Macroraptorial sperm whales (Cetacea, Odontoceti, Physeteroidea) from the Miocene of Peru

Olivier Lambert, Giovanni Bianucci, Christian De Muizon

Abstract

The three extant sperm whale species, the giant *Physeter macrocephalus* and the diminutive *Kogia* species, are relict members of the superfamily Physeteroidea, whose evolutionary history is traced back to the late Oligocene. Although well-preserved and diagnostic cranial remains are relatively scarce, the physeteroid fossil record reveals a considerable degree of morphological disparity (especially during the Miocene), suggesting that sperm whales occupied a broader range of ecological niches in the past. Here, we provide detailed descriptions and a (re)analysis of several new and established middle–late Miocene stem physeteroids from the Pisco Formation of southern Peru. In particular, we (1) further describe the holotype of *Acrophyseter deinodon* from the latest Tortonian–Messinian of Sud-Sacaco, with new information on previously unpublished portions of the skull (including the ear bones) and a discussion of its masticatory musculature; (2) diagnose a new species of *Acrophyseter*, *A. robustus* sp. nov., based on a finely preserved skull with some associated cranial remains from the late Serravallian–Tortonian (> 9.2 Ma) of Cerro la Bruja; (3) provisionally refer a skull from Cerro los Quesos, which has been radiometrically dated to the Messinian (6.9–6.7 Ma), to *Acrophyseter* sp.; and (4) further describe the skull of the giant raptorial sperm whale *Livyatan melvillei* from Cerro Colorado, recently re-dated to the Tortonian (9.9–8.9 Ma) based on the associated diatom fauna and Ar/Ar dating. A phylogenetic analysis based on 53 characters and 21 physeteroid species confirms the monophyly of *Acrophyseter* and groups this genus with the larger, middle to late Miocene macroraptorial stem physeteroids *Brygmophyseter* and *Zygophyseter*. With its unique supracranial basin morphology, *Livyatan* forms a separate, more crownward stem physeteroid lineage. Combined with biostratigraphic information, our cladistic hypothesis allows us to discuss the time of origin of the main physeteroid clades, as well as trends in the evolution of their body size, dentition, temporal fossa and supracranial basin.

Introduction

Three modern physeteroids, the giant sperm whale *Physeter macrocephalus* Linnaeus, 1758 and the pygmy and dwarf sperm whales *Kogia breviceps* (Blainville, 1838) and *K. sima* Owen, 1866, are the only survivors of an odontocete (echolocating tooth cetaceans) group that originated before the end of the Oligocene (more than 23 Ma) and diversified considerably during the Miocene (Mchedlidze, 1970; Fordyce & Muizon, 2001). Fossil sperm whales are known from many parts of the world and display a high degree of morphological disparity, as shown by their great size range and impressive diversity of oral and facial morphologies. The latter include the presence of a large supracranial basin, which is a key physeteroid character (Lydekker, 1893; Kellogg, 1925a, b, 1927, 1965; Barnes, 1973; Muizon, 1988; Hirota & Barnes, 1995; Bianucci & Landini, 2006; Kimura, Hasegawa & Barnes, 2006; Lambert, 2008; Lambert, Bianucci & Muizon, 2008; Whitmore & Kaltenbach, 2008; Lambert *et al*., 2010a; Vélez-Juarbe *et al*., 2015).

Physeteroidea are generally divided into three groups: Kogiidae, comprising all the species more closely related to *Kogia* than to *Physeter*; Physeteridae, comprising all the species more closely related to *Physeter* than to *Kogia*; and a paraphyletic series of stem taxa that are basal to both kogiids and physeterids. Thanks to the presence of several relatively unambiguous synapomorphies, the content of the family Kogiidae is of less debate than that of Physeteridae and stem Physeteroidea (Muizon, 1988; Bianucci & Landini, 2006; Lambert, 2008; Lambert *et al*., 2008, 2010a; Whitmore & Kaltenbach, 2008; Vélez-Juarbe *et al*., 2015).

Although relatively rich, the fossil record of sperm whales is still predominantly represented by isolated teeth, partial mandibles and loose earbones, all of which tend to be poorly diagnostic (but see Hampe, 2006; Fitzgerald, 2011; Vélez-Juarbe, Wood & Pimiento, 2016); well-preserved cranial elements are scarce, which means that much of the past morphological and ecological diversity of sperm whales probably remains hidden.

Here, we considerably add to the physeteroid record by describing four crania, all of them with associated mandibles, from the Miocene Pisco Formation of Peru (Fig. 1). Two of these crania were previously published as the holotypes of *Acrophyseter deinodon* Lambert et al., 2008 and *Livyatan melvillei* (Lambert et al., 2010a), respectively, and are further described here to provide additional details on their morphology and, in the case of *A. deinodon*, take into account the subsequent discovery of additional parts of the specimen (including ear bones). The remaining two skulls both belong to the genus *Acrophyseter*, one of which is the basis for the diagnosis of the new species *A. robustus* sp. nov. To place the new material into context, we perform a cladistic analysis aimed at resolving the content and interrelationships of stem physeteroids. Combined with biostratigraphic information, our cladistic hypothesis allows us to discuss the time of origin of the main

physeteroid clades, as well as trends in the evolution of their body size, dentition, temporal fossa and supracranial basin. Finally some preliminary comments are provided about the marine vertebrate faunal succession in the Pisco Formation.

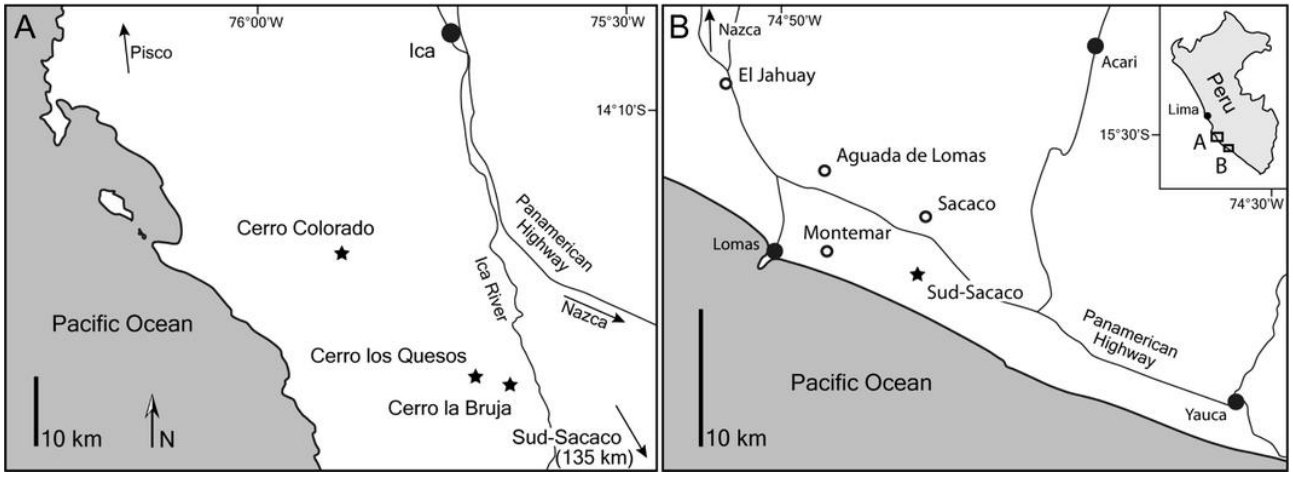

Fig. 1. Schematic maps of the Pisco and Sacaco basins, indicating localities where fossil physeteroids were found (stars). A, northern part of the Pisco Basin, with Cerro Colorado for the holotype of *Livyatan melvillei*, Cerro los Quesos for *Acrophyseter* sp. and Cerro la Bruja for the holotype of *Acrophyseter robustus* sp. nov.; B, Sacaco Basin, with Sud-Sacaco, the type locality of *A. deinodon* as well as other localities of the basin (open circles). The smaller map indicates the position of the two areas along the coast of Peru.

Material and methods

Institutional abbreviations

IRSNB, Institut royal des Sciences naturelles de Belgique, Brussels, Belgium; LSUMG, Museum of Geoscience, Louisiana State University, Baton Rouge, Louisiana, USA; MNHN, Muséum national d'Histoire naturelle, Paris, France; MSNUP, Museo di Storia Naturale, Università di Pisa, Italy; MUSM, Museo de Historia Natural, Universidad Nacional Mayor de San Marco, Lima, Peru; NNML, Nationaal Natuurhistorisch Museum Naturalis, Leiden, The Netherlands; USNM, National Museum of Natural History, Smithsonian Institution, Washington, DC, USA; ZMA, Zoölogisch Museum Amsterdam, The Netherlands.

Anatomical terminology

Our primary source for cranial and mandibular morphology is Mead & Fordyce (2009). For morphological features more specific to sperm whales and for postcranial bones, we also follow Flower (1867), Kellogg (1927, 1965), Reidenberg & Laitman

(1994) and Bianucci & Landini (2006). For jaw muscle terminology, we follow Turnbull (1970). Corresponding references for terms departing from the references listed here are provided directly in the text.

Tooth counts

For specimens with a known total tooth count (holotypes of *Acrodelphis deinodon* and *Livyatan melvillei*; upper jaw of *Acrophyseter* sp. MUSM 2182), lower and upper tooth counts start from the anteriormost tooth, either in the maxilla (in L. melvillei) or in the premaxilla (in *Acrophyseter*). In the case of the latter, we specify if we consider only maxillary teeth, in which case we start counting from the anteriormost maxillary tooth. The exact tooth count is unknown in MUSM 1399, but we hypothesize that it is similar to *A. deinodon* (12 teeth per upper quadrant and 13 per lower quadrant; Lambert et al., 2008). To facilitate comparisons between different species of *Acrophyseter*, we therefore start counting from the hypothetical first premaxillary or mandibular tooth.

Systematic Palaeontology

Cetacea Brisson, 1762
Odontoceti Flower, 1867
Physeteroidea Gray, 1821
Acrophyseter Lambert, Bianucci & Muizon, 2008

Type species

Acrophyseter deinodon Lambert, Bianucci & Muizon, 2008

Other species included

Acrophyseter robustus sp. nov.

Emended diagnosis

Small physeteroid with an upper tooth count of 12, differing from all other members of the superfamily in the following characters: dorsal surface of premaxillae steeply sloping dorsomedially along rostrum; deep and rectilinear groove directed anterolaterally along medial wall of tympanosquamosal recess; conspicuously curved mandible with regularly convex ventral margin in lateral view; considerably enlarged right infraorbital canal, with a transverse diameter > 7% of bizygomatic width; long and greatly thickened medial lamina of the pterygoid along the basioccipital basin. Further differs from all other physeteroids except *Zygophyseter varolai* Bianucci & Landini, 2006 in having a more developed supracranial basin on right side of neurocranium, this basin partly overhanging right orbit and from all other

physeteroids except *Brygmophyseter shigensis* Kimura et al., 2006, *Livyatan* and *Zygophyseter* in having dental roots whose greatest diameter exceeds 5% of the maximum skull width. *Acrophyseter* is further characterized by the following, probably plesiomorphic, features: retention of enamel on teeth; posterior lower teeth transversely flattened; posterior end of upper alveolar groove close to level of antorbital notch; retention of two nasals; elongated contact between jugal and zygomatic process of squamosal; and a high and anteroposteriorly long temporal fossa.

Acrophyseter deinodon Lambert, Bianucci & Muizon, 2008

Holotype

MNHN SAS 1626, a skull lacking part of the left portion of the neurocranium and the right supraorbital process, but including the right periotic, tympanic bulla, incus, stapes and associated mandibles with teeth.

Type locality

Sud-Sacaco, Sacaco Basin, km 540 of the southern Pan-American Highway (Fig. 1B). Geographical coordinates: 15°34′52″S, 74°44′40″W. The holotype was discovered and collected by C. Muizon in 1988.

Type horizon

Pisco Formation, Montemar level (MTM) as defined by Muizon & DeVries (1985), late Miocene. This level was dated to 6.0–5.5 Ma (Messinian) based on molluscan faunas and K–Ar dating of ash layers in levels below MTM (Muizon & DeVries, 1985; Muizon, 1988; Lambert & Muizon, 2013). New Sr analyses on mollusc shells from MTM yielded a somewhat older age coinciding with the Tortonian–Messinian boundary (7.3 Ma, 95% confidence interval 8.7–6.5 Ma) (Ehret et al., 2012). Other marine vertebrates from this level include the phocoenid *Piscolithax* sp. Muizon, 1983, the cetotheriid *Piscobalaena nana* Pilleri & Siber, 1989, an undetermined balaenopterid, the monachine phocid *Acrophoca longirostris* Muizon, 1981, another undescribed monachine phocid, the marine sloth *Thalassocnus natans* Muizon & McDonald, 1995, the penguin *Spheniscus urbinai* Stucchi, 2002, the crocodile *Piscogavialis jugaliperfortatus* Kraus, 1998, and the sharks *Carcharocles megalodon* (Agassiz, 1843) and *Cosmopolitodus hastalis* (Agassiz, 1843) (Muizon, 1981, 1984; Muizon & DeVries, 1985; Muizon & McDonald, 1995; Kraus, 1998; Stucchi, 2002; Muizon et al., 2003).

Emended diagnosis

Differs from *Acrophyseter robustus* sp. nov. in: rostrum being proportionally more pointed in dorsal view, with abrupt anterior decrease of height of maxilla in lateral view; presence of left anterior and posterior premaxillary foramina; presence of a lateral groove on the right side of the rostrum; proportionally broader right infraorbital canal leading to a single anteriorly directed dorsal infraorbital foramen; absence of sulcus anterior to main left dorsal infraorbital foramen; dorsal margin of supracranial basin defined by a sharp rim; dorsal margin of coronoid process of mandible being angular.

Other material

An isolated right periotic MNHN F-PPI 272 (Fig. 12), from the AGL level in the locality of Aguada de Lomas, shares many similarities with the periotic of the holotype of *A. deinodon*; it is referred to *Acrophyster* aff. *A. deinodon* and will be mentioned in the description below. It is noteworthy that this specimen may belong to the same species as the specimen from Cerro los Quesos (MUSM 2182) referred to *Acrophyseter* sp. (see below). In fact, both specimens may prove to be contemporaneous, as the Cerro los Quesos beds that have yielded MUSM 2182 are tentatively correlated to the AGL level of the Sacaco area (see below; Bianucci et al., in press).

Morphological description of *Acrophyseter deinodon*

Ontogenetic stage

Considering the filling of the pulp cavities, the depth of the occlusal facets, the thickness of the cementum layer on roots and the robustness of skull bones (see description below), the holotype of *A. deinodon* was not a juvenile. However, limited apical dental wear and partly open sutures in the rostrum region indicate that it was not an old adult, but rather a fully mature young adult.

Body length estimate

Based on body length (bl) estimates for the closely related *Zygophyseter varolai* (6.5–7.0 m; Bianucci & Landini, 2006), the body length of *Acrophyseter deinodon* is calculated based on equations from Lambert et al. 2010a: supplementary information) and using a bizygomatic width (bzw) and a condylobasal length (cbl) estimated to 466 and 845 mm, respectively.

With the smallest estimate for *Z. varolai* (6.5 m):

$bl = (6.738 \times bzw) + cbl = 4.0$ m

With the largest estimate for *Z. varolai* (7.0 m):

bl = (7.41 × bzw) + cbl = 4.3 m

The proposed size range (4.0–4.3 m) is close to the range proposed in the preliminary description of *A. deinodon* (Lambert et al., 2008: 3.9–4.3 m).

Skull

General morphology

The size of the holotype skull is similar to *Orycterocetus crocodilinus* Cope, 1867, but distinctly smaller than both *Brygmophyseter* and *Zygophyseter* (Table 1). Comparison of the cranial measurements to those of the holotype of *Zygophyseter varolai* indicates that body size of *Acrophyseter deinodon* was approximately half that of the latter (see above for body length estimates).

In lateral view (Figs 2, 3), the ventral margin of the maxilla is markedly convex, which causes the rostrum to taper anteriorly and results in an anterodorsal orientation of the alveolar margin. A similar condition occurs in *O. crocodilinus* (especially on USNM 22926 and 22931, Kellogg, 1965: pl. 24 and 29), whereas the margin of the maxilla is roughly straight in *Zygophyseter*. In dorsal view (Figs 4, 5), the rostrum is wide at its base but then abruptly tapers towards its apex. Although some of the maxillary and premaxillary teeth are missing, the preserved portions of the maxillae and premaxillae suggest an upper tooth count of 12, with three premaxillary and nine maxillary teeth per upper quadrant.

Just posterior to the rostrum, the supracranial basin is dorsoventrally deep and extends far anterolaterally above the right dorsal infraorbital foramen, antorbital notch and orbit (Figs 2–6). This condition differs from *Zygophyseter*, in which the development of the supracranial basin above the right orbit is even more pronounced (Bianucci & Landini, 2006), as well as *Aprixokogia*, *Kogia*, *Livyatan* and *Physeter*, in which the basin is extended further anteriorly along the rostrum. The large temporal fossa is similar in size to that of *Brygmophyseter*, *Livyatan* and *Zygophyseter*, but relatively larger than in *Diaphorocetus* and *O. crocodilinus*, and much larger than in *Aulophyseter morricei* Kellogg, 1927 and *Physeter*. It is as dorsoventrally high as anteroposteriorly long, and anteroposteriorly shorter than in *Brygmophyseter* and *Zygophyseter*. Because of its dorsoventral extension, which is greater than in most other physeteroids, the fossa invades the posterodorsal part of the supraoccipital shield. The supraoccipital shield slopes posteriorly at an average angle of 55° with the horizontal plane, thus causing the medial portion of the elevated nuchal crest to overhang the supracranial basin. The right bony naris is at least four to five times smaller than its left counterpart, with its greatest diameter being less than half (7.2 vs.

30 mm). The mesorostral groove is dorsally open and anteroposteriorly aligned with the right bony naris, as in *O. crocodilinus* and *Zygophyseter*; by contrast, the right naris in *A. morricei* and *Physeter* is located lateral to the longitudinal axis of the mesorostral groove. It therefore seems that the condition in *Acrophyseter deinodon* could either be more derived than in *A. morricei* and *Physeter*, or suggest a reversal in the latter. Further phylogenetic analysis is required to test this hypothesis.

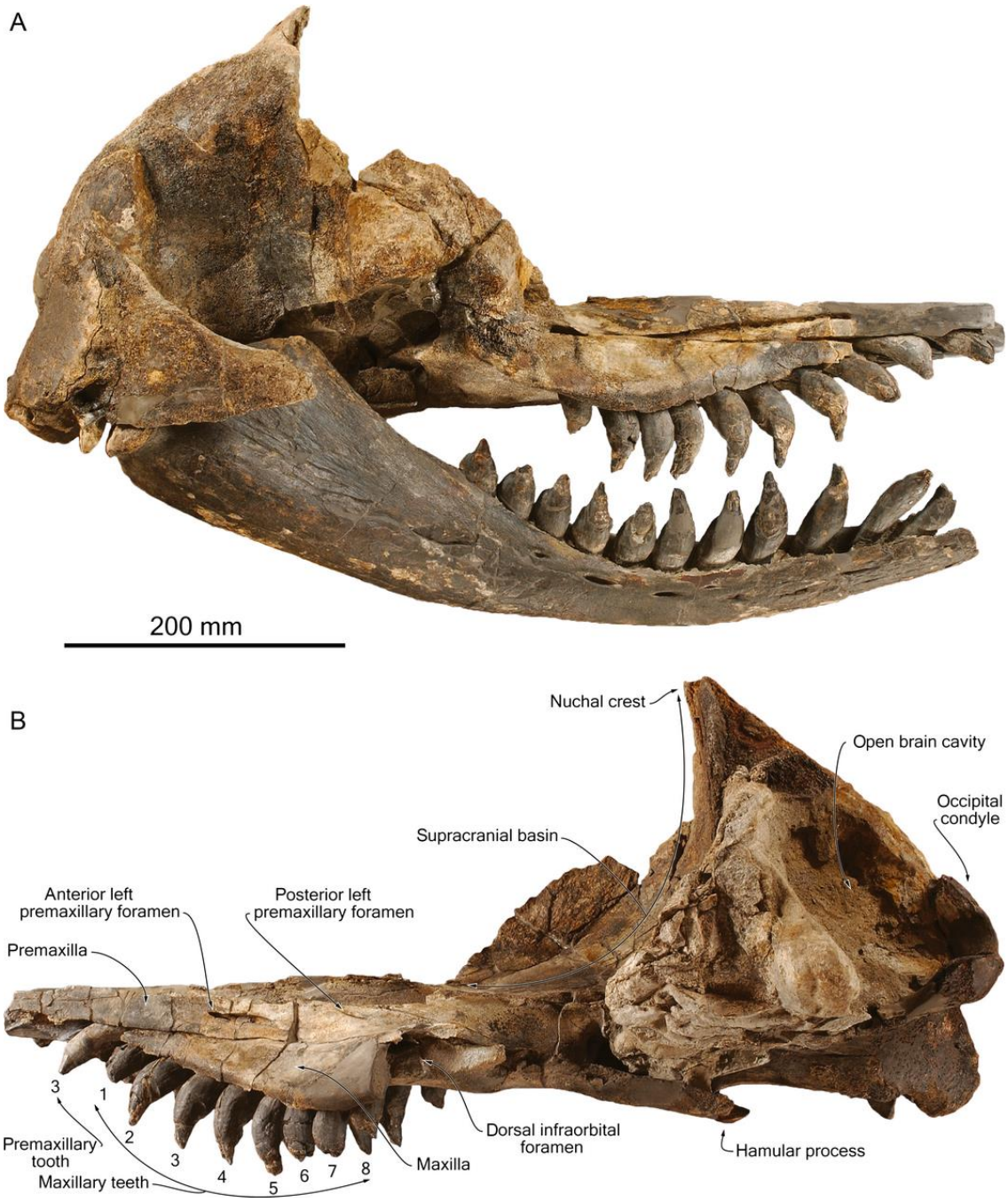

Fig. 2. Skull of *Acrophyseter deinodon* MNHN SAS 1626 (holotype), Sud-Sacaco, late Miocene of the Pisco Basin, Peru. A, right lateral view with articulated mandible; B, left lateral view.

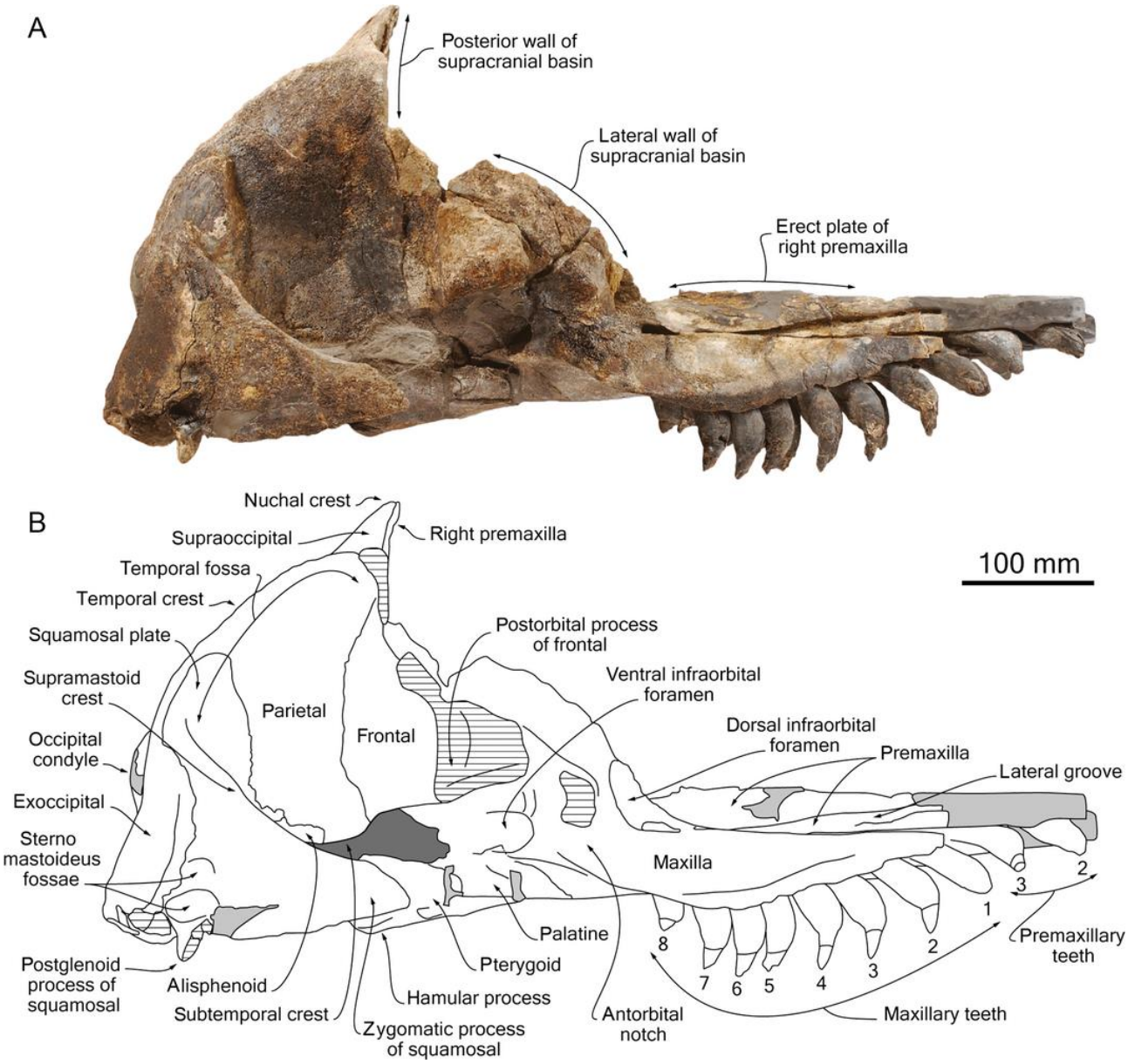

Fig. 3. Skull of *Acrophyseter deinodon* MNHN SAS 1626 (holotype), Sud-Sacaco, late Miocene of the Sacaco Basin, Peru, in right lateral view. A, photograph; B, corresponding line drawing. Light shading for reconstructed parts; hatched surfaces for major break surfaces; stippled lines for incomplete parts; dark shading for sediment.

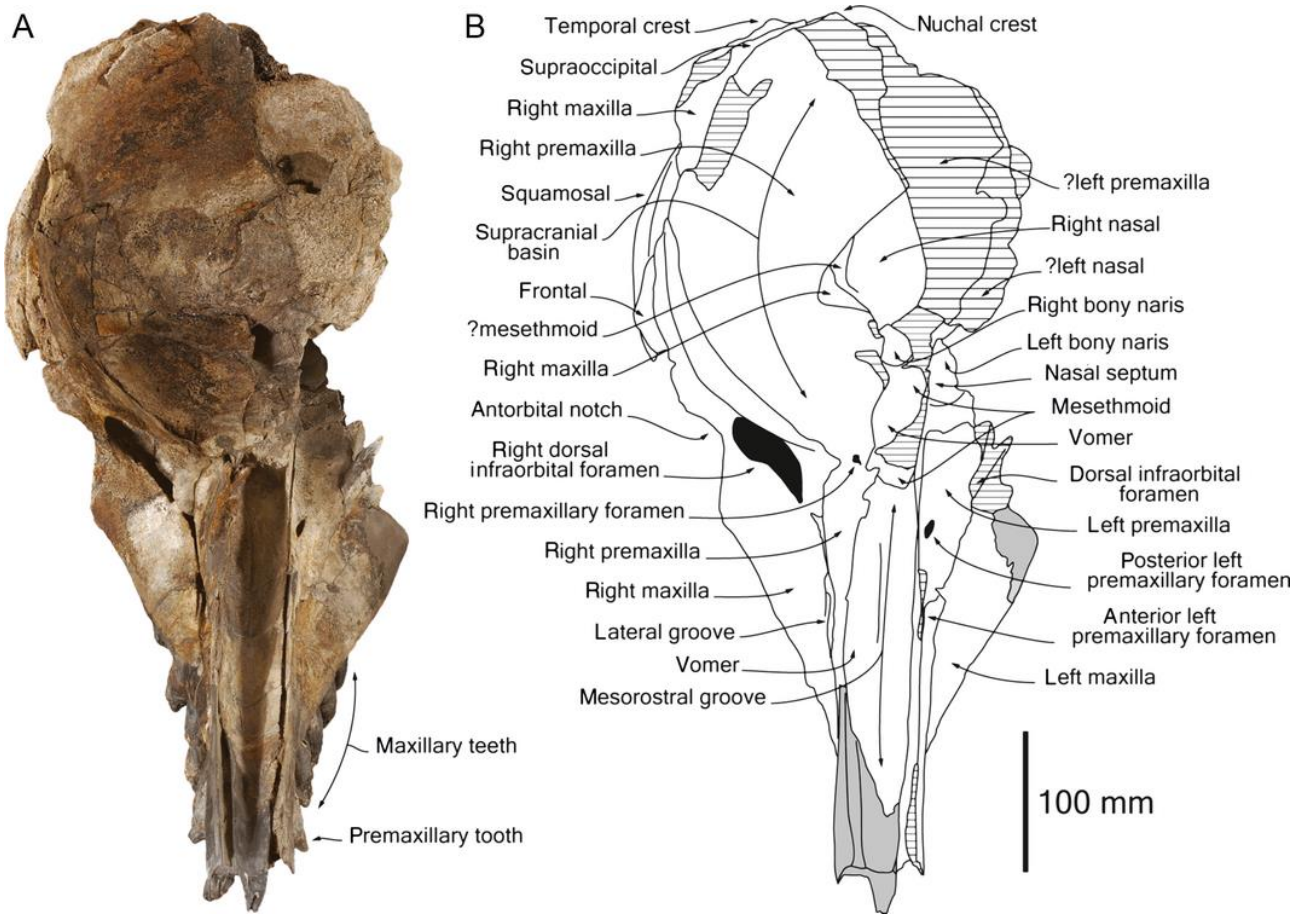

Fig. 4. Skull of *Acrophyseter deinodon* MNHN SAS 1626 (holotype), Sud-Sacaco, late Miocene of the Sacaco Basin, Peru, in anterodorsal view. A, photograph; B, corresponding line drawing. Light shading for reconstructed parts; hatched surfaces for major break surfaces; stippled lines for incomplete parts. Teeth are omitted from the line drawing.

Fig. 5. Skull of *Acrophyseter deinodon* MNHN SAS 1626 (holotype), Sud-Sacaco, late Miocene of the Sacaco Basin, Peru, in dorsal view.

Table 1. Measurements (mm) on the skulls of *Acrophyseter deinodon* MNHN SAS 1626 (holotype), *A. robustus* sp. nov. MUSM 1399 (holotype) and *Acrophyseter* sp. MUSM 2182

	A. Deinodon MNHN SAS 1626	*A. Robustus* MUSM 1399	*Acrophyseter* sp. MUSM 2182
Condylobasal length	+815	-	e930
Rostrum length	e427	-	552
Neurocranium length	-	e460	e378
Length of premaxillary part of rostrum	+100	-	160
Width of rostrum at anterior end of maxillae	e58	-	60
Maximum width of ventral exposure of vomer on rostrum	57	-	33
Distance between lateral margins of alveolar grooves at level of alveoli 3	51	-	50
Distance between lateral margins of alveolar grooves at level of alveoli 8	144	-	108
Distance between lateral margins of alveolar grooves at level of alveoli 12	e228	-	188
Longitudinal distance between last alveolus and antorbital notch	-	63	e50
Width of rostrum at base	e274	-	300
Transverse diameter of right bony naris	21	21	-
Transverse diameter of left bony naris	+44	46	-
Maximum width of supracranial basin	-	272	-
Distance from anteriormost margin of preorbital process of frontal to posteriormost margin of postorbital process	-	-	120
Maximum length of temporal fossa	e234	230	200
Maximum height of temporal fossa	e230	230	-
Distance between anterior tip of zygomatic process and ventral tip of postglenoid process	190	-	e168
Maximum height of skull	+368	-	-
Bizygomatic width of skull	e466	e385	432
Minimum distance between temporal fossae across supraoccipital shield	-	171	-
Maximum distance between lateral margins of basioccipital crests	e252	193	205
Width of occipital condyles	-	-	e162
Maximum width of left condyle	-	71	-
Height of left condyle	-	117	-
Height of right condyle	100	-	-
Transverse diameter of foramen magnum	-	e63	-
Total length of periotic	+42.5	-	-
Maximum dorsoventral height of periotic	+24	-	-
Maximum mediolateral width of periotic	30	-	-
Length of anterior process of periotic (from anterior edge of pars cochlearis to apex)	8	-	-
Length of pars cochlearis of periotic (until anterior margin of fenestra rotunda)	19	-	-
Length of tympanic bulla (without posterior process)	40	43	46
Maximum mediolateral width of tympanic bulla	20.5	-	-
Maximum height of incus	5.7	-	-
Maximum width of incus including crus breve	6.55	-	-
Maximum width of articular facet of incus with malleus	4.3	-	-

+, Incomplete; e, estimate; –, no data.

Premaxilla

At the apex, each premaxilla bears deep, obliquely orientated alveoli for three procumbent incisors, with I1 being the most strongly inclined (Figs 2, 3, 7). As preserved, the incisor-bearing portion of the premaxilla extends 100 mm beyond the anterior end of the maxilla, but may be missing up to 50 mm. In total, the premaxilla could thus have contributed about a third to the total length of the rostrum.

Laterally, the exposed surface of the premaxilla is poorly preserved along the anterior half of the rostrum, but appears to be orientated vertically and relatively low (Figs 2–5). Further posteriorly, the right premaxilla forms a dorsally convex blade medially overhanging the mesorostral groove. On the left premaxilla, the dorsal blade remains low along most of the rostrum length. At the posterior end of the mesorostral groove, approximately 50 mm anterior to the mesethmoid, the blade of the left premaxilla becomes lower than the vomer, the latter forming the left dorsolateral edge of the mesorostral groove. Posteriorly, the left premaxilla–vomer suture enters the enlarged left bony naris. There, it turns posterolaterally on the floor of the naris. The lateral edge of the left naris is broken, obscuring the suture posterolaterally. The extent of the left premaxilla in the supracranial basin is therefore unknown.

Because the premaxillae are far from contacting dorsomedially, the mesorostral groove is widely open dorsally for the whole rostrum length, contrary to the condition in the holotype of *Aulophyseter morricei*, *Idiorophus patagonicus* (Lydekker, 1893) and Scaphokogia (Lydekker, 1893; Kellogg, 1927; Muizon, 1984). Judging from their transverse width in dorsal view, the extent of the premaxillae along the lateral walls of the mesorostral groove is seemingly less asymmetrical in *A. morricei*, *Physeter*, *Scaphokogia* and *Zygophyseter*. However, such delicate elements are often only partly preserved in fossil specimens. The walls of the mesorostral groove are also strongly asymmetrical at the rostrum base in *Orycterocetus crocodilinus*; interestingly in the latter the condition is reversed, with the left premaxilla and left part of the vomer being transversely wider than the right, and more markedly overhanging the mesorostral groove (conspicuous in USNM 22926; Kellogg, 1965).

Dorsally raised lateral walls of the mesorostral groove support our hypothesis that the supracranial basin did not extend far on to the rostrum in *A. deinodon*.

On the right premaxilla is a small right premaxillary foramen (transverse diameter 6 mm) located slightly anterior to the level of the anterior end of the mesethmoid and at approximately 10 mm from the medial edge of the blade of the premaxilla (the latter is damaged in this area for a length of 35 mm, but can be reconstructed based on the preserved anterior and posterior edges) (Figs 4, 6). This foramen is superficially damaged and its anteroposterior diameter cannot be measured. However, it is clear that it was anteroposteriorly elongated, probably at least twice anteroposteriorly long

as transversely wide. On the left premaxilla, a small posterior premaxillary foramen is present 40 mm anterior to the right foramen. It is also located at approximately 10 mm from the medial edge of the premaxilla. This foramen is elongated (22 mm for the longitudinal diameter and 5 mm for the transverse diameter) with a slightly oblique, anteromedially–posterolaterally orientated long axis. Surprisingly the asymmetry of the premaxillae extends more anteriorly on the rostrum: the left premaxilla is pierced by an additional, anteriorly located elongated foramen (61 mm long, maximum transverse diameter of 6 mm), whereas the right premaxilla is excavated by a deep longitudinal groove starting 30 mm anterior to the right premaxillary foramen and 30 mm lateral to it at the maxilla–premaxilla suture (Figs 3, 4, 6). This groove extends anteriorly until the level of the fifth maxillary tooth where it divides. A narrow groove follows the maxilla–premaxilla suture, whereas a wider and deeper groove extends anteriorly and slightly dorsomedially on the lateral surface of the premaxilla until the preserved anterior apex of the bone. Because of its transverse width at this level (ca. 6 mm), it is likely to have extended several centimetres more anteriorly. This groove on the right premaxilla can be followed posterolaterally until the enlarged right dorsal infraorbital foramen. On the left side of the skull, the maxilla is broken from the level of the anterior end of the mesethmoid. However, on the posterior side of this breakage, the section of a large infraorbital canal is observed at the level of the premaxilla–maxilla suture, extending anteriorly under a plate of maxilla. It is likely to have left the suture approximately at the level of the fifth maxillary tooth, continuing anteriorly within the premaxilla only. This assumption is supported by the observation of the elongated left anterior premaxillary foramen, most likely constituting an exit for part of the nerves and vessels of the canal (Fig. 4). Beyond this foramen, the canal extends further anteriorly within the premaxilla for an unknown distance. Such major exits of the infraorbital canal in the premaxilla were not observed in other physeteroids.

At the level of the premaxillary foramen, the right premaxilla is constricted by a medial projection of the maxilla. From that point, the premaxilla strongly widens posteriorly, covering most of the lateral floor of the supracranial basin (Figs 4, 5), as is observed in *Diaphorocetus* and *O. crocodilinus*. *Acrophyseter deinodon* differs in this respect from *Zygophyseter* and the kogiids, in which the right premaxilla is not transversely expanded in its supracranial portion. It also differs from *Aulophyseter morricei* and *Physeter*, in which this posterolateral extension of the premaxilla is considerably less developed.

Although the preservation of the right premaxilla is not optimal on the holotype of *A. deinodon*, sutures of the bone can be followed with reasonable accuracy. The outline of the preserved portions and the sections at broken margins suggest that it originally covered most of the right part of the elevated posterior wall of the supracranial basin, and that it probably crossed the sagittal plane of the skull. On the anterolateral region

of the supracranial basin, the premaxilla–maxilla suture follows the right edge of the basin at a distance from the edge varying from 30 to 60 mm. On the posterolateral portion of the basin, the suture approaches the edge of the nuchal crest. The right premaxilla reaches the top of the nuchal crest in its medial region. There, the premaxilla directly contacts the supraoccipital without any frontal exposure. This condition differs from that in *O. crocodilinus*, in which the right premaxilla is separated from the supraoccipital by the maxilla and a small portion of the frontal, and from that in *Physeter*, in which the posterior part of the premaxilla rests exclusively on the frontal. At the rostrum base, the medial suture of the premaxilla is with the vomer. It passes to the mesthmoid at some point before the right bony naris, but the vomer–mesethmoid suture could not be detected. This medial suture is slightly sigmoidal. Between the premaxillary foramen and the small right bony naris (transverse diameter 21 mm), the dorsal surface of the right premaxilla remains flat, lacking the deep groove, which extends posteriorly from the premaxillary foramen as seen in several physeteroids (e.g. *Aulophyseter morricei*, *'A.' rionegrensis* Gondar, 1975, *O. crocodilinus* and *Placoziphius duboisi* Van Beneden, 1869; Kellogg, 1927, 1965; Gondar, 1975; Lambert, 2008). Approaching the right naris, the premaxilla–mesethmoid suture heads towards the ventrolateral wall of the naris. From the posterolateral corner of the naris, we suspect that a poorly preserved bony element corresponds to the medial exposure of the right maxilla, appearing between the premaxilla and the mesethmoid; such an exposure of the maxilla is indeed observed in many odontocetes. The resulting premaxilla–maxilla suture abruptly turns laterally for approximately 40 mm, and then draws an angle of about 90°. Therefore, posterior to the bony naris, the medial edge of the premaxilla is strongly concave medially. After this turn, the suture is roughly straight and extends posteromedially for approximately 80 mm. Here, the right premaxilla is broken with a longitudinal section visible from the left side of the skull. The bone is relatively thick (from 10 to 15 mm) and the break surface reaches the supraoccipital dorsally. In medial view (with the left side of the skull missing), the dorsalmost part of the posterior plate of the premaxilla overhangs the supracranial basin. Here, the longitudinal axis of the rostrum and the posterior plane of the supracranial basin form an angle slightly < 90°.

From the posterior left premaxillary foramen, the concave dorsal surface of the left premaxilla deepens markedly towards the large left bony naris (transverse diameter > 44 mm), reaching a level 30 mm lower than the right premaxilla. The posterior end of the left premaxilla is not preserved, but anterior to the bony naris, it does not widen as observed on the right premaxilla. The left dorsal infraorbital foramen mentioned above is edged medially for at least 25 mm by the left premaxilla.

On the ventral face of the rostrum (Fig. 7), the premaxillae are adjacent from the apex of the rostrum to the second maxillary teeth, where they diverge posteriorly due to the anterior pointed apex of the ventral exposure of the vomer being wedged between

them. From the third to the fifth right maxillary tooth (to the fourth on the left side of the skull) the premaxilla forms a thin strip of bone bordered by a thin palatal part of the maxilla laterally and by the vomer medially.

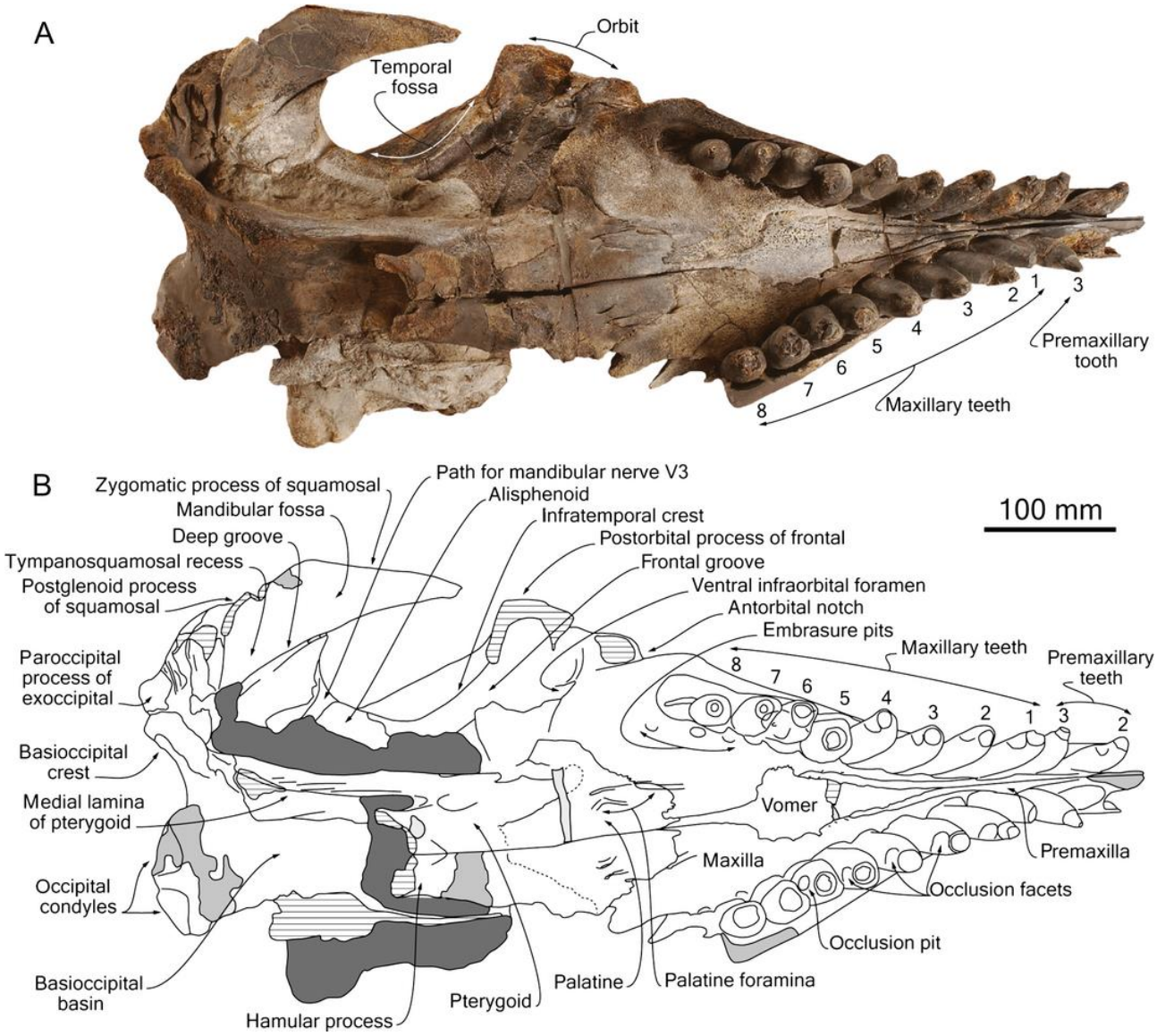

Fig. 7. Skull of *Acrophyseter deinodon* MNHN SAS 1626 (holotype), Sud-Sacaco, late Miocene of the Sacaco Basin, Peru, in ventral view. A, photograph; B, corresponding line drawing. Light shading for reconstructed parts; hatched surfaces for major break surfaces; stippled lines for incomplete parts; dark shading for sediment.

Maxilla

The maxilla is shorter anteriorly than the vomer, ending 100 mm posterior to the preserved apex of the rostrum (see above) (Figs 2, 3). In lateral view, the maxilla forms an elongated triangle that borders the premaxilla ventrally, with a horizontal dorsal edge and a strongly oblique ventral edge bearing teeth. In dorsal view, the

maxillae also form two elongated triangles bordering the premaxillae laterally, with slightly concave lateral edges (Figs 4, 5). Their dorsolateral surface slopes ventrolaterally at an angle of c. 45° from the suture with the premaxilla. At the rostrum base, the lateral margin of the maxilla is much lower than the roof of the orbit (Fig. 1C), differing markedly for that character from *Aprixokogia kelloggi* Whitmore & Kaltenbach, 2008, *Aulophyseter morricei*, *'A.' rionegrensis*, *Brygmophyseter*, *Diaphorocetus poucheti* Moreno, 1892, *Idiorophus*, *Kogia*, *Orycterocetus crocodilinus*, *Physeter*, *Physeterula dubusi* Van Beneden, 1877 and *Placoziphius*.

On the right side of the skull, there is presumably no anteroventrally developed antorbital process of the maxilla. A small break surface on the ventral side of this area is interpreted here as superficial wear, although it cannot be excluded that a narrow antorbital process of the maxilla did originally project anteroventrally. Unfortunately, this region is not preserved on the left side. Based on our favoured interpretation, the antorbital notch was not laterally limited by the maxilla (see below for a comment on the lost jugolacrimal complex). The right antorbital notch is distinctly outside the supracranial basin and much lower than the anterolateral wall of the basin. It is indeed located just ventral to the dorsal infraorbital foramen and slightly posterior to the level of the right premaxillary foramen.

On the right lateral edge of the base of the rostrum is an enormous dorsal infraorbital foramen (see dimensions below), forming the anterior opening of an approximately 80-mm-long funnel-shaped infraorbital canal (Fig. 6). This foramen is oval-shaped with a long axis orientated dorsolaterally–ventromedially. Maximum and minimum diameters of the foramen are c. 60 and 30 mm, respectively. This right dorsal infraorbital foramen is overhung dorsomedially by a thin oblique blade of the maxilla, which forms the anterolateral border of the supracranial basin. From the dorsal infraorbital canal, three large sulci or grooves depart in different directions: (1) a broad saddle-shaped notch is observed at the dorsolateral extremity of the foramen and extends posterolaterodorsally above the orbit, lateral to the edge of the supracranial basin; (2) from the ventromedial margin of the foramen, a 15-mm-wide sulcus divides into two canals: one turns dorsomedially, where it bifurcates again with a branch connecting the right premaxillary foramen and another posteromedial branch seemingly heading to the right bony naris, whereas the other canal strongly narrows anteriorly, is covered dorsally by a thin lamina of the maxilla for only 13 mm, and runs along the premaxilla–maxilla suture, before another bifurcation, with one narrower groove following the premaxilla–maxilla suture and a wider groove that is deeply entrenched in the premaxilla, as described above; and (3) from the medial margin of the infarorbital foramen, a wide and poorly differentiated groove turns medially, runs ventral to the anteromedial end of the thin plate of maxilla forming the anterolateral limit of the supracranial basin, and reaches the maxilla–premaxilla

suture at the level of the premaxillary foramen. All these passages exiting from the dorsal infraorbital foramen are likely to have transmitted blood vessels (infraorbital arteries and veins) and nerves (branches of the trigeminal nerve) to the posterodorsal and anterior regions of the spermaceti organ and surrounding forehead soft tissue elements, and to the anterior region of the rostrum (see Fraser & Purves, 1960; Mead & Fordyce, 2009). These neurovascular passageways do not pierce the maxilla on the floor or on the lateral wall of the supracranial basin, as in many other physeteroids (e.g. *Aprixokogia*, *Aulophyseter morricei*, *'A.' rionegrensis*, *Kogia*, *O. crocodilinus*, *Placoziphius* and *Zygophyseter*). In addition, most physeteroids (including *Livyatan* and *Zygophyseter*) display more than one right dorsal infraorbital foramen (see data-matrix in Appendix S2). At this level, the condition in *A. deinodon* is similar to that in *Physeter*, in which a single dorsal infrorbital foramen (maxillary incisure) pierces the right maxilla, although in the latter, the foramen opens roughly vertically on the anterolateral wall of the supracranial basin. Furthermore, the right dorsal infraorbital foramen and infraorbital canal are proportionnally larger than in all other physeteroids.

The left maxilla is not preserved posterior to maxillary tooth 8. Therefore, the dorsal infraorbital foramen is only partly preserved. At the level of the right premaxillary foramen is the medial edge of an anterior dorsal infraorbital foramen, which penetrates the premaxilla–maxilla suture and extends toward the apex of the rostrum (Fig. 4). This canal is large and its roughly circular section has a diameter of about 20 mm.

On the right side, from the oblique, thin maxillary plate, the maxillary edge of the supracranial basin rises posterolaterodorsally. Dorsal to the orbit, the wall of the basin is subvertical and was originally not distant from the partly eroded lateralmost margin of the orbit (Figs 4–6). The development of the highly asymmetrical supracranial basin above the right orbit is even more pronounced in *Zygophyseter*, with a lateral wall extending laterally beyond the orbit (Bianucci & Landini, 2006). In this region, in lateral view, the portion of the maxilla dorsal to the postorbital process is relatively elevated. Posterodorsally, the maxilla disappears at some distance from the sagittal plane and is most likely barely involved in forming the nuchal crest, constituted predominantly by the right premaxilla and supraoccipital in the preserved region.

On the ventral side of the rostrum, each maxilla bears large alveoli for nine teeth; interalveolar septa are very thin, sometimes nearly absent (Fig. 7). With the three premaxillary teeth, the total count for the upper tooth row is 12, less than in *Idiorophus*, *O. crocodilinus*, and *Zygophyseter*. The upper dentition is reduced to absent in *Aulophyseter morricei*, *Kogia*, *Nanokogia isthmia* Vélez-Juarbe et al., 2015, *Physeter*, *Placoziphius* and *Scaphokogia* (Muizon, 1988; Kimura et al., 2006;

Lambert, 2008; Vélez-Juarbe et al., 2015). The tooth rows strongly converge anteriorly; the first left and right maxillary teeth are only separated by 12 mm whereas the distance increases to 108 mm at the level of maxillary tooth 7 and 140.5 mm at the level of maxillary tooth 9.

On the palate, the maxilla is very narrow anteriorly from the level of the fourth upper tooth to the ninth. Posteriorly, the maxilla greatly widens medially from the tenth tooth until the level of the suture with the palatine.

Following our hypothesis that the antorbital process of the maxilla does not project anteroventrally in *A. deinodon*, we propose that an almost flat subcircular facet on the ventral surface of the right maxilla posterolateral to the antorbital notch corresponds to a facet for the articulation of the jugolacrimal complex, which is not preserved. Posterior to this articular facet is a shallow and short, posteriorly concave, and c. 10-mm-wide sulcus, extending from the lateral edge of the ventral infraorbital foramen medially to the orbit laterally. We have no interpretation for this structure. Only slightly smaller than the more funnel-shaped dorsal infraorbital foramen, the ventral (posterior) opening of the infraorbital canal (= maxillary foramen sensuWible, 2008; ventral infraorbital foramen sensuMead & Fordyce, 2009) has transverse and dorsoventral diameters of 35 and c. 30 mm, respectively. It opens anteromedial to the orbit.

Vomer–mesethmoid

In the mesorostral groove, the right lateral wall of the vomer follows medially the dorsomedial curve of the elevated right premaxilla, partly closing the groove dorsally (Figs 4, 5). More posteriorly, this part of the vomer partly covers the ossified portion of the mesethmoid as a subhorizontal plate. However, the path of the mesethmoid–vomer suture could not be followed in that region. As in other physeteroids, the mesethmoid is distinctly tilted towards the left side, from the nasal septum to the rostrum base; the nasal septum draws an angle of < 40° with the horizontal plane of the skull (90° in a symmetrical skull). Posterolateral to the right bony naris, a narrow exposure of the mesethmoid is tentatively identified between a medial exposure of the right maxilla and the right nasal.

The roughly flat and triangular ventral surface of the rostrum between the tooth rows is mostly occupied by the vomer (Fig. 7). The palatal exposure of the bone has a characteristic lanceolate morphology, with an elongated, narrow anterior end wedged between the premaxillae. Posteriorly, the vomer widens markedly until the level of maxillary tooth 6 (maximum width of 57 mm). From that level, the vomer abruptly narrows, wedges between the maxillae posteromedially and contacts the apex of the right palatine.

Nasal

Based on a comparison with A. robustus, only a part of the right nasal could be detected posterior to the right bony naris (Fig. 4). As a relatively thin plate of bone, the right nasal is bordered anteriorly and laterally by the mesethmoid, and posterolaterally by the right premaxilla. The right nasal crosses the sagittal plane and may have covered the left nasal dorsally. However, this region is too poorly preserved to allow a firm identification of individual bones, apart from the right nasal.

Frontal

The anterior part of the supraorbital process of the right frontal is missing (Figs 2, 3, 7). The postorbital process is partly preserved; its lateral and ventral regions are abraded and the dorsoventral extent cannot be estimated. With the shape of a roughly equilateral triangle, its preserved base is massive. Its vertical posterior edge gently turns posteromedially in the temporal fossa. Above the orbit, a distinct crack resulting from post-mortem breakage follows the suture between the maxilla and the frontal (Fig. 3). In the temporal fossa, the frontal has a subvertical suture with the parietal. The ventral edge of the frontal in the temporal fossa forms a sharp infratemporal crest, which corresponds to the posterolateral border of the wide and deep frontal groove. The latter forms an angle of 40° with the longitudinal plane; it is more anteriorly directed than in Aulophyseter morricei, Diaphorocetus, Orycterocetus crocodilinus and Physeter. Because the dorsal edge of the supracranial basin is damaged, the frontal is mostly obscured in this region.

Palatine

Anteriorly, the palatine reaches the level of the last maxillary alveolus. It is wide and its anterior portion is roughly rectangular, with an irregular transverse suture with the maxilla (Fig. 7). Several palatine foramina are observed on each side: one major palatine foramen is located along the suture with the maxilla at the anterolateral angle of the bone, and several accessory palatine foramina (two on the right side, three on the left side) pierce the palatine itself. Each major palatine foramen extends anteriorly in a deep groove excavating the maxilla, whereas the accessory palatine foramina are followed anteriorly by sulci in the palatine. Posterior to the level of the accessory palatine foramina, the palatine greatly widens and almost reaches the ventromedial edge of the ventral infraorbital foramen. As in other physeteroids, the palatine is not invaded by the pterygoid sinus (Fraser & Purves, 1960).

Pterygoid

The right pterygoid is nearly complete, whereas a large anterior portion of the left is lost. The anterior portion of the bone is a thin plate, which partly overlaps the palatine

anterolaterally (Fig. 7). Not reaching anteriorly the level of the antorbital notch, apices of the right and left pterygoids are widely separated by the palatines; both pterygoids contact only at a level posterior to the level of the postorbital process. The anterior portion of the pterygoid is narrow and distinctly thickened on its lateral edge. This thickened edge is the medial margin of a shallow fossa in the palatine, laterally delimitated by the ventral infraorbital foramen. A similar condition of the pterygoid and palatine is observed for example in *Eudelphis mortezelensis* du Bus, 1872, *Kogia* and *Physeter*, and may correspond to a locally deeper fossa for the anterior extension of the pterygoid sinus (see Fraser & Purves, 1960, for Kogia and Physeter). Anterior to the Eustachian notch, the surface of the pterygoid presents a rounded shallow depression, also possibly related to the pterygoid sinus. An alternative interpretation of this fossa as an area of origin for a pterygoid muscle is presented below. Neither hamular process is complete posteroventrally. Although it is probable that each process did project for some distance posterolaterally, we cannot evaluate the outline of the posterior margin. Laterally limiting the basioccipital basin, the medial lamina is proportionally much elongated (146 mm from the Eustachian notch to the posterior contact with the basioccipital) and greatly transversely thickened (Figs 7, 8); its posterior portion has a robust triangular section. This condition is not recorded in any other physeteroid for which this region is known, with *Zygophyseter* as a possible noteworthy exception (basicranium moderately well preserved displaying a relatively robust and long medial lamina); the medial lamina of the pterygoid is generally shorter and relatively slender (e.g. in *Diaphorocetus*, *Kogia*, *Orycterocetus crocodilinus* and *Physeter*).

Parietal

Only the right parietal is preserved. It forms most of the median portion of the temporal fossa, comprising more than one-third of the lateral wall of the braincase between the frontal and the squamosal (Fig. 3). This is considerably wider than in *Aulophyseter morricei* and *Physeter*, and is more similar to *Idiophyseter Kellogg*, 1925 and probably relating to the anteroposteriorly longer temporal fossa. It extends from the temporal crest dorsally to the subtemporal crest ventrally. It has a subvertical suture with the frontal anteriorly and with the squamosal plate posteriorly. Ventrally, it contacts the alisphenoid and probably reaches the subtemporal crest anterior to the latter.

The temporal crest is distinct until a level slightly dorsal to the dorsal edge of the squamosal plate (Figs 3, 5, 9). Judging from the spongy aspect of the bone in that area, some degree of abrasion eroded the ventrolateral portion of the crest, which was probably originally connected to the supramastoid crest of the squamosal (forming the posterior edge of the squamosal plate and the dorsal edge of the zygomatic process). From its posterior margin, the temporal crest turns anterodorsomedially,

indicative of a temporal fossa extending far dorsomedially. The crest then turns anterolaterally to reach the posterolateral edge of the supracranial basin. The posterior suture of the parietal with the exoccipital and supraoccipital is not discernible (see the condition in a young *Physeter macrocephalus* in Kellogg, 1925a, pl. 2).

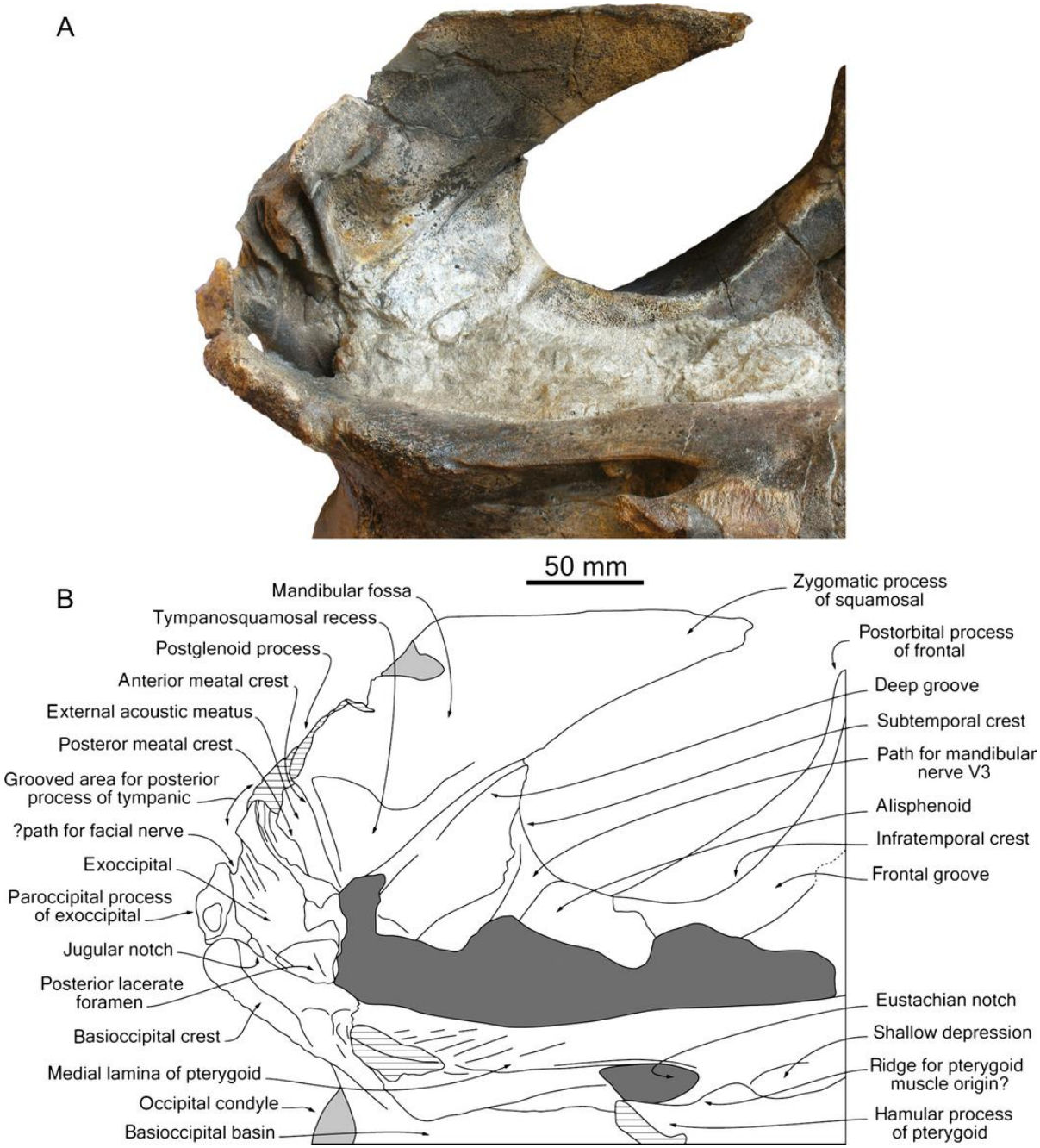

Fig. 8. Skull of *Acrophyseter deinodon* MNHN SAS 1626 (holotype), Sud-Sacaco, late Miocene of the Sacaco Basin, Peru. Detail of the right side of the basicranium in anteroventral and slightly lateral view. A, photograph; B, corresponding line drawing. Light shading for reconstructed parts; hatched surfaces for major break surfaces; stippled lines for incomplete parts; dark shading for sediment.

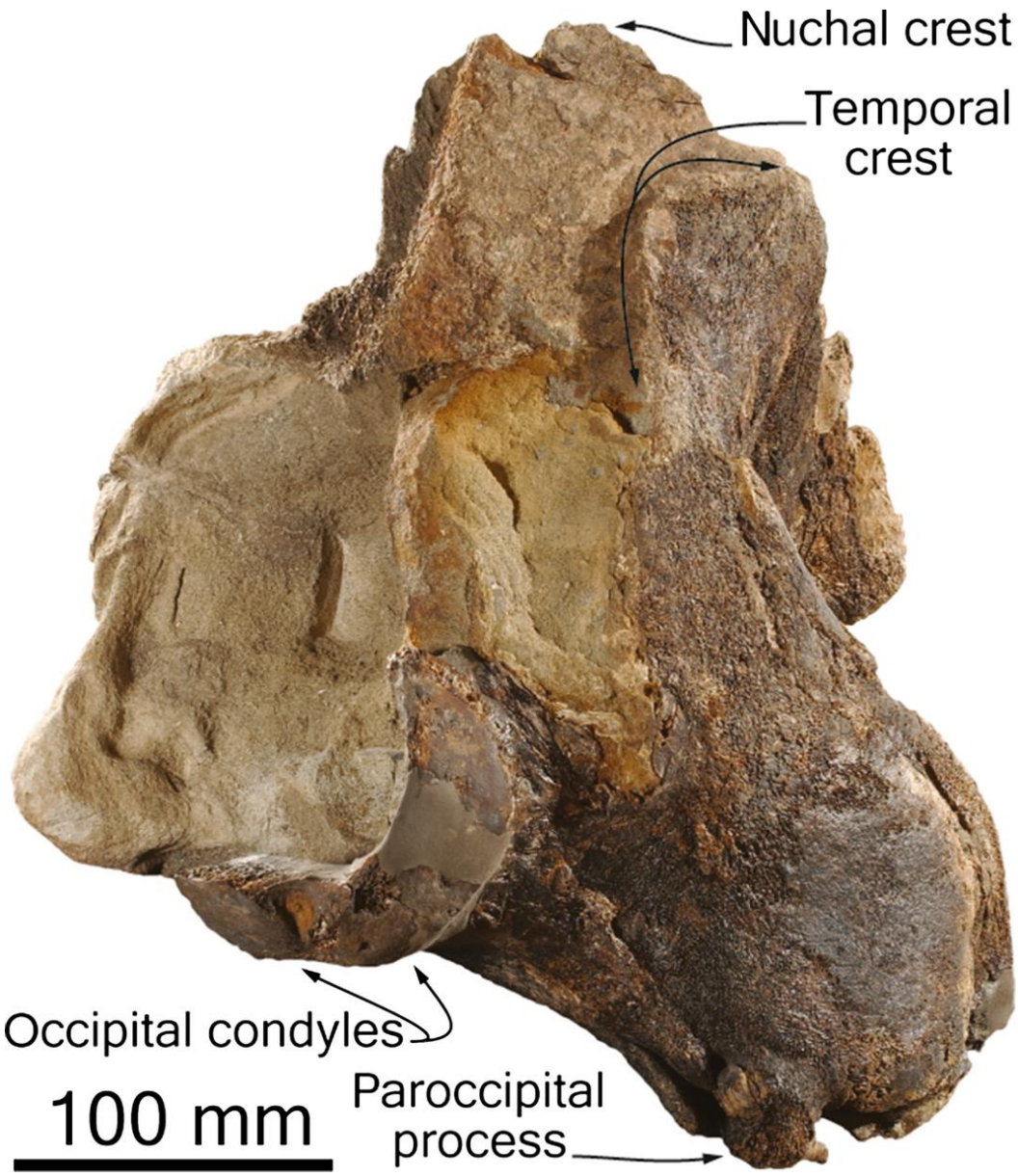

Fig. 9. Skull of *Acrophyseter deinodon* MNHN SAS 1626 (holotype), Sud-Sacaco, late Miocene of the Sacaco Basin, Peru, in posterior view.

Squamosal

The zygomatic process of the squamosal is moderately elongated (Fig. 3), but much less than in *Zygophyseter*. The anterior tip of the process is abraded, so its accurate outline cannot be provided. However, considering its anteroposterior position close to the level of the postorbital process of the squamosal, it is probably nearly complete. Its dorsoventral height increases considerably posteriorly, making a triangular shape in lateral view, with the supramastoid crest rising steeply towards the temporal crest.

Just anterior to the suture with the exoccipital, two moderately excavated sternomastoideus fossae (the lower being deeper and somewhat larger) end before the zygomatic process anteriorly. In the temporal fossa, the squamosal plate is dorsoventrally elongated and anteroposteriorly narrow. Constituting the floor of the temporal fossa, the squamosal fossa is a wide, transversely concave and roughly longitudinally flat surface descending steeply from the squamosal plate to the subtemporal crest. The squamosal contacts the alisphenoid along that crest.

The nearly flat mandibular fossa (= glenoid cavity) is anteroventromedially orientated and barely demarcated from the shallow tympanosquamosal recess (Figs 7, 8). The latter is L-shaped with the small branch being posterior and pointing laterally. The long branch almost reaches the subtemporal crest. Along this long branch of the tympanosquamosal recess is an elongated, deep and narrow rectilinear groove, which extends anterolaterally from the posteromedial angle of the tympanosquamosal recess (the region of the spiny process) to the subtemporal crest. An anteriorly shorter, narrow groove is observed in *Physeter*, not reaching the subtemporal crest, whereas only a shallower and less rectilinear groove is present in Aulophyseter morricei, *Eudelphis mortezelensis* and *Orycterocetus crocodilinus* (IRSNB M.1936). Similarly present in other specimens of *Acrophyseter* this groove may correspond to the passage of a branch of the external carotid artery, for example the proximal portion of the mandibular or the internal maxillary artery, considering the passage of these arteries close to this region in the dog and several delphinids (Fraser & Purves, 1960: fig. 7; Evans & de Lahunta, 2013). The falciform process is only preserved as a low, inconspicuous prominence in the medialmost corner of the squamosal; it is too incomplete to estimate its original extent.

The postglenoid process is a thin, obliquely directed plate. Its ventral apex is not fully preserved, but it is continuous with the medially located, thin, high and long anterior meatal crest (Figs 7, 8). The latter margins anteriorly the deep and narrow external acoustic meatus, which is slightly obliquely orientated, with its lateral end being slightly anterior to the partly preserved spiny process. Posterior to the meatus is a slender posterior meatal crest. Posterior to this crest is a deeply grooved, irregular surface probably corresponding to the contact of the squamosal with the enlarged posterolaterally directed posterior process of the tympanic bulla (not preserved). This grooved area extends until the exoccipital posteriorly and bears a larger crest and groove just anterior to the squamosal–exoccipital suture. In lateral view, there is no deep notch for the posterior process of the tympanic between the postglenoid process of the squamosal and the paroccipital process of the exoccipital, a clear difference with *Kogia* and *Praekogia cedrosensis* Barnes, 1973 (Barnes, 1973: fig. 3).

Alisphenoid

Only the lateral portion of the alisphenoid could be prepared. In lateral view the alisphenoid occupies a reduced area on the posteroventral border of the temporal fossa, where it articulates with the squamosal posteriorly and the parietal anteriorly (Figs 3, 7, 8). No contact with the frontal could be detected in that area. The foramen ovale is hidden by hardened sediment. The shallow and wide groove for the path for the mandibular nerve V3 exits with an anterolateral direction in the temporal fossa, just anterior to the squamosal–alisphenoid suture.

Basioccipital–exoccipital

The basioccipital basin is proportionately long anteroposteriorly, as shown by the elongated and thick medial lamina of the pterygoid, and posteriorly wide (Figs 7, 8). Only the right basioccipital crest is preserved. Nevertheless, because the sagittal plane can be located in the basioccipital basin, a strong posteroventral divergence of the basioccipital crests is noted, as in other physeteroids and most ziphiids (Muizon, 1991).

The robust occipital condyles are separated from the lateral plate of the exoccipital by a short and barely constricted neck (Figs 7, 9). The articular facet on the condyle faces posteriorly and slightly dorsally relative to the horizontal plane of the neurocranium and rostrum; therefore, the rostrum did not project anteroventrally relative to the vertebral column, contrasting with the condition in kogiids, *Idiophyseter* and *Physeter*.

In posterior view, the exoccipital presents a transversely wide and dorsoventrally high lateral plate along the posterior edge of the squamosal as usual in physeteroids (Figs 9, 10). On the ventral border, the paroccipital process is small but well differentiated from the rest of the bone. Its ventral face is a flat to slightly concave surface for the articulation for the stylohyal. Medially, the paroccipital process contacts the lateral surface of the basioccipital crest. The jugular notch is therefore ventrally closed, constituting a true foramen. Two notches are observable on the dorsomedial wall of this large foramen. The lateral notch is relatively wide and U-shaped, corresponding probably to the path for the jugular vein (jugular notch sensu stricto). The narrower, pinched medial notch is interpreted as separating the exoccipital from the basioccipital. This notch defines a short and narrow process of the exoccipital between the jugular notch and the basioccipital crest, interpreted here as a vestigial medial crest of the exoccipital (or falcate process of the exoccipital). A similar notch is generally absent in odontocetes, but is observed in basilosaurids (e.g. *Cynthiacetus peruvianus* Martínez-Cáceres & Muizon, 2011 MNHN.F.PRU 10). However, in the latter the contribution of the exoccipital to the basioccipital crest is much larger and roughly square (see Kellogg, 1936; Uhen, 2004). The lateral edge of the paroccipital process of *A. deinodon* is also deeply notched, as seen in several

physeteroids, including *Eudelphis*, *Orycterocetus crocodilinus*, *Physeter* and *Placoziphius* (Lambert, 2008). In *Physeter*, this notch is partly filled with the enlarged posterior process of the tympanic (as observed for example in USNM 395398). Nevertheless, there could be space left in this notch for the passage of a nerve (possibly the facial nerve, as proposed for Simocetus rayiFordyce, 2002 and *Waipatia maerewhenua* Fordyce, 1994, 1994, 2002; Lambert, 2008) or a vessel leaving the basicranium in a ventrolateral direction. A tiny foramen, opening ventrolaterally, pierces the exoccipital lateral to the occipital condyle; this foramen seems too small and distant from the jugular notch to represent the hypoglossal foramen.

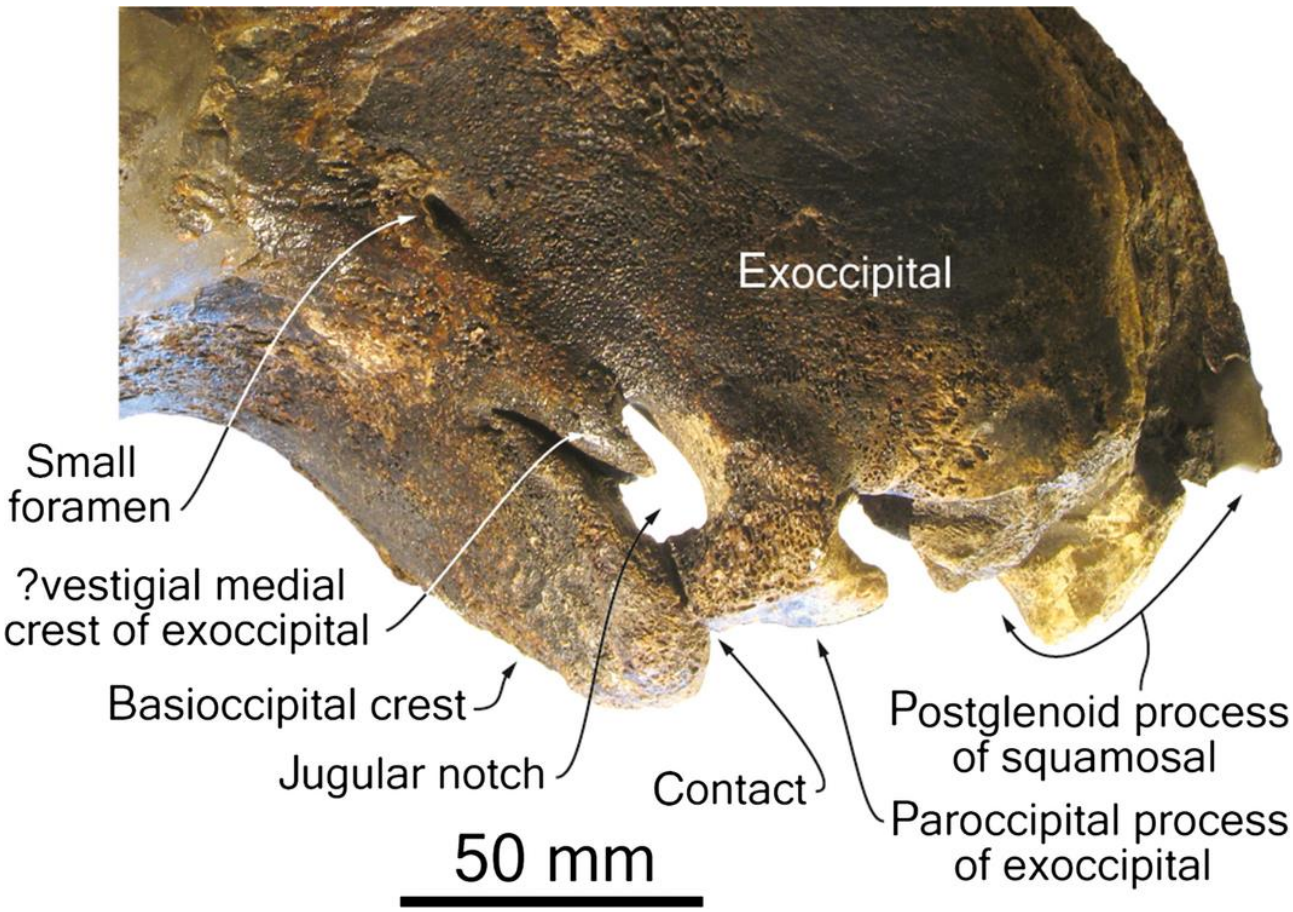

Fig. 10. Skull of *Acrophyseter deinodon* MNHN SAS 1626 (holotype), Sud-Sacaco, late Miocene of the Sacaco Basin, Peru. Detail of the right ventrolateral portion of the basicranium in posterior view.

Ear bones

On both the right periotic and the right tympanic bulla of the holotype of *Acrophyseter deinodon* MNHN SAS 1626, the outer surface of the bone is

moderately damaged; at some levels a thin crust of concretion remains, whereas at other levels a thin layer of bone has been removed during preparation (Figs 11, 13). Nevertheless, most of the morphological features of the periotic are preserved, apart from the posterior surface of the pars cochlearis and the end of the posterior process. The stapes is preserved in connection with the fenestra ovalis. The tympanic is less well preserved, with a part of the outer lip, the sigmoid process and elements of the posterior process missing. The right incus is complete. The isolated right periotic MNHN F-PPI 272 (Fig. 12), from Aguada de Lomas referred to *Acrophyster* aff. *A. deinodon*, will be mentioned in the description below when it differs from the holotype of *A. deinodon*.

Periotic (Figs 11, 12)

Measurements of the periotic of MNHN SAS 1626 are provided in Table 1. The almost complete periotic MNHN F-PPI 272 is slightly larger than MNHN SAS 1626, with a preserved total length of 50.3 mm, the anterior process 11.2 mm long, the pars cochlearis 19.7 mm long, the maximum dorsoventral height 29.5 mm and the mediolateral width 32 mm. Nevertheless, this difference clearly fits in the range of intraspecific variation observed in *Physeter macrocephalus* and *Kogia* spp. (Kasuya, 1973).

The apex of the short anterior process is pointed and anteroventrally directed. The small ventral surface anterior to the accessory ossicle is slightly longitudinally concave, corresponding to a small anterior bullar facet. This facet is also present in MNHN F-PPI 272, but is approximately twice as long. As in other physeteroids and some ziphiids, the fovea epitubaria is occupied with a large (12 mm long), ovoid and slightly dorsoventrally flattened accessory ossicle, and a fragment of the outer lip of the tympanic fused to the anterior process. The accessory ossicle is still proportionally smaller than in *Physeter*. The ossicle is even smaller in MNHN F-PPI 272; it is less globular, dorsoventrally flattened, but slightly longer anteroposteriorly than in the holotype. Against the anterior margin of the pars cochlearis, the dorsomedial region of the anterior process is occupied by a voluminous, rounded prominence, which is somewhat anteriorly longer than the accessory ossicle. This pointed prominence is especially developed on MNHN F-PPI 272. A similar prominence is observed in *Kogia*, an isolated periotic tentatively referred to Scaphokogia (MNHN PPI 240, Muizon, 1988: fig. 37), isolated kogiid periotics from Lee Creek Mine, North Carolina (e.g. Whitmore & Kaltenbach, 2008: fig. 80), and in *Zygophyseter*. It is smaller in *Aulophyseter morricei* and in *Physeter*, and seemingly absent in *Orycterocetus crocodilinus*. The mallear fossa (the anterior part of the epitympanic recess) is deep and roughly circular on the holotype and shallower and oval-shaped on MNHN F-PPI 272. The lateral tuberosity is poorly developed laterally, with a slightly convex ventral surface. It is separated from the posterior

process by a shallow hiatus epitympanicus. Medial to the distal opening of the facial canal (the secondary facial foramen), the fenestra ovalis (fenestra vestibuli) of the holotype is obscured by the stapes preserved in situ. This fenestra is more oval than in *A. morricei*, *O. crocodilinus* and *Physeter*.

At the anterior tip of the posterior process, the oval-shaped fossa incudis is posterolateral to the distal opening for the facial canal. As in other physeteroids except kogiids, the preserved part of the posterior bullar facet is slightly convex transversely and concave longitudinally. The facet curves posteroventrally, a condition absent in *Kogia* and other isolated kogiid periotics. No grooves and ridges are observed in the proximal part of the facet in the holotype. However, MNHN F-PPI 272 displays in the distal part of the better-preserved facet a series of prominent ridges. In the latter, the facet is also transversely convex and curves distinctly laterodorsally and mediodorsally. In both specimens, the medial part of the facet floors the facial suclus. In lateral view, the posterodorsal margin of the posterior process forms an angle of approximately 90° with the dorsal edge of the bone. This resembles the condition in *Aulophyseter* morricei and *O. crocodilinus*, but the angle is larger than in *Physeter*, in which it approaches 70°. The posterodorsal margin of the process bears a sharp and elevated keel, deeply excavated on its lateral wall. Such a keel is also present in *A. morricei* and *O. crocodilinus*, but absent in *Physeter*. The posterior process differs significantly from that of kogiids, in which it bears a plate-like posterior extension and an articular facet fully facing ventrally (e.g. Vélez-Juarbe et al., 2016).

In ventral view, the pars cochlearis is raised medially, slightly tilted towards the anterior process. As in MNHN F-PPI 272, the outline of the pars cochlearis in ventral view presents a slight angulation posteromedially, more pronounced than in kogiids, *O. crocodilinus* and *Physeter*. This condition is due to a pointed projection on the medial edge of the fenestra rotunda (external aperture of the cochlear fossula). In medial view, the pars cochlearis is narrow, more dorsoventrally flattened than on MNHN F-PPI 272 and in other physeteroids. On the posterodorsomedial area of the pars cochlearis, a slightly concave surface separates the fenestra rotunda from the internal acoustic meatus (IAM). The fenestra rotunda is oval, with its great diameter orientated dorsoventrally. It is separated from the wide and deep stapedial muscle fossa by a wide and moderately elevated bar, without angular posteroventral corner (and therefore without conspicuous caudal tympanic process). On the posterodorsal edge of the pars cochlearis, the aperture for the cochlear aqueduct (external aperture of the cochlear canaliculus) is small and anteroposteriorly elongated, whereas it is circular on MNHN F-PPI 272. The aperture for the vestibular aqueduct is even more flattened, along the posterior margin of the IAM. The IAM is oval, not anteriorly pinched, with a great diameter directed mediolaterally. The large and circular proximal opening of the facial canal is located inside the IAM, lateral to the spiral

cribriform tract, and separated from the latter by a low transverse crest. The opening for the facial canal is more anterior in *O. crocodilinus* and *Physeter*. The mediolaterally flattened singular foramen, smaller than in *Zygophyseter*, is located roughly at the top of the crest, whereas it is on the medial wall of the crest in MNHN F-PPI 272. More similar to kogiids and *Zygophyseter*, the dorsal process (dorsal crest sensuMead & Fordyce, 2009) is low and little differentiated from the rest of the dorsal margin of the bone in medial view. This process is longer beyond the lateral margin of the IAM and more pointed in *A. morricei* and *O. crocodilinus*, and longer but more massive in *Physeter*.

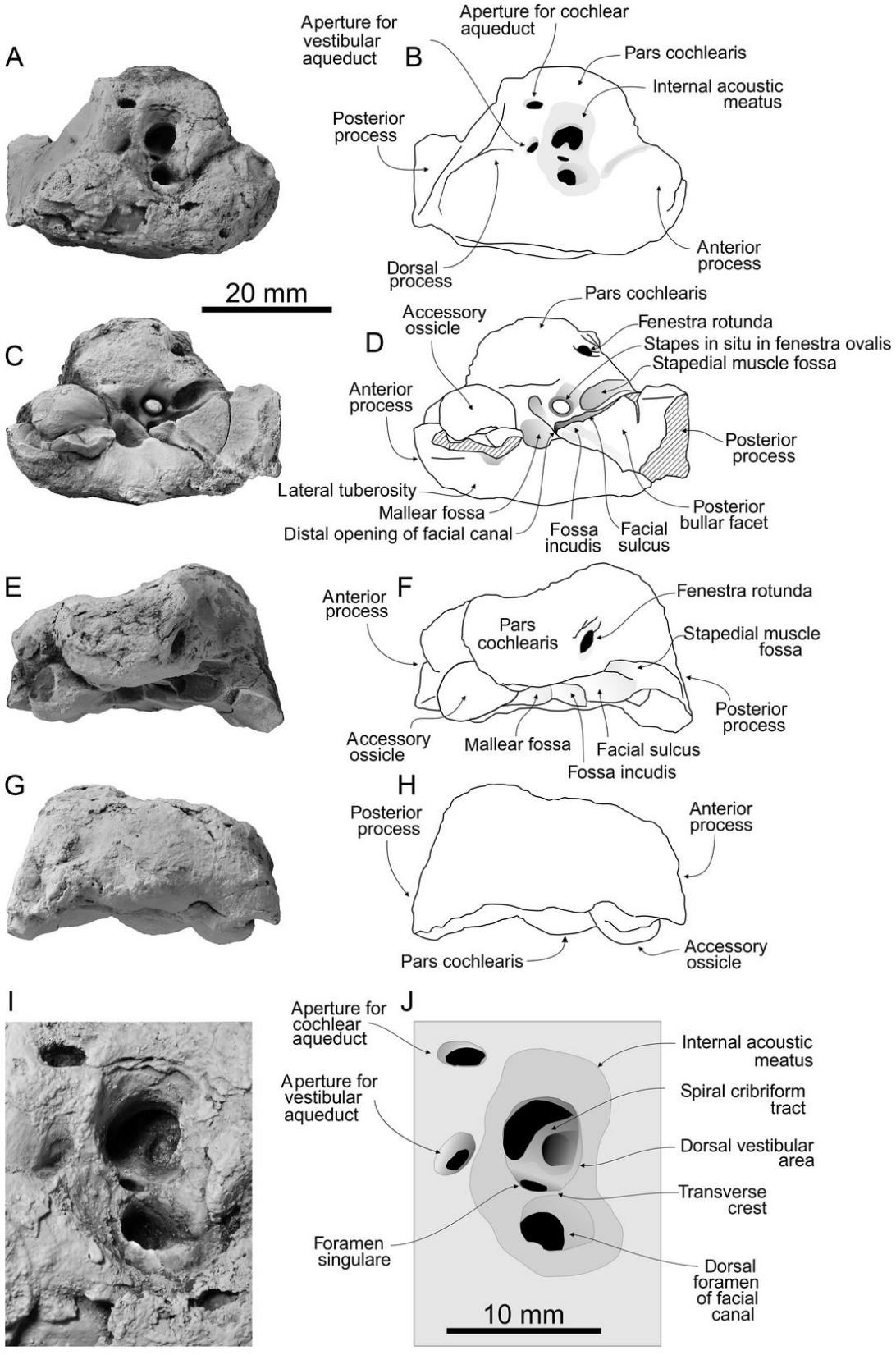

Fig. 11. Right periotic of *Acrophyseter deinodon* MNHN SAS 1626 (holotype), Sud-Sacaco, late Miocene of the Sacaco Basin, Peru. A, dorsal view; B, corresponding line drawing; C, ventral view; D, corresponding line drawing; E, medial view; F, corresponding line drawing; G, lateral view; H, corresponding line drawing; I, detail of the pars cochlearis in anterodorsal view; J, corresponding line drawing. Hatched surfaces for major break surfaces. Scale bar for A–H = 20 mm, for I, J = 10 mm.

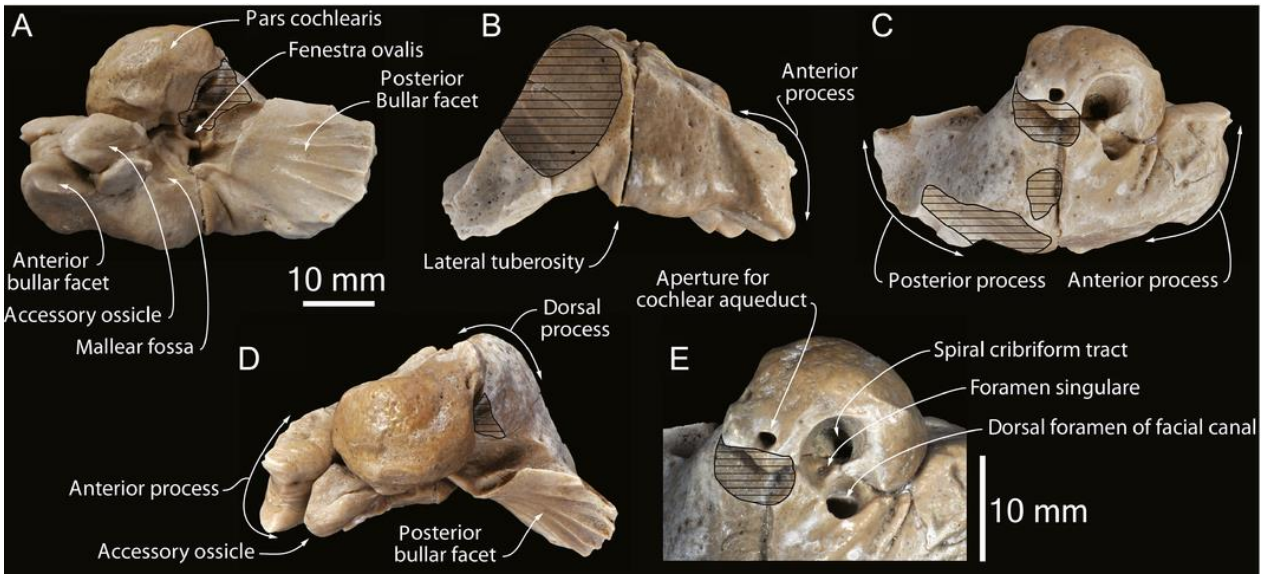

Fig. 12. Isolated right periotic of *Acrophyster* aff. *A. deinodon* MNHN F-PPI 272, Aguada de Lomas, late Miocene of the Sacaco Basin, Peru. A, ventral view; B, lateral view; C, dorsal view; D, medial view; E, detail of the pars cochlearis in anterodorsal view. Hatched surfaces for major break surfaces.

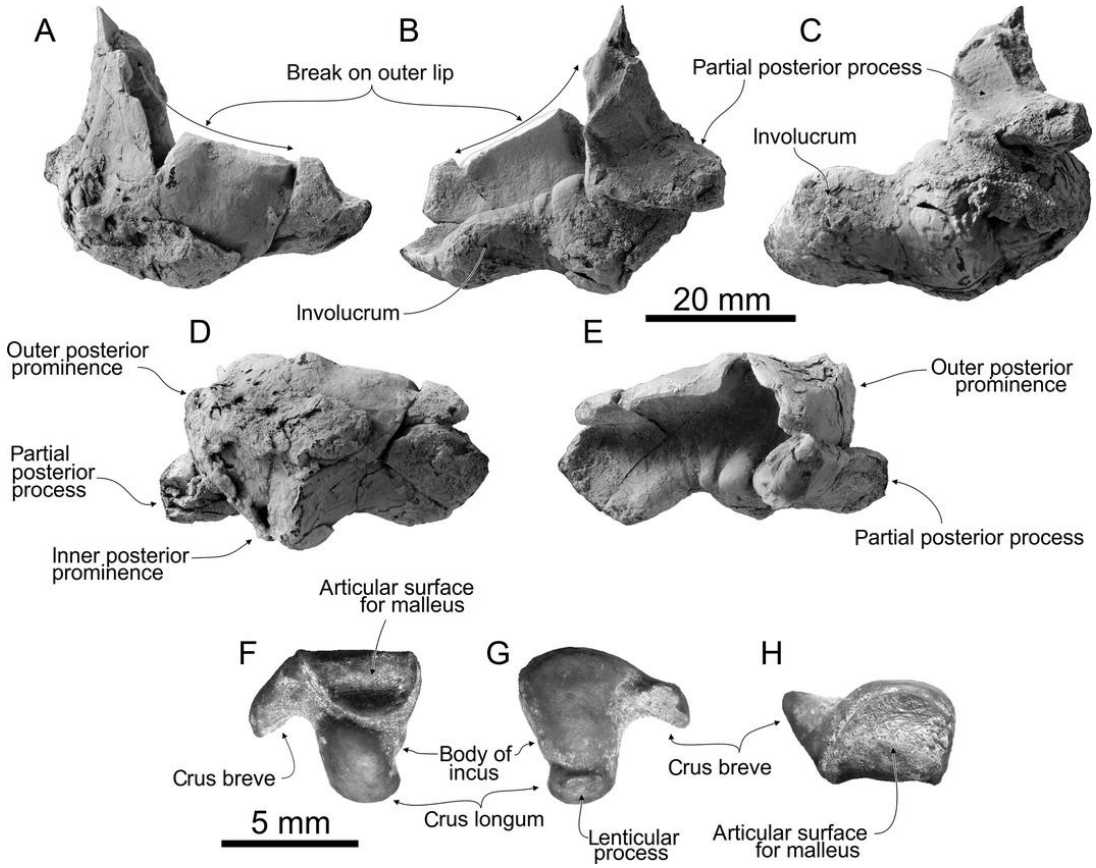

Fig. 13. Right tympanic bulla and incus of *Acrophyseter deinodon* MNHN SAS 1626 (holotype), Sud-Sacaco, late Miocene of the Sacaco Basin, Peru. A–E, tympanic bulla. A, ventral view; B, dorsal view; C, dorsomedial view; D, ventromedial view; E, lateral view. F–H, incus. Scale bar for A–E = 20 mm, for F–H = 5 mm.

Tympanic bulla (Fig. 13; Table 1)

As for many features of the skull, the physeteroid tympanic has an unusual morphology compared to other odontocetes. For that reason, it is necessary to specify the orientation of the different parts of the bone. In the following description, the dorsal side is identified by a deep concavity in the involucrum, which receives the pars cochlearis of the periotic. The dorsal face of the bone also bears the articular facet for the periotic, which faces dorsally. The medial aspect of the tympanic is a relatively flat area, which bears posteriorly the inner and outer prominences. The ventral and lateral aspects are formed by the outer lip with the large dorsoventrally elongated sigmoid process. On the holotype of *Acrophyseter deinodon*, most of the outer lip is missing, with its ventral part only being preserved. Furthermore, the posterior spongy extension of the posterior process is broken off. Unsurprisingly, and as detailed below, the general shape of the tympanic differs strikingly from non-physeteroid odontocetes. In dorsal view, the involucrum is curved anteromedially, with a deep notch at mid-length of its medial margin, as in *Kogia*, *Orycterocetus crocodilinus*, *Physeter* and *Zygophyseter*. This condition is especially obvious in medial view. As in all other known physeteroids, the anterior part of the involucrum is transversely thickened. Nevertheless, in *Acrophyseter deinodon*, this part is transversely narrower (in dorsal view) than in Zygophyseter. Furthermore, because the notch of the involucrum is deeper in *Acrophyseter* than in *Zygophyseter*, in medial view, the thickened anterior part of the involucrum appears more salient dorsally than in *Zygophyseter*. As a consequence, in medial view the dorsal and ventral margins of the anterior part of the tympanic are diverging anteriorly, while they are roughly parallel in *Zygophyseter*. In dorsal view, the lateral edge of the involucrum presents two lateral tubercles: the larger one is located at the anterior angle of the posterior process and the smaller one is slightly more medial. In medial view, the anterior margin of the tympanic is orientated anteroventrally–posterodorsally, a condition also observed in specimens of *Kogia*, whereas this margin is roughly vertical in *Physeter* and *Zygophyseter*. No median furrow is observed on the medial surface of the tympanic. The inner posterior prominence (dorsal according to the conventional orientation adopted above) is much shorter posteriorly than the outer (ventral) prominence, a condition more pronounced than in Physeter and more similar to *Kogia* (see e.g. Kasuya, 1973, pl. 8). The inner (dorsal) posterior prominence is even more dorsally projected in *Zygophyseter*, but the outer (ventral) prominence is unknown in the latter. The outer (ventral) posterior prominence of *Acrophyseter* is less swollen than in *Physeter*. No conspicuous interprominental notch could be detected, whereas a shallow notch is present in *Kogia* and *Physeter*. However, this area is poorly preserved in MNHN SAS 1626. The posterior process is pressed against the high posterior wall of the body of the tympanic for about three-quarters of the height of the latter. Although the process is

partly broken, the contact of the process on the wall of the tympanic is clearly observable. The posterior wall–posterior process contact is similarly long in *Physeter*, but much less in *Kogia*. The facet for the posterior process of the periotic is saddle-shaped (transversely concave and anteroposteriorly convex) and orientated posteroventrally, as in *Physeter*. No elliptical foramen is present between the inner and outer posterior pedicles.

Incus (Figs 13, 14; Table 1)

As in *Kogia* (K. breviceps USNM 302040) and *Physeter* (MHNP 1913-286, USNM 487416), the crus breve of the incus of the holotype starts directly from the margin of the large articular surface with the malleus, differing from most other odontocetes observed (Fig. 14). This feature is specially different from ziphiids, with a crus breve far from the articular surface. In addition, the latter are characterized by a longer crus breve, with an expanded apex, and a proportionally shorter crus longum. Compared to *Physeter*, the incus of *A. deinodon* is slightly more stocky, the crus breve has roughly the same extent and is slightly more divergent from the body of the bone, and the crus longum is more massive. The small articular surface for the malleus is lower and the large articular surface is less buckled than in *Physeter*. In *Kogia*, the apex of the crus breve is more swollen and the crus longum is proportionally shorter compared to the articular surface with the malleus. The lenticular process, for the contact with the stapes, is oval, on a part of the crus longum separated from the rest of the bone by a slight constriction.

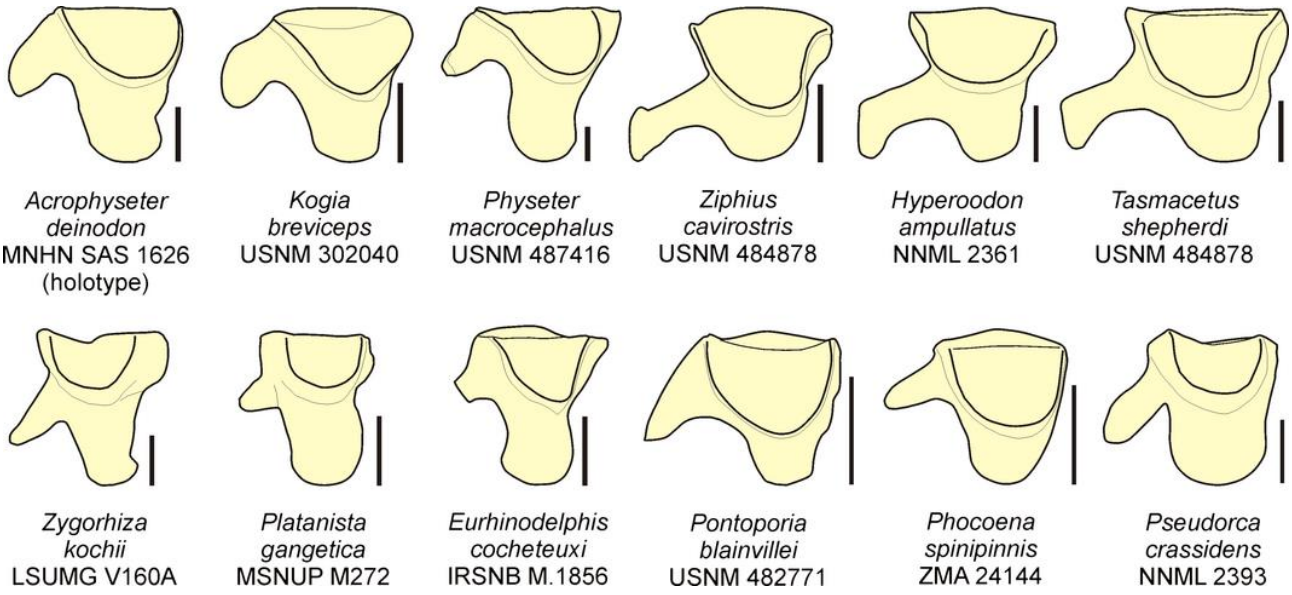

Fig. 14. Comparison of the shape of the incus of *Acrophyseter deinodon* MNHN SAS 1626 (holotype) with other extinct and extant odontocetes, in posterolateral to lateral view. Image of *Zygorhiza kochii* modified from Lancaster (1990); image of *Eurhinodelphis cocheteuxi* modified from Lambert (2005). Scale bars = 2 mm.

Stapes (fig. 11C)

The body of the stapes of the holotype, in situ in the fenestra ovalis, is short and stocky, similarly to *Kogia* and *Physeter*. In ziphiids, the stapes is more slender and conical. In addition, the footplate has the oval outline of physeteroids, differing from the subcircular outline in ziphiids and *Platanista gangetica* (Roxburgh, 1801) (Lambert, Bianucci & Post, 2009). As in *Physeter*, the stapedial foramen is reduced to a tiny hole (seen only via computer tomography scan).

Mandibles (Figs 15, 16; Table 2)

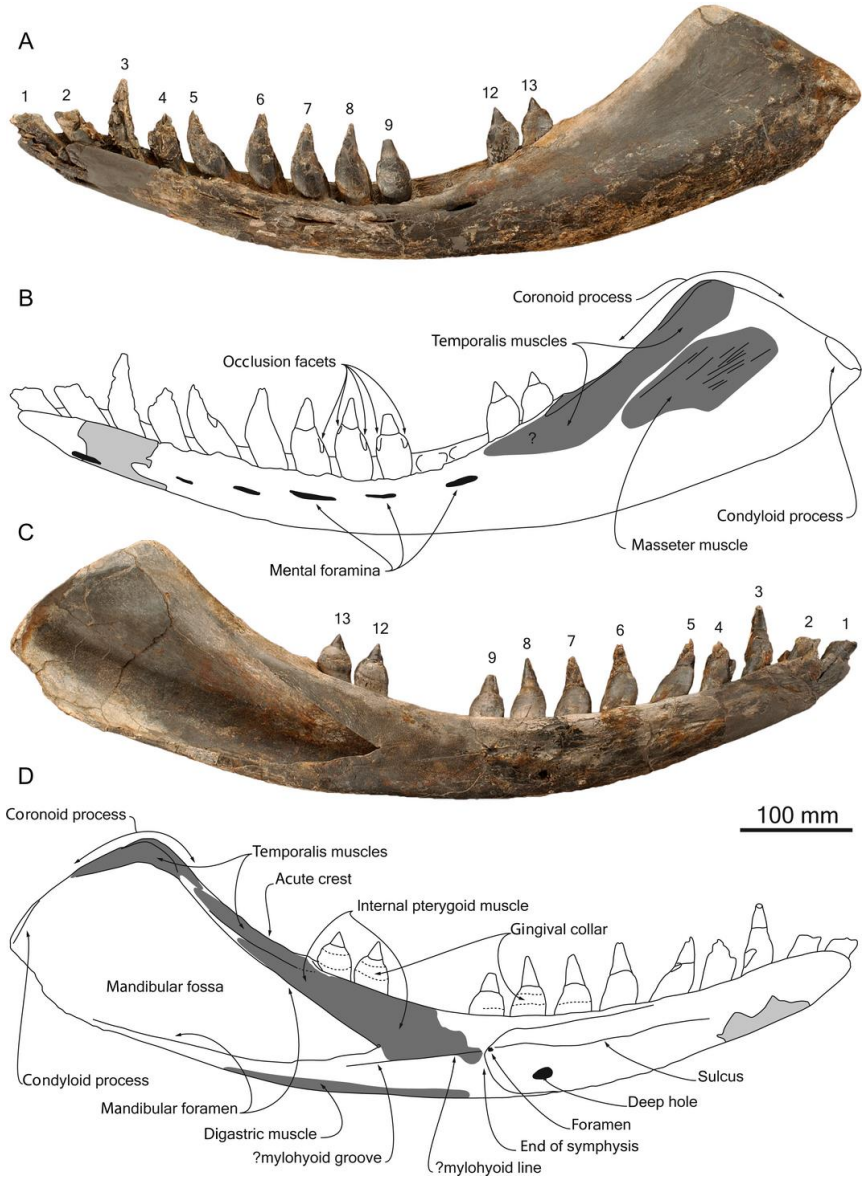

Fig. 15. Left mandible of *Acrophyseter deinodon* MNHN SAS 1626 (holotype), Sud-Sacaco, late Miocene of the Sacaco Basin, Peru. A, lateral view; B, corresponding line drawing; C, medial view; D, corresponding line drawing. Dark shading for reconstructed parts; light shading for proposed muscle insertion areas; stippled lines for incomplete parts and, in D, for gingival collar.

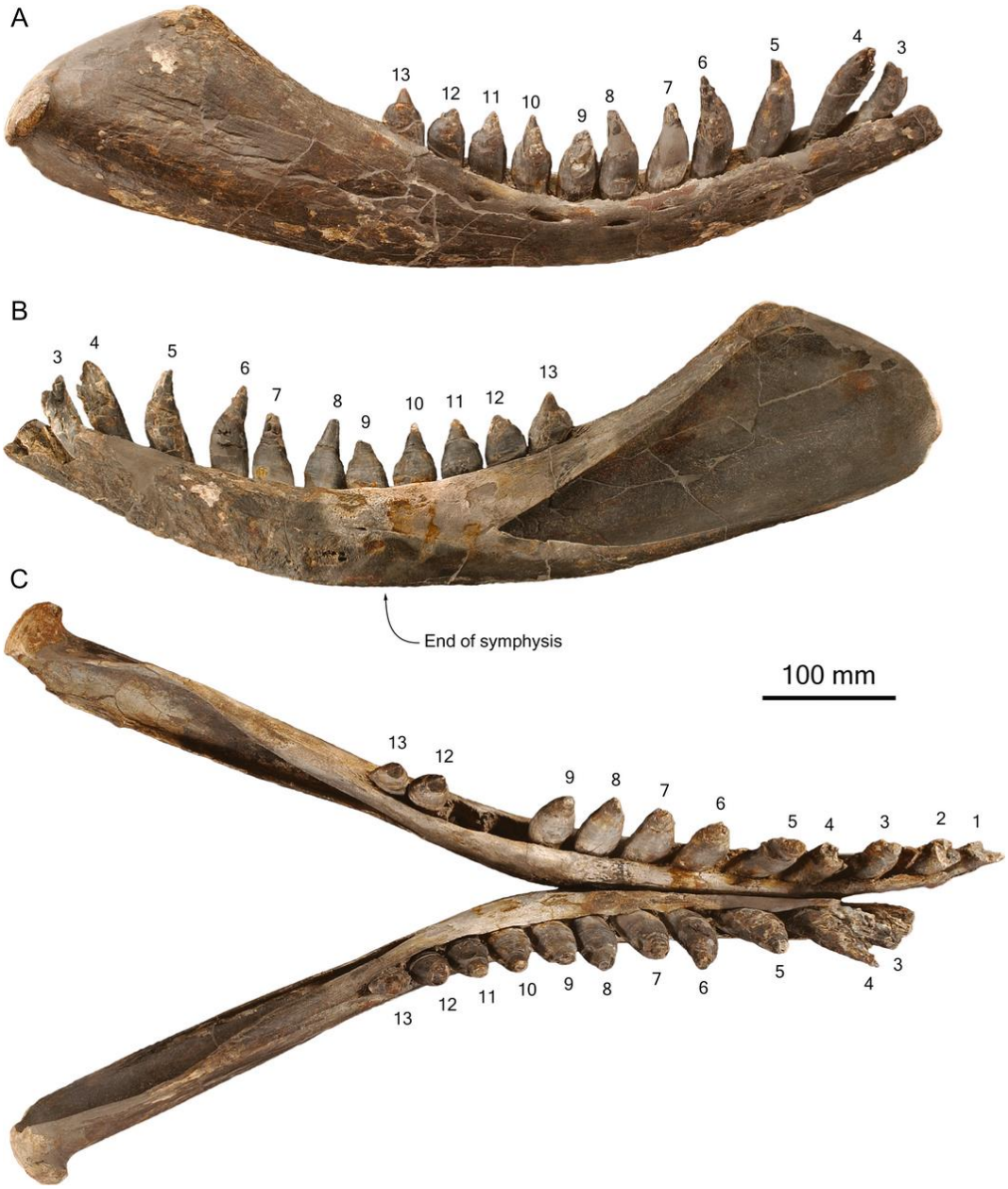

Fig. 16. Mandibles of *Acrophyseter deinodon* MNHN SAS 1626 (holotype), Sud-Sacaco, late Miocene of the Sacaco Basin, Peru. A, lateral view of right mandible; B, medial view; C, both mandibles in dorsal view.

Table 2. Measurements (mm) on the mandibles of Acrophyseter deinodon MNHN SAS 1626 (holotype), A. robustus sp. nov. MUSM 1399 (holotype) and Acrophyseter sp. MUSM 2182

	A. deinodon MNHN SAS 1626	*A. robustus* MUSM 1399	*Acrophyseter* sp. MUSM 2182
Total length (straight line)	760	-	+880
Length of symphyseal portion	355	-	-
Length of tooth row (straight line)	485	-	-
Length of postsymphyseal portion	405	465	e420
Distance from condyle to posterior end of tooth row	278	-	e280
Distance from condyle to anterior end of mandibular fossa	342	315	-
Height of mandible from ventral margin to top of coronoid process	174	+136	+148
Height of mandible at level of last posterior alveolus	115	-	+98
Height of mandible at posterior end of symphysis	73	70	68
Width of mandible at posterior end of symphysis	47	-	-
Height of mandibular condyle	57	67	56
Width of mandibular condyle	50	-	+44

Measurements were taken on the left side. +, Incomplete; e, estimate; –, no data.

Each mandible bears 13 large alveoli (Figs 15, 16). This is two more than in *Livyatan*, one less than in *Zygophyseter*, and distinctly less than in the presumably oldest known physeteroid *Ferecetotherium kelloggi* Mchedlidze, 1970 (up to 30), *Idiorophus* (24), *Physeter* (usually more than 20), and *Physeterula* (about 19) (Lydekker, 1893; Mchedlidze, 1970; Rice, 1989; Bianucci & Landini, 2006; Lambert, 2008; Lambert et al., 2010a). As for the upper tooth count, this lower tooth count corresponds to limited polydonty [only two teeth in excess over the permanent dentition of the *basilosaurid Dorudon atrox* (Andrews, 1906); Uhen, 2004]. The posterior limit of the unfused symphysis is at the level of alveolus 9. The ventral margin of the mandible is strongly and regularly convex, and the dorsal margin (alveolar border) follows this convexity in being strongly concave. This characteristic feature of *Acrophyseter deinodon* gives the mandible a distinctly ventrally bowed morphology, which matches the convexity observed on the ventral border of the rostrum. Also present in *Acrophyseter* sp. MUSM 2182 and the holotype of A.

robustus, this curve is absent in the other recent and fossil physeteroids and probably represents a synapomorphy of *Acrophyseter*. As a consequence of this morphology, even if the distance between the slender angular process and the mandibular condyle is short, the position of the condyle is elevated relative to the ventral-most portion of the mandible. If an artificial horizontal line is drawn from the ventral edge of the condyle to the apex of the mandible, the ventral edge of the condyle is c. 50 mm higher than the alveolar border of the seventh or eighth tooth. The coronoid process is elevated and well developed when compared to that of other physeterids. It is salient dorsally and its anterior and posterior edges form an angle of approximately 110°; in *Physeter* and *Zygophyseter*, the angle is approximately 135° and 130°, respectively. In Acrophyseter sp. MUSM 2182 and *A. robustus*, the coronoid process is distinctly less salient dorsally and more rounded, being regularly and continuously convex. In *A. deinodon*, the elevation and robustness of the coronoid process further emphasize the concavity of the dorsal margin of the bone. The condyloid process (mandibular condyle) is large and slightly convex. Its lateral edge is U-shaped and strongly salient laterally, whereas its medial edge is slightly concave medially. The condyle has its greatest height medially, with a decrease in height toward its lateral rounded edge. Ventral to the condyloid process, the angular process is hardly present, being reduced to a very thin crest slightly protruding ventromedially, which resembles the angular process observed in *'Aulophyseter' rionegrensis*, *Physeter* and *Zygophyseter*.

The mandibular foramen is large and distinctly pointed anteriorly, as seen in young *Physeter* and in *Zygophyseter*. It is long and occupies more than 40% of the total length of the mandible. Its anterior edge is located ventral to the anterior edge of the root of mandibular tooth 12 (penultimate tooth). From this point the edges of the fossa diverge posteriorly, being slightly concave dorsally. The mandibular fossa is bordered dorsally and ventrally by subvertical shelves, whose width decreases posteriorly and which disappear at the level of the coronoid process. The lateral wall of the fossa (pan bone) is transversely concave laterally in its anterior half and in the ventral portion of its posterior half (anteroventral to the condyloid process). This lateral wall is convex or flat in the dorsal portion of its posterior half (area of the coronoid process). Due to the excellent preservation state of the specimen, the thickness of the pan bone could be measured along the mandibular fossa for both mandibles. The thickness varies widely from one point to the other, so the minimum thickness was measured along a transect at one-quarter the length of the mandibular foramen (taken from the anterior tip), one half and three-quarters. The results are: for the right mandible, 3.0, 3.8 and 3.1 mm, respectively, and for the left mandible, 3.7, 3.9 and 3.6, respectively. Minimum thicknesses are generally located at around mid-height of the foramen, except for the second measurement on the left side, at about two-thirds of height. The left mandible is thus slightly thicker at each level. Asymmetry of the pan bone was also noted in an individual of the *basilosaurid*

Basilosaurus isis Andrews, 1904 (Fahlke et al., 2011), but it was expressed differently, with the thinnest region being located more anteriorly on the left mandible. This is not the case here, and more work is required on extant odontocetes (including *Kogia* and *Physeter*) to test the relevance of these observations of *A. deinodon.*

Seven mental foramina pierce the right mandible: the anteriormost is ventral to the alveolus of tooth 3 and extends anteriorly in a deep groove; the second is ventral to the alveolus of tooth 4; the third is ventral to the interalveolar septum that separates the alveoli for teeth 6 and 7; the smaller fourth is ventral to the alveolar border of tooth 7; the fifth is ventral to tooth 8; the sixth (the largest) is ventral to the interalveolar septum between teeth 9 and 10; and the small seventh is ventral to tooth 11 (Fig. 15). Five foramina are preserved on the left mandible: a small foramen ventral to the alveolus of tooth 4, and four larger foramina: ventral to the septum between the alveoli of teeth 6 and 7, ventral to the alveolus of tooth 7, ventral to the septum between the alveoli of teeth 8 and 9, and ventral to the alveolus of tooth 11 (the largest). The alveoli are posteroventrally orientated in the anterior portion of the tooth row, with anterior teeth being strongly procumbent (the preserved root of tooth 1 is almost parallel to the ventral margin of the mandible). Alveoli for teeth 8–12 are roughly vertical and alveolus 13 is anteroventrally directed.

Additional morphological details about the mandibles are provided below in the section about masticatory musculature.

Teeth and tooth wear

Teeth are conical and robust, with a swollen root and a relatively short enamelled crown (Figs 2, 3, 7, 15–17; Table 3). The enamel layer is moderately thick (1.0–1.2 mm as measured in transverse section) and superficially ornamented with shallow longitudinal grooves, on both the lingual and the labial sides of the crown. Roots are deeply embedded in the alveoli, particularly the anterior upper and lower teeth with an elongated, posteriorly projected root. The posterior lower teeth are transversely flattened, a feature more pronounced posterior to the end of the symphysis, with a posterior bulge of the root at the crown–root boundary. In contrast, the flattening of the posterior upper teeth is anteroposterior; it is most likely increased by the development of deep occlusal facets along the distal surface of the crown and root. Anterior upper and lower teeth are more cylindrical. On the maxilla, the median maxillary teeth (from maxillary tooth 2 to maxillary tooth 5) exhibit a strong angulation between the crown and the root, which approaches 120°. Such a marked bending is apparently much less developed in *A. robustus*, but is present in *Acrophyseter* sp. from Cerro los Quesos and *Zygophyseter* (Bianucci & Landini, 2006: fig. 9). The fragmentary maxillary teeth of *Brygmophyseter* and *Livyatan* obscure testing of this character.

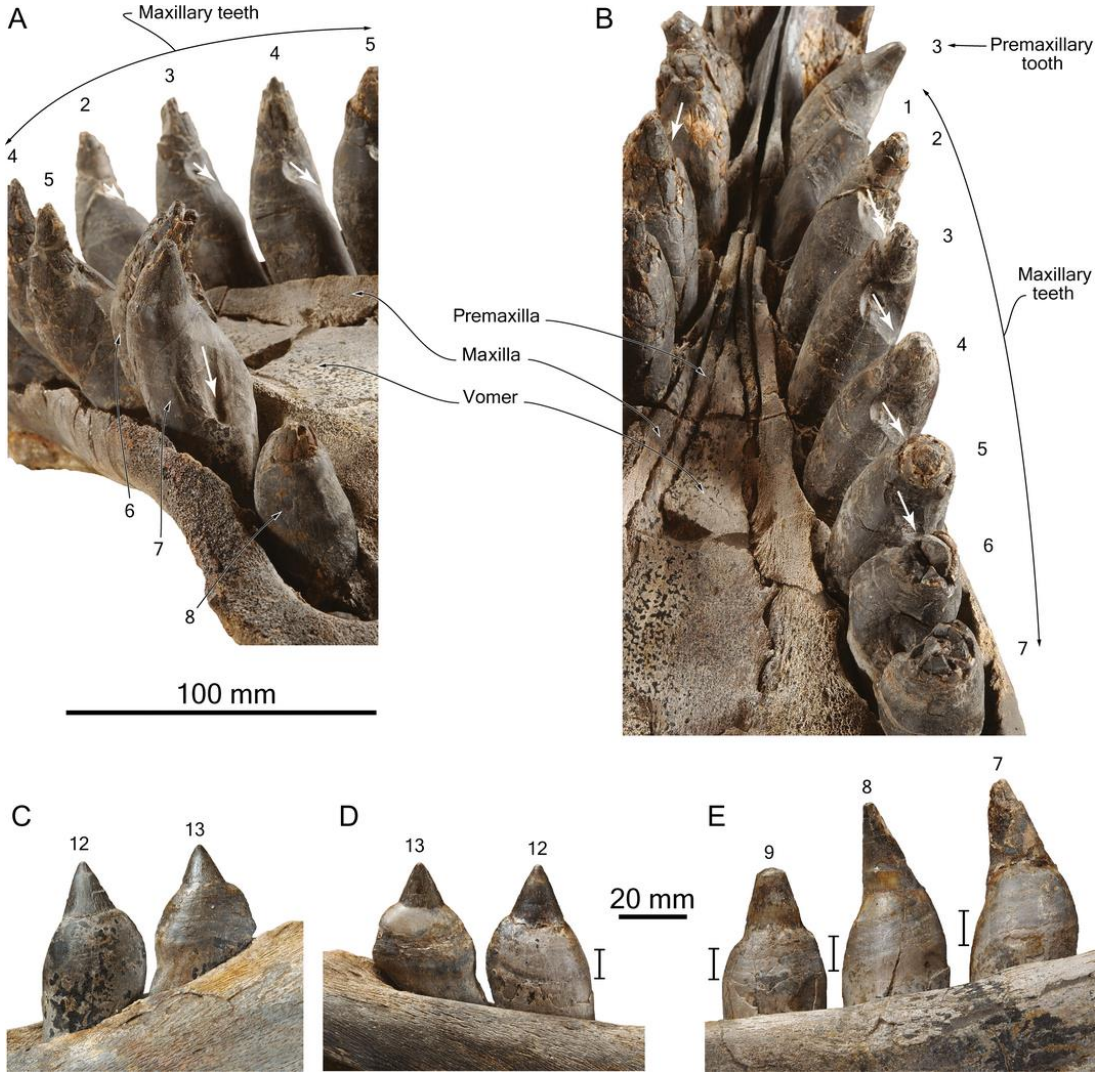

Fig. 17. Teeth of *Acrophyseter deinodon* MNHN SAS 1626 (holotype), Sud-Sacaco, late Miocene of the Sacaco Basin, Peru. A, detail of the rostrum in right posterolateral and slightly ventral view; B, detail of the rostrum in posterodorsal view; C, D, posteriormost teeth from the left mandible in lateral (C) and medial (D) view; E, three posterior teeth from the left mandible in lateral view. White arrows indicate main occlusal facets. Vertical bars indicate the extent of the gingival collar. Scale bar for A, B = 100 mm, for C–E = 20 mm.

Table 3

Measurements (mm) on teeth of Acrophyseter deinodon MNHN SAS 1626 (holotype)

Tooth number	Maximum transverse diameter of root	Maximum mesiodistal diameter of root	Transverse diameter at crown base	Mesiodistal diameter at crown base	Total length
Upper right					
2	23	26	-	-	+90
3	24	28	-	-	-
4	24	26	-	-	-
5	25	26	-	-	-
6	26	27	-	-	-
7	30	27	-	-	-
8	32	27	-	-	-
9	31	27	16	15	-
10	31	27	16	15	+93
11	26	22	13	12	-
Lower left					
3	28	27	-	-	-
4	28	28	-	-	-
5	30	29	-	16	-
6	30	32	-	17	28
7	29	31	17.5	17	30
8	27	31	17.5	17	19
12	21	30	15	16	19
13	18	30	12.5	14	14

+, Incomplete; e, estimate; –, no data.

The best-preserved teeth display limited apical wear; the crowns of the left lower teeth 12 and 13 are nearly complete, with only a small portion of the tip missing (Fig. 17C, D), whereas the right lower tooth 13 and the left upper tooth 3 lack a few millimetres. Crowns of other teeth are too damaged to estimate apical wear. Additional wear is detected at the surface of the crown, as demonstrated by the

reduction of the ornamentation; longitudinal grooves become attenuated from the crown base to the tip. Described in other physeteroid teeth (Hampe, 2006), this wear probably corresponds to repeated contact with food items. Cementum is similarly smooth in the portion of the root just below the crown–root boundary (a feature conspicuous along the buccal surface of the posterior lower teeth), supporting the hypothesis that a part of the root was emergent from the gums, in physeteroids such as *Zygophyseter* (Bianucci & Landini, 2006). Based on the observation of a multi-layered darker region at the surface of the root, an extensive gingival collar is indeed detected on several teeth (Fig. 17); this collar ends before the crown–root boundary.

On many teeth, the mesial and distal surfaces of the root are cut by deep and long occlusal facets (Figs 7, 15, 17). These facets are more developed in teeth from the second third of the tooth row, on both upper and lower dentition. Facets are generally deeper on the distal surface of the roots, with sometimes more than 5 mm of cementum removed. On the anterior upper teeth, these deeper occlusal facets are more bucccodistal whereas they tend to be more distal in posterior upper teeth. On maxillary tooth 6, the deep distal occlusal surface ends in a pit (Fig. 17A); the tip of the crown of the opposing lower tooth progressively entered the thick cementum layer of the root in a way that is unusual for an odontocete. The deep occlusal facets are related to: (1) the short distance between the succeeding teeth along the tooth row and (2) the great thickness of cementum on the roots. The second and not completely independent parameter is most likely linked to ontogeny. In *Physeter macrocephalus*, cementum layers are deposited on the outer surface of the continuously growing tooth (Hohn, 2002). Tooth wear in *A. deinodon* should therefore be considered as a dynamic process in which cementum is continuously deposited all around the root and worn at some specific levels. The resulting occlusion pattern is similar to the pattern in the modern killer whale *Orcinus orca* (Linnaeus, 1758). Small depressions in the maxilla posteromedial to the 2–3 last posterior alveoli are interpreted as embrasure pits, indicating that the posteriormost lower teeth contacted the palate instead of the corresponding upper teeth. A similar condition is observed in basilosaurids (e.g. *Cynthiacetus*, *Dorudon*; Uhen, 2004; our pers. observ.), in *Simocetus* (Fordyce, 2002), in *Orycterocetus crocodilinus* (Kellogg, 1965) and in pomatodelphinine platanistids (Lambert, 2006).

Masticatory musculature of Acrophyseter deinodon

The mandibles and skull of the holotype of *Acrophyseter deinodon* are finely preserved compared to most other fossil physeteroids. Here, we present hypotheses on the masticatory musculature reconstruction of this specimen as a preliminary model for a discussion of the jaw muscles in fossil raptorial physeteroids. For the discussion of jaw muscles, we mostly used the following references: Berzin 1971; fetus of *Physeter macrocephalus*), (Mead & Fordyce 2009; *Tursiops truncatus*

Montagu, 1821), (Murie 1873*; Globicephala melas* (Traill, 1809)), (von Schulte & Smith 1918, fetus of *Kogia breviceps*), (Seagars 1982; delphinids), (Turnbull 1970; terrestrial mammals) and (Uhen 2004; Dorudon atrox).

As a preliminary remark, the insertion areas for jaw muscles in the proposed schematic drawings do not correspond to the exact boundaries. These are the regions that are relatively well defined, by crests or with rough surfaces (grooves and ridges); they correspond therefore to minimum insertion areas. The identification of muscles corresponding to these areas is mostly based on published data on extant physeteroids, delphinids (including *Orcinus orca*, the basilosaurid *Dorudon* and terrestrial mammals, and on direct observations of extant odontocete skulls and mandibles.

Mandibular muscle attachments

On the dorsal edge of the medial surface of the coronoid process of the holotype of *A. deinodon*, a flat triangular to crescentic region is limited ventrally and anteroventrally by the mandibular foramen and anterodorsally by the dorsal crest of the coronoid process. This region is interpreted as the area of insertion for part of the temporalis muscles (deep portion) (Fig. 15C, D). The surface is larger than in the fetus of *Kogia breviceps*. It is more similar to some delphinids, but not as large as in Orcinus orca (see Seagars, 1982: fig. 11). This area extends anteriorly on the anterior crest of the coronoid process. Posteromedial to the alveolar groove in the anterior coronoid region, the surface of the bone makes a narrow, transversely flat, strip facing dorsomedially and laterally defined by a sharp crest. This crest extends from the last mandibular tooth anteriorly for approximately 120 mm and posteriorly vanishes 60 mm anterior to the apex of the coronoid process. The surface of this strip of bone is also rough, with longitudinal grooves and ridges. We interpret this region as an anterior extension of the area of insertion for the temporalis muscle. In delphinids, the limit between pterygoid and temporalis muscles on the dorsomedial portion of the mandible varies from one species to another (Seagars, 1982). This limit is not marked by distinct osteological features, so this area may also correspond to the insertion of the internal pterygoid muscle (pterygoideus internus, see below).

Posteroventral to the long mandibular foramen, the medial surface displays only limited space for the insertion of one of the pterygoid muscles. Furthermore, the bone is thin in that area. Therefore, the insertion of the pterygoid muscles probably differed from the proposed attachment area for the medial (internal) pterygoid muscle in *Dorudon* (Uhen, 2004). The surface of the bone anterodorsal to the mandibular foramen is rougher and is tentatively interpreted as the area of insertion for part of the internal pterygoid muscles, as in delphinids (Seagars, 1982: fig. 11). This region is anteroventrally limited by an oblique groove. We interpret the posterior portion of the groove as the mylohyoid groove, lodging mylohyoid vessels and nerves in several

terrestrial mammals (tentatively identified in *Tursiops*; Mead & Fordyce, 2009). The anterior part, until the mandibular symphysis, may correspond to the mylohyoid line, for the attachment of the mylohyoideus muscle. The mylohyoid line may be absent in *Physeter* (our pers. observ.), possibly in relation to the posterior position of the tongue in the latter (Werth, 2004, 2006). However, this structure is not easy to detect on specimens and a more exhaustive mapping of its presence/absence in other odontocete families would be necessary; it is, for example, not described in *Tursiops* (Mead & Fordyce, 2009). The groove runs anteriorly and slightly dorsally until a foramen at the posterior limit of the mandibular symphysis. From that foramen, a sulcus extends anteriorly towards the apex of the mandible, a feature also observed in *Physeter*; in the basilosaurid *Cynthiacetus*, the sulcus seems less continuous. A subcircular deep hole with smooth margins and a maximum diameter of 13 mm is present on the left symphyseal surface, 55 mm from the posterior end of the symphysis; it may be involved in the attachment of the two mandibles.

A part of the ventromedial region of the mandible, posterior to the symphysis, displays longitudinal ridges. It is interpreted as an area of attachment for the digastric muscle, the main abductor of the mandible. The attachment area probably originally extended on the ventrolateral portion of the mandible, as in delphinids, but the surface of the bone in that area is not as finely preserved.

On the lateral surface of the mandible, where much more space is available for muscle attachment than on the medial surface cut by the large mandibular foramen, deep and wide longitudinal grooves are concentrated in a region between the level of the last alveolus and the condyloid process, and approximately 50 mm ventral to the anterior edge of the coronid process. In *Kogia breviceps* and *Physeter*, this region corresponds to the insertion of masseter muscles (von Schulte & de Smith, 1918; Berzin, 1971), whereas in delphinids, the masseter insertions are located more posteroventrally, on the angular process. We propose that the condition in A. deinodon is more similar to extant physeteroids than to delphinids, with a more central position of the attachment of masseter muscles (Fig. 15A, B; no distinction between superficial and deep portions), as suggested for *Dorudon* (Uhen, 2004) and many terrestrial mammals (Turnbull, 1970). Similar longitudinal grooves are observed in *Physeter*, but they are shallower. In *Cynthiacetus*, this area is smooth, possibly indicating weaker muscle attachment. Interestingly, the larger and more central surface of attachment for the masseter in these physeteroids and this basilosaurid is associated with a jugolacrimal complex that is much more robust in the antorbital region and ventral to the orbit, compared to non-physeteroid odontocetes (see below). More ventrally on the lateral surface of the mandible, the bone is more damaged, precluding identification of other attachment areas. More superficial fibres of the masseter may have inserted there, as in delphinids, *Kogia* and

many terrestrial mammals (von Schulte & de Smith, 1918; Turnbull, 1970; Seagars, 1982).

Similarly to the condition on the medial surface, the area posterolateral to the alveolar groove was probably the region of attachment for another jaw muscle; medially defined by a thin crest making the dorsal edge of the coronoid process, this narrow and slightly transversely concave area may have constituted the insertion region for the internal pterygoid muscle, as observed in several delphinids (Seagars, 1982: fig. 9). However, the anterior portion of this concave area is positioned lateral to the last alveolus. Any muscle leaving from there to the palatine region would be cut by the posterior teeth during closure of the jaws. Therefore, either the pterygoid muscle did not occupy the entire anterior extent of the concave area, or the muscle inserting there was instead either a temporalis muscle, leaving posterodorsally towards the temporal fossa, or part of the masseter, or even the buccinator [as proposed for *Neophocanea phocoenoides* (Cuvier, 1829) by Howell, 1927]. From the apex of the coronoid process to the region lateral to the last posterior teeth, ridges on the surface of the bone suggest a long insertion area for the temporalis muscle, dorsal and anterior to the masseter region. In *Cynthiacetus*, ridges and grooves with a similar posterodorsal direction on the anterior part of the lateral surface of the coronoid process and extending in the area ventrolateral to the last alveoli probably similarly define an area of insertion for the temporalis muscle.

Cranial muscle attachments

The most obvious area for the attachment of jaw muscles on the skull is the temporal fossa. As previously mentioned, the temporal fossa of *A. deinodon* is proportionally much larger than in *Kogia* and *Physeter*, occupying most of the lateral surface of the neurocranium posterior to the postorbital process (Figs 2, 3, 5, 9). A similar condition is observed in *A. robustus* and in Acrophyseter sp. Therefore, a much larger volume of temporalis muscles than described in the two extant physeteroids (see von Schulte & de Smith, 1918; Berzin, 1971) is expected. A voluminous temporal fossa is also present in *Brygmophyseter*, *Livyatan* and *Zygophyseter*, denoting powerful temporalis muscles; in contrast, the smaller temporal fossa of *Aulophyseter morricei* and *Orycterocetus crocodilinus* is an indication of a less developed temporalis musculature, a condition probably related to the relatively more slender teeth. In delphinids, a similar variation of the size of the temporal fossa is observed, with *Orcinus* orca displaying the largest fossa and corresponding volume of temporalis muscles (Seagars, 1982). As detected in *Kogia* (von Schulte & de Smith, 1918), part of the temporalis muscles may have originated from the medial surface of the zygomatic process of the squamosal of *A. deinodon*. The presence of a large zygomatic process in *Livyatan* and *Zygophyseter* may confirm the presence of powerful temporalis muscles in these genera.

The jugolacrimal complex is not preserved in the holotype of *A. deinodon*. However, an extremely robust jugolacrimal complex is preserved on the holotype of *A. robustus* (see below) and we expect that the condition of this complex was similar in the two species. A very robust jugolacrimal complex is also observed in *Livyatan* and *Zygophyseter* (Bianucci & Landini, 2006; Lambert et al., 2010a). We propose that the jugolacrimal complex is an important region of origin for the masseter in several extinct physeteroids, as already demonstrated in extant species, in which the masseter is most likely the main adductor of the mandibles, as compared to the reduced temporalis (von Schulte & de Smith, 1918; Berzin, 1971). Furthermore, the posteriormost part of the upper alveolar groove extends medially from the lateral margin of the rostrum in *Acrophyseter*, *Livyatan* and *Zygophyseter*, clearing a space between the alveolar groove, the lateral margin of the rostrum and the antorbital notch (Fig. 7). This space may correspond to an enlarged area of origin for the masseter muscle.

In delphinids, a large part of the pterygoid muscles (both the internal and the external portions) has an origin on the lateral lamina of the pterygoid and palatine, anterior to the Eustachian notch (Seagars, 1982). The lateral lamina of the pterygoid is absent in physeteroids, with a large sinus occupying this region (at least in *Kogia* and *Physeter*, see Fraser & Purves, 1960: fig. 16, pl. 16). Therefore, the pterygoid muscles attach on the ventral margin of the medial lamina of the pterygoid in *Kogia*, from the posterior tip of the bone, beyond the Eustachian notch, to the palate (von Schulte & de Smith, 1918). Considering the condition in *Kogia* and in many terrestrial mammals (see Turnbull, 1970), the internal pterygoid muscle of *A. deinodon* probably originated from the ventral margin of the pterygoid. As highlighted above, the medial lamina of the pterygoid along the basioccipital basin is indeed robust and anteroposteriorly long in *A. deinodon*. Distinct grooves are observed on the ventrolateral surface of the medial lamina, posterior to the Eustachian notch (Figs 7, 8), suggesting an important area of muscle attachment. In contrast, the shorter and more slender medial lamina of the pterygoid observed in O. crocodilinus suggests a weaker pterygoid muscle than in *A. deinodon*. In addition, a robust ridge with a rough surface runs from the tip of the hamular process of the pterygoid in an anterodorsal and slightly lateral direction. The ridge, also seen in *Kogia* and *O. crocodilinus*, is interpreted as the medial limit of the attachment area for the pterygoid muscle (internal or external). A fossa cuts the ridge a few centimetres anterior to the Eustachian notch, possibly corresponding to the origin of another pterygoid muscle. A somewhat different interpretation is provided for *Dorudon*; Uhen (2004) proposed that the pterygoid muscles originate mostly from the well-developed lateral lamina of the pterygoid and from the palatine more anteriorly. The loss of the lateral lamina in physeteroids may have led to an important change, with the muscles getting attached to the medial lamina. The latter is indeed much more robust in *A. deinodon* than, for example, in the basilosaurid *Cynthiacetus*.

In the delphinid *Tursiops*, the internal pterygoid is the most robust of all the muscles aiding in closing the jaw (Seagars, 1982). Considering the proposed larger area for the origin of the pterygoid muscle in *A. deinodon*, with comparatively stronger bones, an even more powerful muscle can be expected.

Acrophyseter robustus sp.nov.

Acrophyseter sp. Lambert et al., 2014: figs 1, 2

Holotype

MUSM 1399, a skull with both mandibles and teeth in situ, lacking the anterior part of the rostrum and mandibles, the right part of the rostrum base and the right supraorbital region. The atlas, a fragment of the axis and several hyoid bones (basihyal, partial right and left thyrohyals and stylohyals) are still attached to the skull with hardened sediment.

Referred specimen

MNHN PPI 239, a symphyseal fragment of the right mandible, found in Cerro la Bruja by C. Muizon and previously identified as Physteridae indet (Muizon, 1988: fig. 111).

Etymology

From Latin *robustus*, in relation to the thick bone making the margins of the supracranial basin and the rostrum base.

Type locality

Cerro la Bruja, Pisco-Ica desert, 52 km SSE of Ica (Fig. 1A). Geographical coordinates 14°31′27.9″S, 75°40′13.0″W, altitude 380 m. The holotype was discovered and collected by Mario Urbina.

Type horizon

Pisco Formation, Cerro la Bruja level (CLB) as defined by Muizon & DeVries (1985). CLB corresponds to some of the lowest levels of the Pisco Formation, dated to late middle to early late Miocene (c. 13–11 Ma; Muizon & DeVries, 1985; Muizon, 1988). Ar/Ar dating of biotite from a volcanic ash layer approximately 50 m higher than the CLB layers yielded an age of 9.2 Ma (Brand et al., 2011), providing a minimum age for the fossil-bearing layers. Many marine vertebrates were described or mentioned from this locality and level: among odontocetes, the pontoporiid Brachydelphis mazeasiMuizon, 1988, the ‘pithanodelphinine’ *Atocetus iquensis* Muizon, 1988, the ‘kentriodontid’ *Belonodelphis peruanus* Muizon, 1988, and an undetermined ziphiid, but also undetermined mysticetes, an undescribed monachine

phocid, the penguin *Spheniscus muizoni* Göhlich, 2007, sea turtles, crocodiles, and the sharks *Carcharocles megalodon, Cosmopolitodus hastalis* and *Carcharhinus* sp. (Muizon & DeVries, 1985; Muizon, 1988; Göhlich, 2007). In addition, a new inioid and the stem ziphiid *Messapicetus gregarius* Bianucci et al., 2010 were identified from layers somewhat lower than CLB, in a locality about 4 km south of the main Cerro la Bruja locality (Bianucci et al., 2010; Lambert et al., in press).

Diagnosis

Differs from *A. deinodon* in: rostrum not as attenuate in dorsal view and lacking abrupt anterior decrease of height of maxilla in lateral view; absence of left anterior and posterior premaxillary foramina; absence of a lateral groove on the right side of the rostrum; proportionally narrower right infraorbital canal, probably dividing into two foramina, one dorsal in the supracranial basin and one anterior; deep sulcus anterior to the main left dorsal infraorbital foramen; dorsal margin of supracranial basin thick and rounded; dorsal margin of coronoid process of mandible smoothly rounded.

Morphological description of *Acrophyseter robustus* sp. nov. and comparison

Skull

General morphology

The skull of the holotype may have undergone some degree of crushing, transversely and slightly obliquely. Consequently, lack of precision is expected for cranial measurements (Table 1), with minor overestimates for dorsoventral heights and minor underestimates for transverse widths. The measured bizygomatic width (385 mm) is about 17% smaller than in the holotype of *Acrophyseter deinodon*. The anterior portion of the rostrum (and mandibles) is missing. Because the preserved part of the left maxilla only includes seven teeth, either the rostrum of the holotype included at least the same number of teeth (12) as in *Acrophyseter deinodon*, which would thus correspond to a rostrum proportionally longer than in the latter, or the tooth count was lower for a similarly short rostrum. Considering that the ventral and dorsal margins of the rostrum (and mandible) are parallel in the preserved distal region, a proportionally longer rostrum is more likely. We estimate that at least 200 mm of the rostrum is missing anteriorly; total rostral length was thus probably over 530 mm, proportionally longer than in *A. deinodon*. This proposed difference between the two species is further supported by the less pointed outline of the proximal part of the rostrum of *A. robustus* in dorsal view (Figs 18, 19).

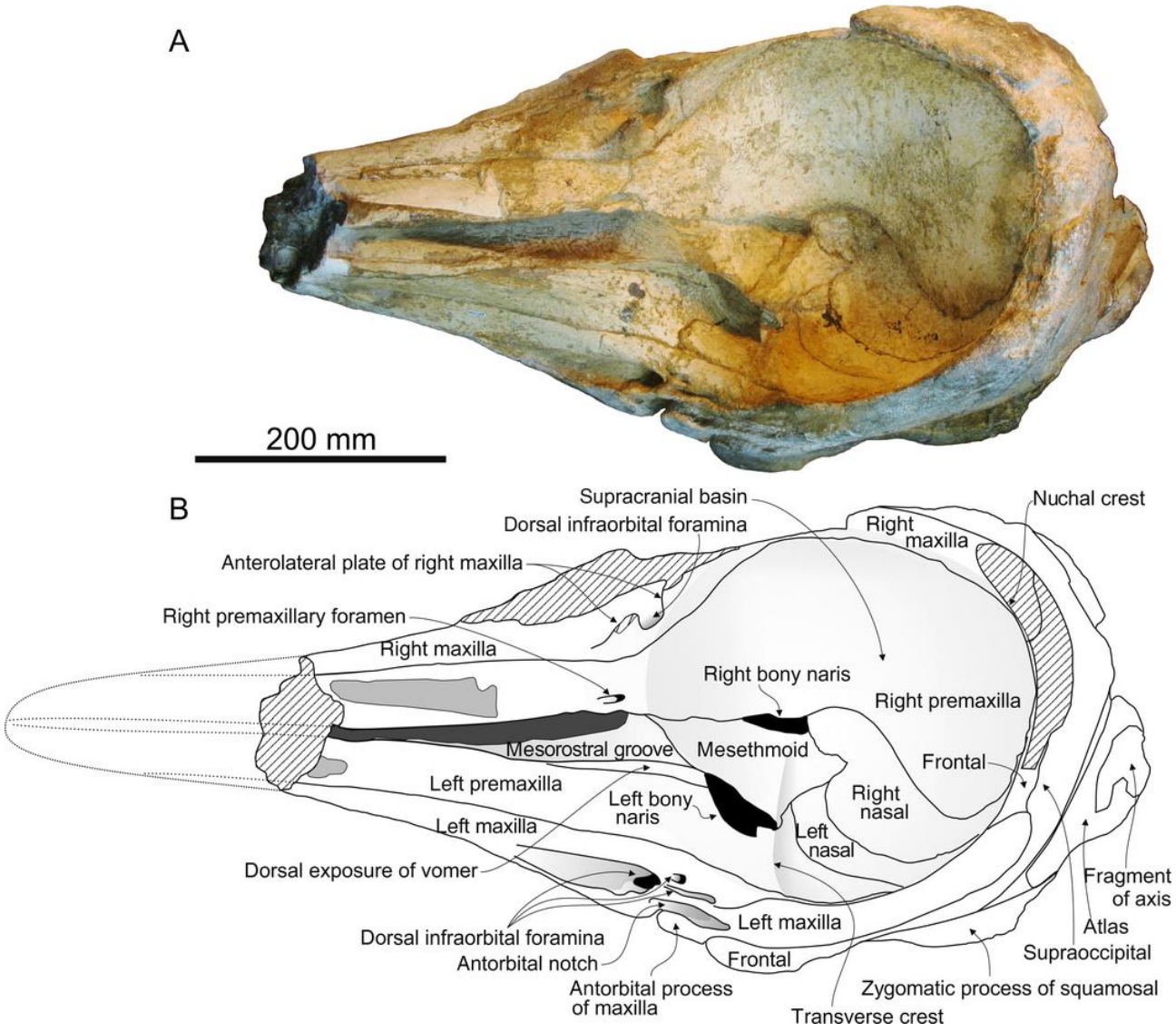

Fig. 18. Skull of *Acrophyseter robustus* sp. nov. MUSM 1399 (holotype), Cerro la Bruja, late middle to early late Miocene of the Pisco Basin, Peru, with articulated mandibles. A, photograph in dorsal and slightly anterior view; B, corresponding line drawing. Light shading for reconstructed parts; hatched surfaces for major break surfaces; stippled lines for the reconstructed anterior part of the rostrum; dark shading for sediment.

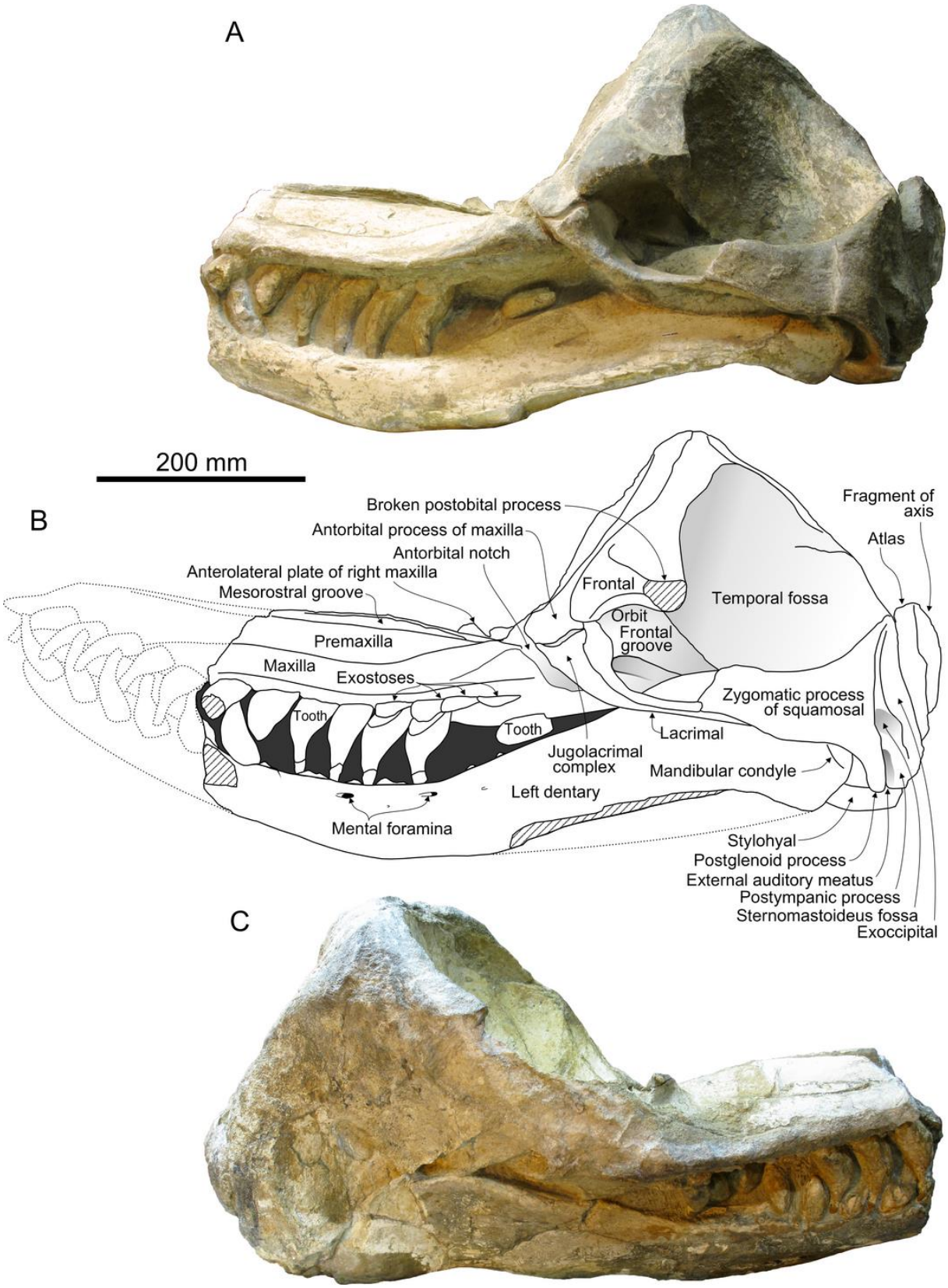

Fig. 19. Skull of *Acrophyseter robustus* sp. nov. MUSM 1399 (holotype), Cerro la Bruja, late middle to early late Miocene of the Pisco Basin, Peru, with articulated mandibles. A, photograph in left lateral view; B, corresponding line drawing; C, photograph in right lateral view. Hatched surfaces for major break surfaces; stippled lines for the reconstructed anterior part of the rostrum and the posteroventral part of the left mandible; dark shading for sediment.

The preserved anterior section of the rostrum is higher than wide (Fig. 20A, B) and the rostrum broadens abruptly towards its base. As in *A. deinodon*, the wide and deep supracranial basin is limited to the neurocranium and is distinctly asymmetrical, extending farther laterally on the right side, with a right lateral boundary more lateral than the corresponding dorsal infraorbital foramen(ina) (Figs 18, 20A, B). The posterior wall of the basin is high, with the upper part (nuchal crest) somewhat overhanging the basin. The right bony naris is significantly smaller than the left (transverse width 46% of width of left naris). As high as long, the vast and mediolaterally deep temporal fossa has a roughly circular outline, with a dorsal border more than twice higher than the orbit roof when compared to the ventral surface of the rostrum. Its posterodorsal margin projects posteriorly beyond the level of the medial region of the supraoccipital shield.

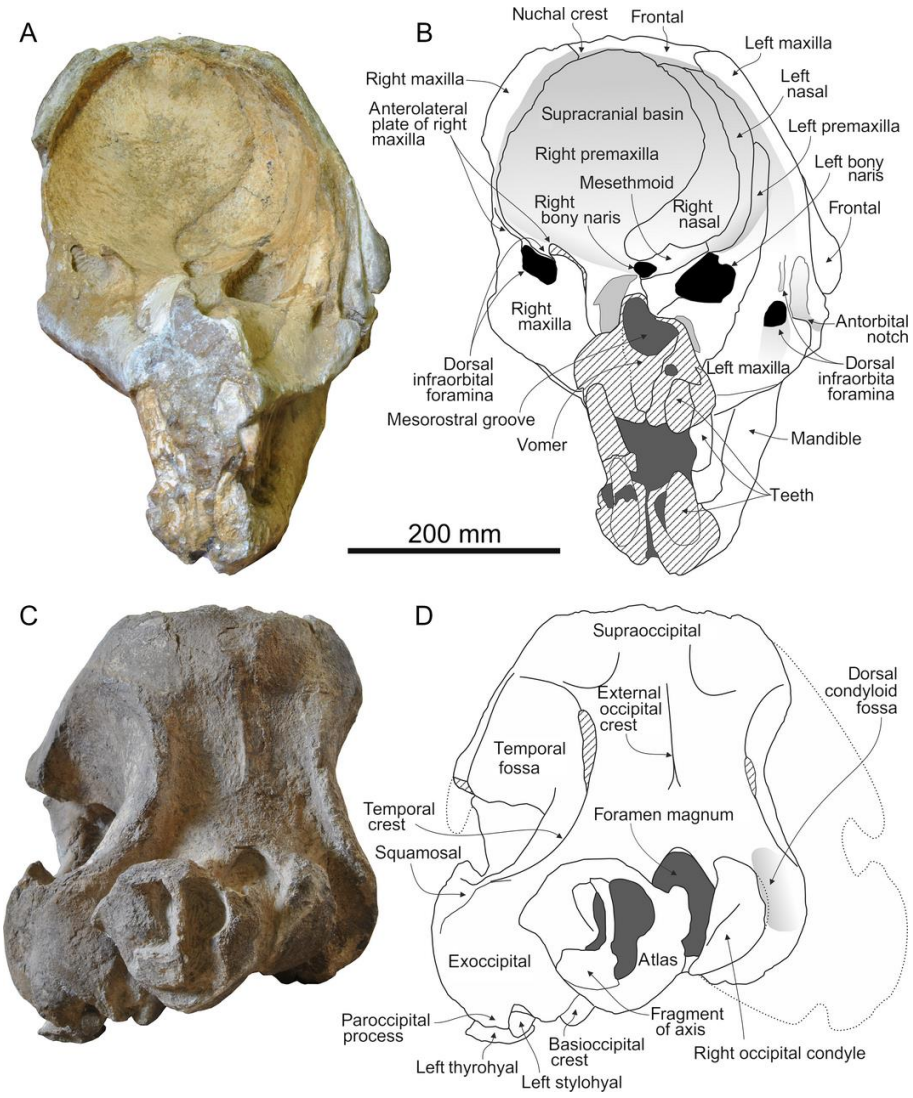

Fig. 20. Skull of *Acrophyseter robustus* sp. nov. MUSM 1399 (holotype), Cerro la Bruja, late middle to early late Miocene of the Pisco Basin, Peru, with articulated mandibles. A, photograph in anterior view; B, corresponding line drawing; C, photograph in posterior view; D, corresponding line drawing. Light shading for reconstructed parts; hatched surfaces for major break surfaces; dark shading for sediment.

Premaxilla

The steep lateral slope of the right premaxilla in the preserved anterior part of the rostrum decreases towards the rostrum base, where the dorsal surface of the premaxilla is horizontal and slightly convex (Figs 18, 20A, B). Anterior to the level of the antorbital notch and close to the mesorostral groove, the right premaxillary foramen is longitudinally elongated in the holotype, with a transverse diameter of 9 mm. The level of the right premaxillary foramen corresponds to the minimum width of the premaxilla. Posteriorly, the lateral margin of the right premaxilla diverges abruptly and is directed posterolaterally along the dorsal infraorbital foramen. The right premaxilla covers more than half the surface of the supracranial basin, reaching the right lateral border and the posterior border of the basin, even crossing the sagittal plane of the skull and extending for some distance on the left side. The last feature is similarly observed in *Acrophyseter* sp. MUSM 2182; it also confirms the interpretation made above for the right premaxilla of *Acrophyseter deinodon*. Along the right bony naris, the medial margin of the right premaxilla rises slightly, before its abrupt ascent towards the nuchal crest.

No left premaxillary foramen is detected on the holotype. Differing from the right premaxilla, the left premaxilla is transversely concave at the rostrum base and descends with a steeper slope towards the corresponding bony naris. Furthermore, the posterolateral divergence of the lateral margin is more moderate than on the right side. Better seen in anterior view, the covering of the left part of the supracranial basin by the left premaxilla is limited to a long and narrow stripe between the left nasal and left maxilla. Posterior to the small left bony naris, the premaxilla sends a medial projection. At this level, a partly worn transverse crest on the premaxilla is continuous with the nasal septum and extends until the lateral edge of the bone. This low crest apparently represents the left anterolateral limit of the supracranial basin; the left bony naris would therefore be oustide the basin.

Maxilla

Linked to the posterior widening of the rostrum, the ventrolateral margin of the maxilla expands posterolaterally, bounding a wide, transversely flat surface with a steep ventrolateral slope (Figs 18–20). Just before the antorbital notch, the lateral margin of the rostrum is highly convex in dorsal view, laterally projected to close the notch anteriorly. This lateral margin is considerably thickened dorsoventrally, making a robust anteromedial wall of the antorbital notch. Whereas the right antorbital notch is not preserved, the left antorbital notch is deep and narrow, opening anterolaterally. The notch extends posteriorly for more than 36 mm, remaining outside the supracranial basin. The left notch is followed posterodorsally by a longitudinal groove on the antorbital process of the maxilla.

A large right dorsal infraorbital foramen is located along the thin oblique plate of maxilla anterolaterally bounding the supracranial basin. This plate being incomplete, it is probable that the broad infraorbital canal was originally divided into two foramina: an anteriorly opening large foramen with a transverse diameter of about 30 mm and located anteroventrolateral to the anterolateral crest of the maxilla (and therefore external to the supracranial basin), and a smaller foramen posteromedial to the crest of the maxilla, and opening inside the supracranial basin. This condition differs from the seemingly derived condition in the holotype of *Acrophyseter deinodon*, with a single and larger dorsal infraorbital foramen located outside the supracranial basin. On the left side of the holotype of *A. robustus*, a large dorsal infraorbital foramen (transverse diameter of 9 mm) opens medial to the antorbital notch, well outside the supracranial basin; its ventral edge extends anteriorly in a wide and deep sulcus, a feature absent in *A. deinodon*. There are two additional left dorsal infraorbital foramina posteriorly: the medialmost foramen is small, whereas the lateralmost foramen is narrow but longitudinally elongated (transverse diameters of 5 and 6 mm, respectively). The left antorbital process of the maxilla is dorsoventrally thick; its ventral contact with the lacrimal/jugal is anteroposteriorly long. In the left supraorbital region, the lateral maxilla–frontal suture draws an angle of about 65° from the horizontal plane. Along the robust posterolateral border of the supracranial basin, the maxilla is thick, more than in *A. deinodon*; such a robust region may correspond to the origin of a powerful maxillonasolabialis muscle (inserting on the hypertrophied soft tissue nasal complex in the extant *Physeter macrocephalus*; see Huggenberger, André & Oelschläger, 2016). On the posterior wall of the basin, left and right maxillae do not contact.

In ventral view, the transverse diameter of alveoli for the maxillary teeth ranges from 30 to 36 mm (Figs 19, 21). At least some of the alveoli are proportionally shallow (18 mm depth for the alveolus corresponding to right tooth 9). The maxilla displays thick bony pads around several posterior alveoli: on the left side, anterolateral to each of the last three alveoli and posterolateral to the last alveolus; on the right side, anterolateral to each of the six last alveoli and lateral to the last alveolus (Figs 19, 21). The dorsoventral thickness and the anteroposterior length of the exostoses decrease distinctly anteriorly. Based on a comparison with human oral exostoses and on a lever arm analysis, these exostoses are interpreted as maxillary buccal exostoses, hypothesized to have developed during powerful bites (Lambert et al., 2014). In a posterior direction, the alveolar row diverges medially from the lateral margin of the maxilla, leaving a wide space between the last alveolus and the antorbital notch (distance from alveolus 12 to lateral margin of maxilla 35 mm).

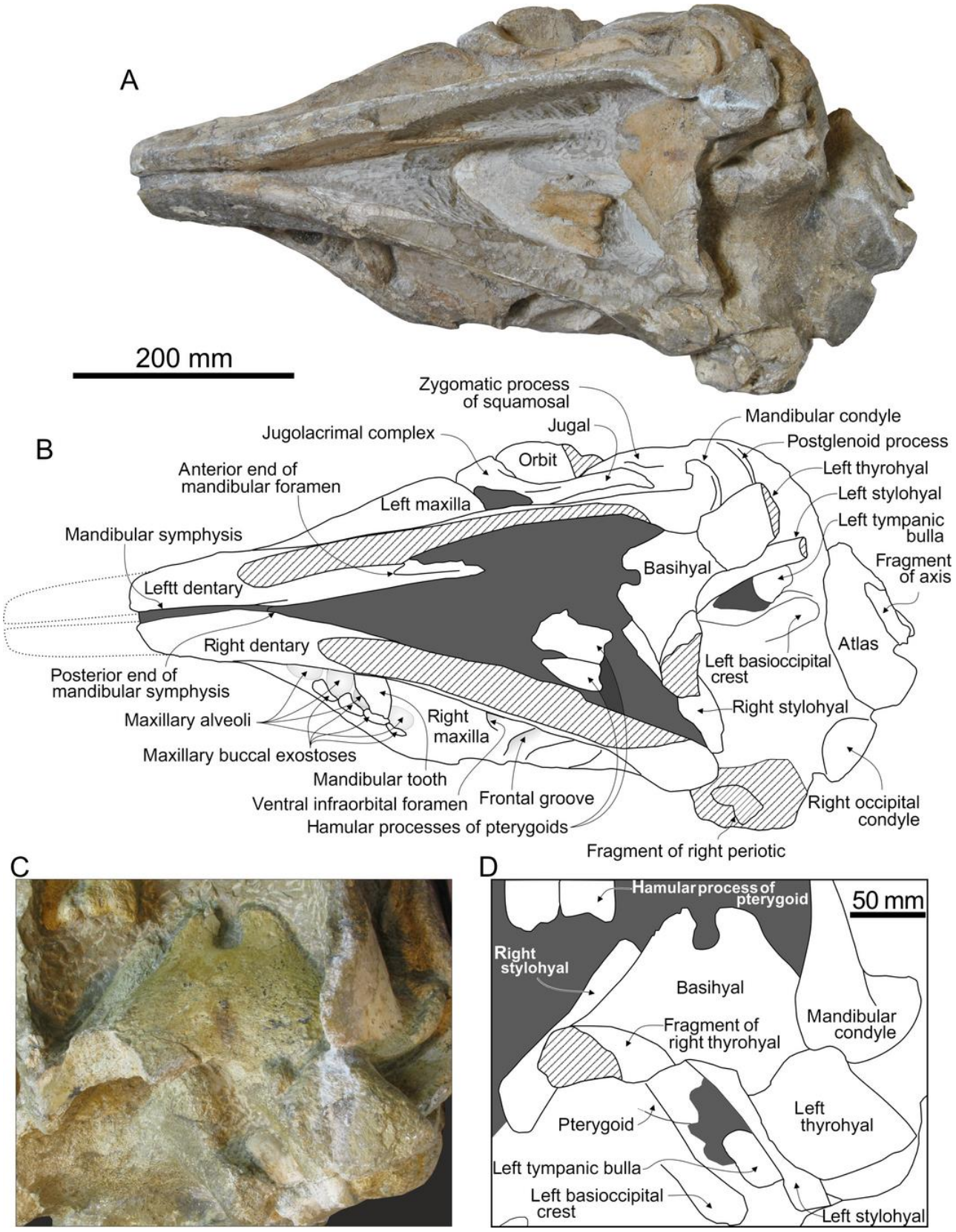

Fig. 21. Skull of *Acrophyseter robustus* sp. nov. MUSM 1399 (holotype), Cerro la Bruja, late middle to early late Miocene of the Pisco Basin, Peru, with articulated mandibles. A, photograph in ventral view; B, corresponding line drawing; C, photograph of the hyoid bones in the basicranial region, in ventral view; D, corresponding line drawing. Hatched surfaces for major break surfaces; stippled lines for the reconstructed anterior part of the rostrum; dark shading for sediment.

Vomer–mesethmoid

The vomer constitutes the lateral walls of the mesorostral groove. On the left side, the dorsal exposure of the vomer broadens towards the left bony naris, forming an elongated triangular surface similarly observed in *A. deinodon*. On the transverse anterior section of the rostrum of the holotype, the vomer is thick below the mesorostral groove.

The mesethmoid is ossified from a level 40–45 mm anterior to the antorbital notch. The nasal septum overhangs the large left bony naris; the right wall of the septum is nearly horizontal, sloping slightly posterolaterally towards the posterior margin of the left bony naris.

Nasal

In the supracranial basin, a long and thin sheet of bone starting from the mesethmoid, rising posterodorsally along the medial wall of the right premaxilla, and nearly reaching the top of the nuchal crest, is interpreted as the right nasal (Figs 18, 20A, B). This bone is partly overlapped by the right premaxilla, whereas it overlaps another elongated sheet of bone interpreted as the left nasal. The latter similarly leaves from the mesethmoid towards the posterolateral wall of the supracranial basin; it slightly overlaps the left premaxilla and maxilla. The identification of these two bones as nasals (instead of frontals or even maxillae) is based on several arguments: (1) the frontals are roughly symmetrical in the supracranial basin of *Physeter* (our pers. observ. on the disarticulated fetal skull USNM 487416); (2) even if much flattened, the two bones on the holotype of *A. robustus* display the contacts with the mesethmoid, premaxillae and frontals typical for the nasals of odontocetes; (3) the right and left bones have a roughly similar outline, despite the right being wider; (4) the medial suture between the two bones starts from the mesethmoid and extends towards the sagittal plane on the nuchal crest; and (5) in *Physeter*, one of the nasals is identified in the same position, but is proportionally smaller (Flower, 1867). The outline of such thin plates of bone is undoubtedly difficult to detect on fossil specimens; it is not surprising that the nasal region could be interperted in only a few other fossil physeteroids: in *Orycterocetus crocodilinus* and *Zygophyseter*, with only one nasal retained, and in the kogiids *Aprixokogia*, *Nanokogia*, *Praekogia* and *Scaphokogia*, which lack any nasal, as in the extant *Kogia* (Kellogg, 1965; Barnes, 1973; Muizon, 1988; Bianucci & Landini, 2006; Whitmore & Kaltenbach, 2008; Vélez-Juarbe et al., 2015). *Acrophyseter robustus* is therefore the first physeteroid in which the plesiomorphic retention of two nasals is unambiguously recorded (although a similar condition is probably present in *A. deinodon*).

Frontal

In the supracranial basin, the frontals are only seen as a narrow strip on the posterior wall, between the supraoccipital posteriorly, the maxillae laterally, and the nasals and right premaxilla anteriorly. The left premaxilla does not contact the corresponding frontal.

The robust preorbital process of the frontal has a blunt anterior end, far posterior to the anterior end of the antorbital process of the maxilla and probably was not in contact with the lacrimal/jugal. In lateral view, the dorsoventral thickness of the bone increases above the orbit, with a concave lateral surface in its posterior part (Fig. 19). The postorbital process is incomplete on the holotype.

In ventral view, the frontal groove is oblique and posteromedially long (Fig. 21A, B). The posterolateral margin of the groove is a sharp crest corresponding to the anteroventral wall of the temporal fossa.

Supraoccipital

The depressed medial portion of the supraoccipital shield bears a low external occipital crest (Fig. 20C, D). The slope of the shield is 55–60° to the horizontal on the holotype, in which the thick nuchal crest may be incomplete dorsomedially. The dorsal margin of the foramen magnum is deeply concave and nearly V-shaped.

Jugal/lacrimal

The jugolacrimal complex comprises most of the lateral and posterior walls of the antorbital notch, with a contribution of the maxilla to the upper part of the notch (Figs 19, 21A, B). The portion of the complex contacting the antorbital process of the maxilla is robust. On the zygomatic arch, the jugal becomes progressively dorsoventrally thinner, but retains a greater transverse width. At the level of the tip of the zygomatic process of the squamosal, the jugal of the holotype is 16 mm wide. The contact between the jugal and the ventral surface of the zygomatic process of the squamosal is long (84 mm). Such an elongated contact is similarly observed in *Zygophyseter* and, to a greater extent, in basilosaurids (Uhen, 2004; Bianucci & Landini, 2006; Martínez-Cáceres & Muizon, 2011); although the jugal is only rarely finely preserved in fossil skulls, this condition may represent the archaic condition for odontocetes. The jugal–squamosal contact is proportionally somewhat shorter in *Physeter* and is absent in *Kogia*.

Pterygoid

The robust hamular process is roughly rectangular in ventral view (Fig. 21A, B). The maximum width of the left process is 32 mm; only a slight posterolateral projection of the process is observed. As in *A. deinodon*, the medial lamina of the pterygoid is

long along the basioccipital basin. Its posterior portion is robust, with a transverse section that is more rounded than in the latter.

Squamosal

The zygomatic process of the squamosal is anteriorly long (Table 1) and dorsoventrally thick. In lateral view, the anterior apex is nearly rectangular (Fig. 19). Most of the dorsal margin of the process is concave, with a marked posterodorsal elevation towards the posterior boundary of the temporal fossa typical for physeteroids. The ventral margin of the process is transversely thick anteriorly, while thinning posteriorly. A ventral swelling is developed at the posterior end of the contact with the jugal. Posterior to the zygomatic process, the surface of the squamosal is excavated by two posterolaterally facing sternomastoideus (or sternocephalicus, pars mastoideus, see Evans & de Lahunta, 2013) fossae. The postglenoid process is an anteroposteriorly flattened and transversely wide blade that is ventrally longer than the posttympanic process and the exoccipital (Figs 19, 21A, B). The mediolaterally wide mandibular fossa is orientated anteroventrally; its surface is transversely flat. The tympanosquamosal recess is mostly marked posteromedial to the mandibular fossa, extending on the medial surface of the postglenoid process. Medial to the recess, as in *A. deinodon*, a deep and rectilinear narrow groove leaves anterolaterally from the region of the spiny process towards the medial wall of the zygomatic process, exiting into the temporal fossa.

Alisphenoid

The path for mandibular nerve V3, leaving laterally, is a shallow but distinct groove.

Basioccipital

The thick and low basioccipital crests strongly diverge posteriorly and delimit a short and wide basioccipital basin (Fig. 21).

Exoccipital

In posterior view, the outline of the robust occipital condyles is rounded (Fig. 20C, D). The posterior (articular) surface of the condyles is roughly perpendicular to the longitudinal axis of the rostrum, contrasting with the condition in *Physeter* and kogiids, where the rostrum is anteroventrally projected when the articular surface of the condyles is set vertically. The condylar neck is poorly developed, but a dorsal condyloid fossa is present. Differing little from the holotype of *A. deinodon*, the paroccipital process of the exoccipital nearly contacts the posterolateral surface of the basioccipital crest. A vestigial medial crest of the exoccipital is present in the nearly closed jugular notch, as in *A. deinodon*.

Tympanoperiotic

Tympanic bulla

Slightly longer (Table 1) than in the holotype of *A. deinodon*, the in situ tympanic of the holotype of A. robustus lacks a clear median furrow (Fig. 21). The outer posterior prominence is rounded and well defined. The anterior margin is roughly straight, differing from *A. deinodon*. The posterior process of the tympanic is a massive rod directed posterolateroventrally. It widens and thickens distally, making a swollen region between the postmeatal crest of the squamosal and the exoccipital. The maximum extent of the swollen part of the bone is 30–40 mm wide and 40–50 mm high in posterolateral view on the holotype. However, in this area, the surface of the spongy bone is crossed with irregular grooves and ridges; therefore, the sutures with the exoccipital and squamosal are difficult to define. The general morphology of the posterior process roughly matches the condition in *Physeter*, differing from *Kogia* in which the process lies in a deep and angular notch.

Periotic

The right periotic of the holotype is only partly visible in situ (Fig. 21A, B). The bone is robust with a strong anterior process and a prominent lateral tuberosity. The partly preserved accessory ossicle is roughly spherical. The diameter of the fenestra ovalis is 4.5 mm.

Mandibles

As in *Acrophyseter deinodon*, the symphysis is not ankylosed. In terms of robustness, no significant difference is detected between the two species. The exact lower tooth count is unknown in *A. robustus*. Posterior to the alveolar groove, the dorsal margin rises towards the moderately elevated coronoid process, which is slightly transversely swollen (Fig. 19). The outline of the process in lateral view is regularly curved, lacking the marked angle seen in *A. deinodon* (Fig. 28). The robust mandibular condyle is located close to the ventral margin of the bone; its lateral and dorsolateral margins are convex. The mandibular foramen is somewhat shorter than in the holotype of *A. deinodon*, with a more rounded anterior end.

The isolated fragment of the right mandible MNHN PPI 239, from the same locality as the holotype, roughly matches the latter in the dorsoventral height of the symphyseal portion and for the diameter of the alveoli (around 35 mm; Muizon, 1988).

Teeth

As in *Acrophyseter deinodon*, teeth are large compared to the size of the jaws (Table 4). None of the preserved teeth displays a curvature as marked as in maxillary teeth 2

and 3 of *A. deinodon*. The short crown is conical; the diameter at the base reaches 16 mm and the length of the best-preserved crowns reaches 22 mm. The crown is covered with a distinct layer of enamel; it is ornamented with longitudinal ridges, less marked apically. The large root is proportionally slender at the contact with the crown (Fig. 19), and this may be related to wear of the part of the root outside the gum. From this area, the diameter of the root increases markedly, with a maximum diameter usually before mid-length, ranging from 29 to 34 mm. This thickest area is followed proximally by a progressive narrowing. The root of the upper posterior teeth is anteroposteriorly flattened in the holotype, which is at least partly due to the contact with the opposite tooth, as in *A. deinodon*. Indeed, deep and long occlusal facets occur in several teeth. The surface of the root of some teeth (e.g. upper right tooth 11 and upper left tooth 12) is fluted.

Table 4. Measurements (mm) on teeth of Acrophyseter robustus sp. nov. MUSM 1399 (holotype)

Tooth number	Maximum transverse diameter of root	Maximum mesiodistal diameter of root	Mesiodistal diameter at crown base	Crown length
Upper left				
6	-	31	-	-
7	-	31	-	-
8	-	33	+12	+16
9	-	31	+13	+22
10	-	34	16	+18
11	-	29	-	-
12	21	28	-	-
Upper right				
6	-	32	-	-
7	-	34	-	-
8	-	31	-	-
12	-	30	15	+22

+, Incomplete; e, estimate; –, no data. Exact tooth count being unknown in MUSM 1399, a tooth count similar to A. deinodon (12 teeth per upper quadrant and 13 per lower quadrant) is hypothesized, starting numbering with hypothetical first premaxillary tooth or anteriormost mandibular tooth.

Atlas

Partly preserved in the holotype (Figs 18–21), the atlas bears a pointed and prominent transverse process, contrasting with the straight lateral margin of the atlas of *Physeter* in posterior view, and being more similar to *Zygophyseter*. From the base of the process, the ventral margin is regularly convex.

Axis

A fragment of the axis is preserved posterior to the atlas. It is shifted to the left compared to the latter, indicating the lack of ankylosis between the two vertebrae (contrasting with Kogia, for which all the cervicals are fused).

Hyoids

The roughly complete basihyal of the holotype (Fig. 21C, D) has a maximum breadth of 120 mm and a medial length (from bottom of anterior notch to posterior margin) of 67 mm. This bone is more triangular than in *Brygmophyseter* (Hirota & Barnes, 1995), with a longer anterolateral margin. This outline is more similar to *Kogia*, but a narrow, 35-mm-deep notch marks the anterior margin of the bone in *Acrophyseter robustus*, separating two long articular processes. This feature is absent or barely developed in both *Kogia* and *Physeter*; in the former, the anterior articular processes are elements separated from the basihyal (Flower, 1867; Reidenberg & Laitman, 1994; our pers. observ.). The deep notch is present in *Brygmophyseter*, and, to a lesser extent, in several other odontocetes (e.g. *Ziphius cavirostris*; Heyning & Mead, 1996). Along the anterior notch, the left articular process is wider than the right; asymmetry is also noted at this level in other odontocetes (Reidenberg & Laitman, 1994; our pers. observ.). The posterior margin of the basihyal is more concave than in *Kogia* and *Physeter*. The preserved portions of the right and left thyrohyals indicate that these bones were massive in their proximal part, with a long and probably ankylosed contact with the basihyal. The maximum proximal width of the left thyrohyal is at least 56 mm. The exposed surface of the right stylohyal, originally more than 166 mm long, does not differ significantly from *Brygmophyseter*.

Acrophyseter sp.

Specimen

MUSM 2182, a skull with both mandibles and teeth. The whole dorsal part of the supracranial basin, as well as the right supraorbital region, is worn away. The medial surface of the right mandible is closely appressed to the basioccipital basin and right orbital region, whereas the medial surface of the left mandible crosses the ventral surface of the rostrum at about mid-length, in an oblique direction. Five or six teeth or tooth fragments are in situ in the right upper tooth row, three in the left upper tooth

row, and four or five in the left mandible. Twelve teeth of the same specimen were found detached around the skull and mandibles.

Locality

Cerro los Quesos, 50 km south of Ica, at the top of the main hill (Fig. 1A). Geographical coordinates: 14°30′52.8″S, 75°43′05.8″W, altitude 696 m. The specimen was discovered by Mario Urbina in 2008 and collected in November 2010. The locality of Cerro los Quesos yielded other marine vertebrate remains: the ziphiid *Nazcacetus urbinai* Lambert et al., 2009, a phocoenid tentatively referred to *Lomacetus ginsburgi* Muizon, 1988, a kogiid displaying affinities with *Scaphokogia cochlearis* Muizon, 1988, several mysticetes including a small cetotheriid sharing similarities with *Piscobalaena nana*, and at least two large balaenopteroids, phocids, and the sharks *Carcharocles megalodon* and *Cosmopolitodus hastalis* (Lambert et al., 2009; Bianucci et al., in press; our pers. observ.).

Horizon

The specimen was discovered in the upper layers of the Pisco Formation outcropping in Cerro los Quesos, namely in Member F of the local section (Di Celma et al., in press; Bianucci et al., in press; Fig. 22). 40Ar/39Ar dating of the biotite from ash layers under (lower portion of Member F) and above the level of the specimen gave absolute ages of 6.9 and 6.7 Ma, respectively; this Messinian (latest Miocene) interval is confirmed biostratigraphically with diatoms providing an interval of 7.3–7.1 Ma for the base of Member F (Di Celma et al., in press; Fig. 22). The beds having yielded MUSM 2182 were tentatively correlated to the AGL level as defined by Muizon & DeVries (1985) and Muizon (1988) in Aguada de Lomas, Sacaco area on the basis of the possible occurrence of the phocoenid *Lomacetus ginsburgi* and a kogiid sharing similarities with Scaphokogia cochlearis (Bianucci et al., in press). This correlation is compatible with the age estimates (c. 7.5–7.0 Ma) provided by Muizon (1988) for the AGL level.

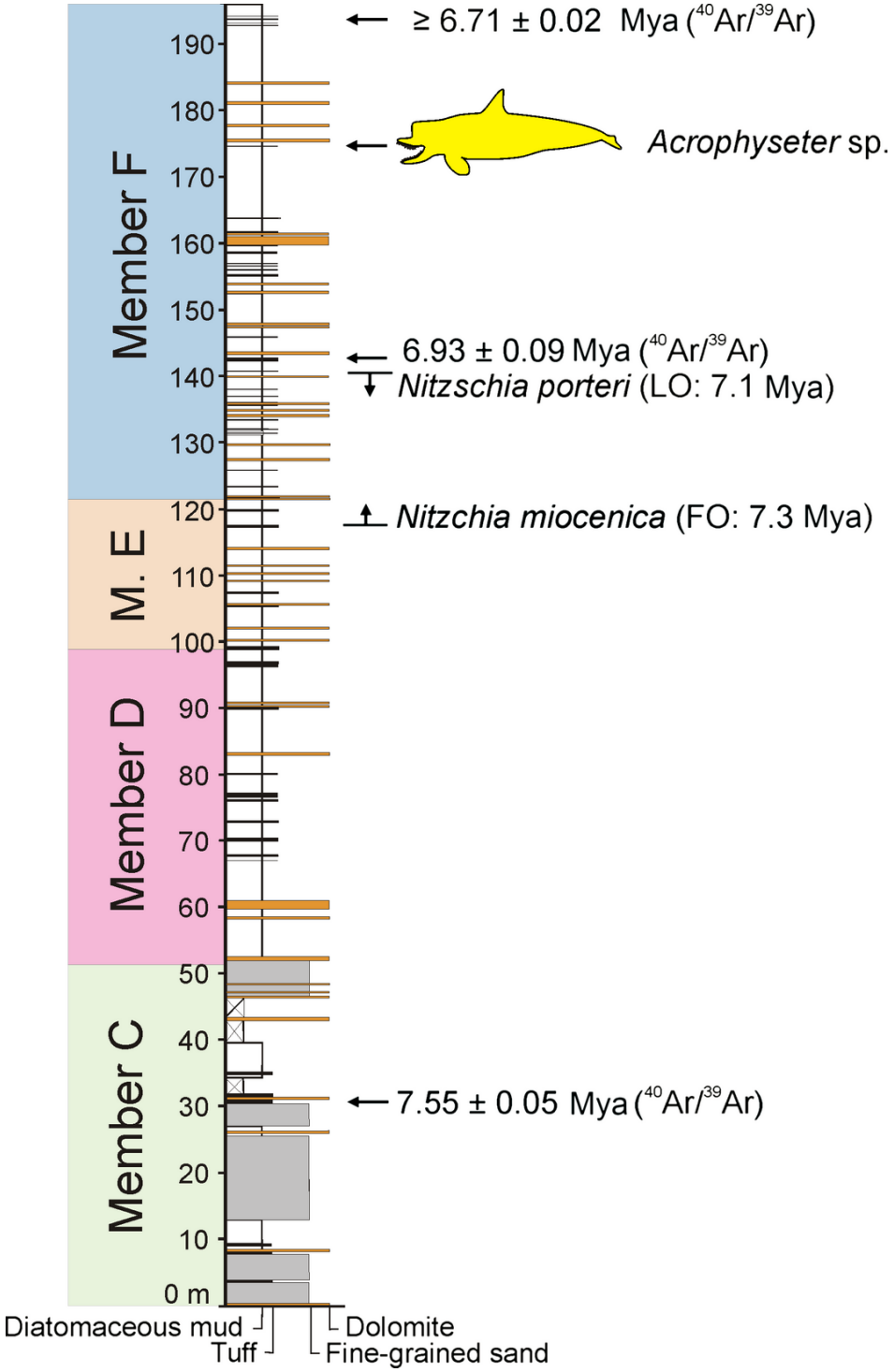

Fig. 22. Stratigraphic column of late Miocene deposits of the Pisco Formation in the locality of Cerro los Quesos, indicating the stratigraphic level where the specimen *Acrophyseter* sp. MUSM 2182 originates from together with ash layers from which radiometric dates were obtained. A few tens of metres below the *Acrophyseter* level the co-occurence of the diatoms *Nitzschia porteri* and *Nitzschia miocenica* indicates an interval ranging from 7.3 to 7.1 Ma (Barron, 2003). Modified from Bianucci et al. (in press: fig. 5).

Morphological description of *Acrophyster* sp. MUSM 2182 and comparison with *A. deinodon* and *A. robustus* sp. nov.

Contrasting with the holotypes of *Acrophyseter deinodon* and *A. robustus*, the apex of the rostrum of MUSM 2182 is preserved. The rostrum constitutes about 60% of the condylobasal length (Table 1; Figs 23, 25, 26), with a tooth count of 12 for each upper tooth row. Considering that the upper tooth count is the same as in *Acrophyseter deinodon* and that the teeth have roughly similar dimensions, the proportionally longer rostrum of MUSM 2182 implies longer interalveolar septa. The bizygomatic width is intermediate between the larger holotype of *A. deinodon* and the smaller holotype of *A. robustus*.

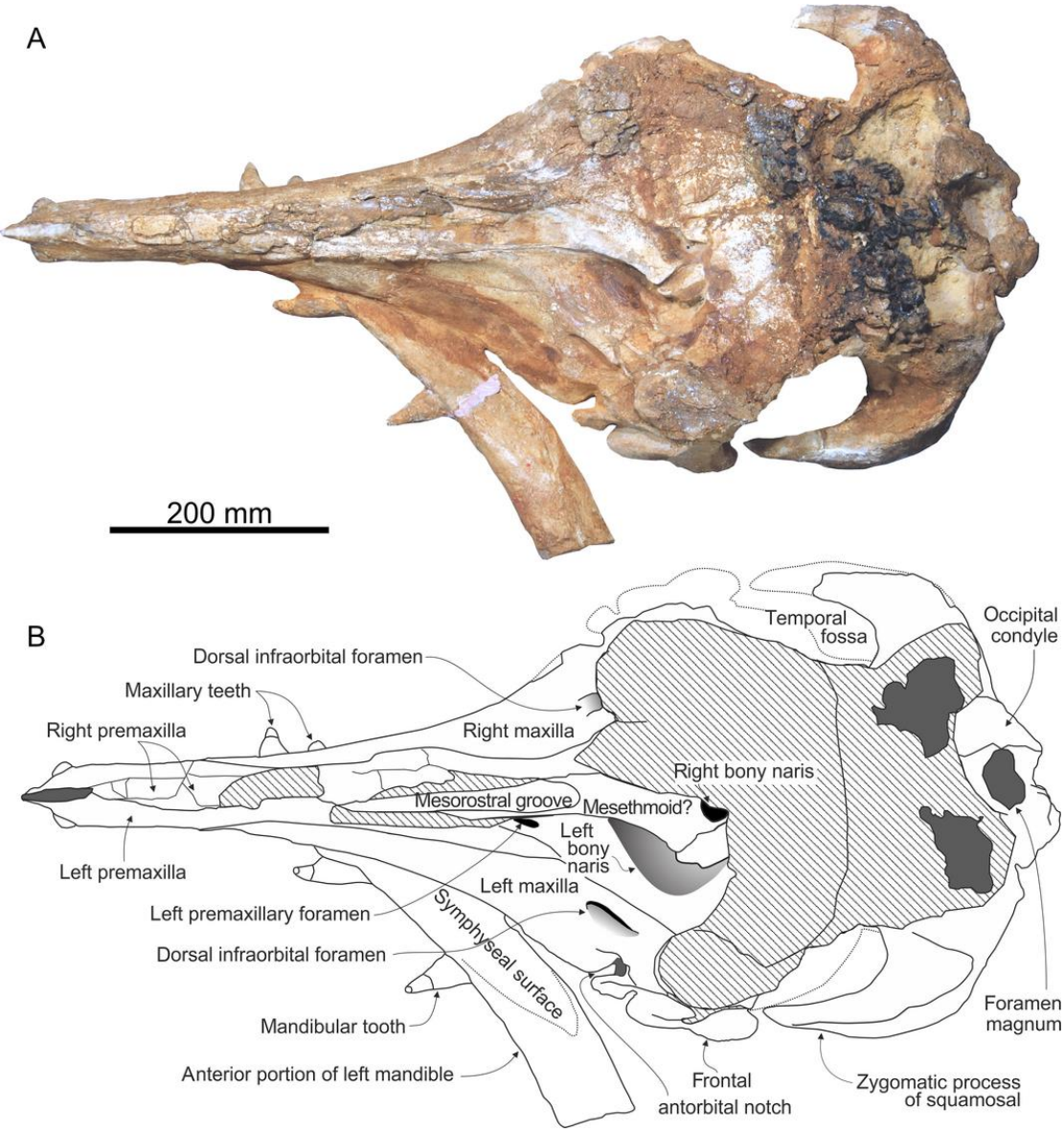

Fig. 23. Skull of Acrophyseter sp. MUSM 2182, Cerro los Quesos, late Miocene of the Pisco Basin, Peru. A, photograph in dorsal view, with anterior portion of left mandible in medial view; B, corresponding line drawing. Hatched surfaces for major break surfaces; dark shading for sediment.

Premaxilla

Anterior to the first alveolus, each premaxilla sends an anteromedial finger-like projection bounding the narrow apex of the mesorostral groove (Figs 23, 25, 26). The premaxilla–maxilla suture can be detected on the lateral surface of the rostrum, descending anteroventrally between alveoli for teeth 3 and 4. Three teeth were therefore present in each premaxilla. On most of the anterior part of the rostrum, the premaxillae of MUSM 2182 are crushed in the mesorostral groove. Taking into account the medial overlap of both premaxillae, they originally had raised walls along the groove, differing on that point from the low walls and widely open mesorostral groove in *A. deinodon*. No right premaxillary foramen could be detected in MUSM 2182, possibly due to damage on the bone. Differing from the holotype of A. robustus, a left premaxillary foramen is present along the mesorostral groove, 70 mm anterior to the antorbital notch of MUSM 2182. This elongated foramen has a transverse diameter of 5.4 mm, smaller than on the right premaxilla of the holotype of *A. robustus*. Differing from the holotype of *A. deinodon*, no additional anterior left premaxillary foramen is observed. Posterior to the corresponding naris, the right premaxilla crosses the sagittal plane; its extent on the left side is nevertheless unknown.

In ventral view, as in *A. deinodon*, the large alveoli for the right and left premaxillary teeth are closely appressed (Figs 25, 26); for example, a distance of 9.5 mm separates right and left alveoli 2 in MUSM 2182.

Maxilla

The lateral margins of the maxillae are roughly parallel in the narrow anterior part of the rostrum of MUSM 2182. For more than one-third of the rostrum length, the lateral surface of the maxilla is nearly vertical. Towards rostrum base, the lateral margin of the maxilla is more concave in dorsal view and dorsoventrally thinner than in the holotype of *A. robustus*. The well-preserved left antorbital notch is deep, U-shaped and opens anterolaterally. Its nearly vertical medial wall is dorsoventrally thick, with a sharp dorsal border. From that border, the surface of the maxilla slopes ventromedially towards the left dorsal infraorbital foramen.

Only one large dorsal infraorbital foramen is preserved on the left side, more distant from the antorbital notch than in *A. robustus*. This foramen is followed posteriorly by a wide and elongated sulcus, whereas no sulcus is observed anteriorly, contrasting with the holotype of *A. robustus*. No lateral groove is observed along the right side of the rostrum, a difference with the holotype of *A. deinodon*. Best seen in dorsal view, a deep notch separates the antobital processes of the maxilla and frontal.

Vomer

In ventral view, the vomer is widely exposed, but less so than in A. deinodon, between the maxillae, with a maximum width of 33 mm at the level of alveoli 9 and 10 (Figs 25, 26).

Frontal

The preorbital process of the frontal is robust in lateral view, with a blunt anteroventral apex (Fig. 24). On the preserved left side, the transversely convex dorsal surface of the process transforms into a crest that rises posterodorsally, laterally limiting a deep and wide longitudinal groove. In lateral view, the supraorbital region of the frontal abruptly thickens posteriorly. The postorbital process is incomplete laterally and ventrally. Nevertheless, the preserved posterodorsal surface of the process draws a smooth curve in lateral view, from vertical to nearly horizontal towards the zygomatic process of the squamosal. This unusually shaped postorbital process closes the temporal fossa anteroventrally.

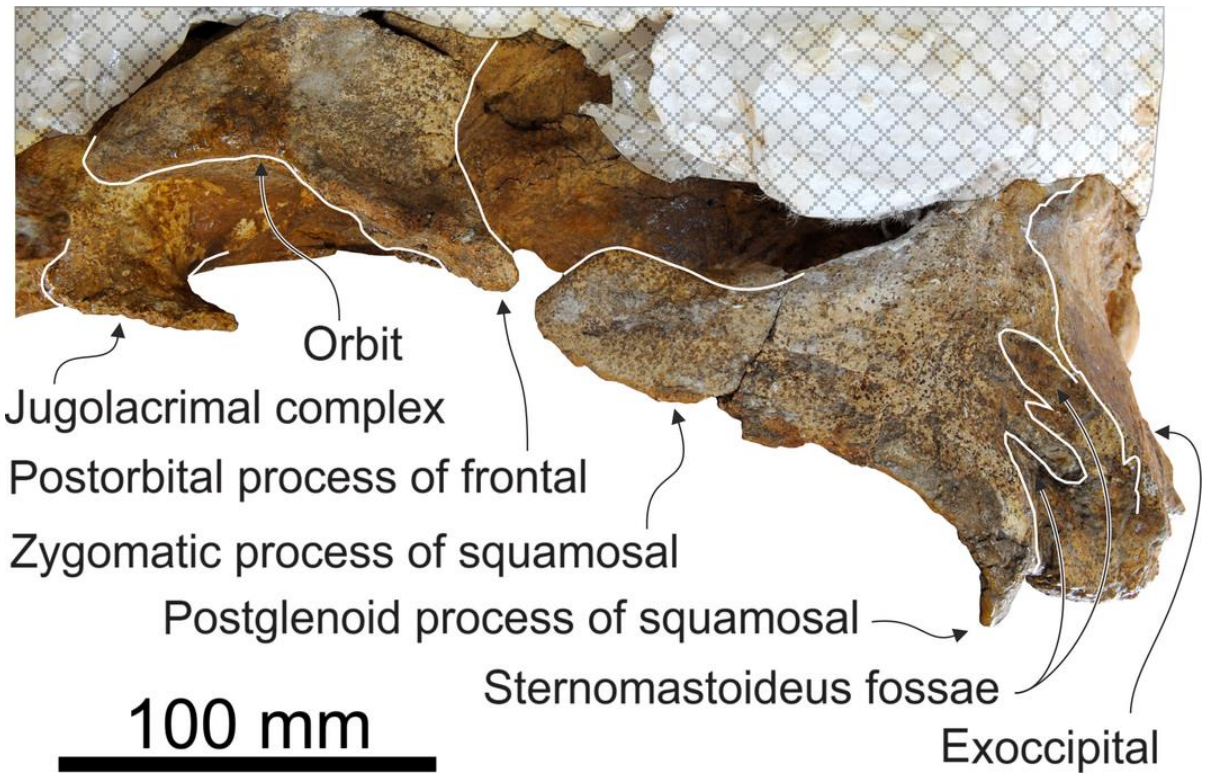

Fig. 24. Skull of *Acrophyseter* sp. MUSM 2182, Cerro los Quesos, late Miocene of the Pisco Basin, Peru. Photograph of the neurocranium in left lateral view.

Palatine

On the wide and slightly convex palate, the anterior margin of the palatine–maxilla suture is interdigitated and roughly transversely directed (Figs 25, 26). A major palatine foramen is located at the anterolateral corner of each palatine, extending anteriorly in a deep and wide sulcus. A slight parasagittal crest is present at that level. From this foramen, the palatine–maxilla suture is directed posterolaterally, towards a curved crest similarly observed in *A. deinodon* and possibly corresponding to an area of origin for a pterygoid muscle (internal or external, see above). An alternative interpretation is that the crest marks the anterior and anterolateral boundaries for a pterygoid sinus fossa.

Pterygoid

In our interpretation, the anterior tip of the pterygoid–palatine suture is 23 mm posterior to the anterolateral corner of the palatine (Figs 25, 26). Together, the right and left pterygoid–palatine sutures draw a ‘W’. The anterior part of the pterygoid is a thin plate (lost on both sides in the holotype of *A. deinodon*). In the palate, the surface of the pterygoid is excavated. As mentioned above, this area was probably occupied by the pterygoid sinus fossa, but the anterior limit of the fossa may correspond to an area of origin for a pterygoid muscle. The posterior portion of the medial lamina of the pterygoid is robust, with a more rounded section compared to *A. deinodon*.

Squamosal

In lateral view, the anterior apex of the long and dorsoventrally thick zygomatic process is more rounded in MUSM 2182 than in the holotype of *A. robustus*, with a slightly concave anterior margin and a more developed anterodorsal bulge (Fig. 24). A smaller oval dorsal fossa and a more elongated ventral fossa represent the two sternomastoideaus fossae in MUSM 182, which are better defined than in *A. robustus*. Complete on the left side, the postglenoid process forms a transversely directed blade that is ventrally longer than the exoccipital and posttympanic process of the squamosal. The wide mandibular fossa faces anteroventrally (Figs 25, 26). Better defined posteromedial to the mandibular fossa, the tympanosquamosal recess extends on the medial surface of the postglenoid process. More anteriorly, the lateral limit of the recess is less abrupt. The deep and rectilinear narrow groove observed in *A. deinodon* and *A. robustus* is present in MUSM 2182. The shallow and wide path for the mandibular nerve V3 is directed laterally.

Fig. 25. Skull and mandibles of *Acrophyseter* sp. MUSM 2182, Cerro los Quesos, late Miocene of the Pisco Basin, Peru. Photograph of the skull in ventral view; left mandible in lateral view with condyle pointing upwards and right mandible in lateral view with apex pointing downward.

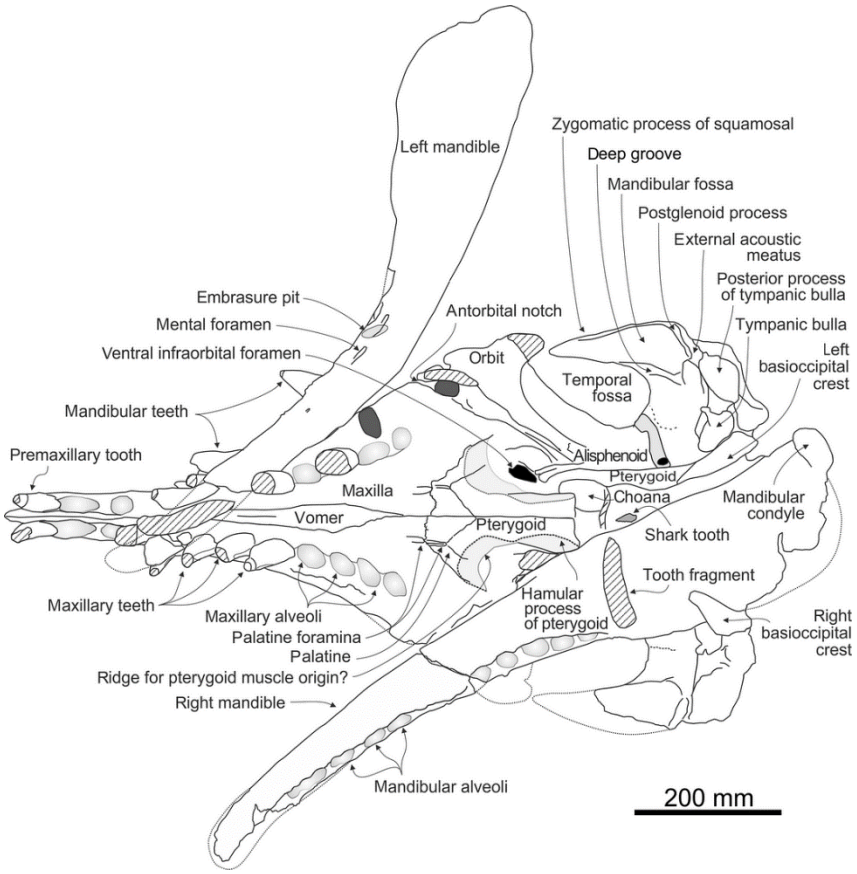

Fig. 26. Skull and mandibles of *Acrophyseter* sp. MUSM 2182, Cerro los Quesos, late Miocene of the Pisco Basin, Peru. Line drawing of the skull in ventral view; left mandible in lateral view with condyle pointing upwards and right mandible in lateral view with apex pointing downward. Hatched surfaces for major break surfaces; dark shading for sediment.

Exoccipital

A contact between the paroccipital process of the exoccipital and the basioccipital crest is only present on the right side (Fig. 27). Such an asymmetry is possibly related to the slight differential deformation of that area.

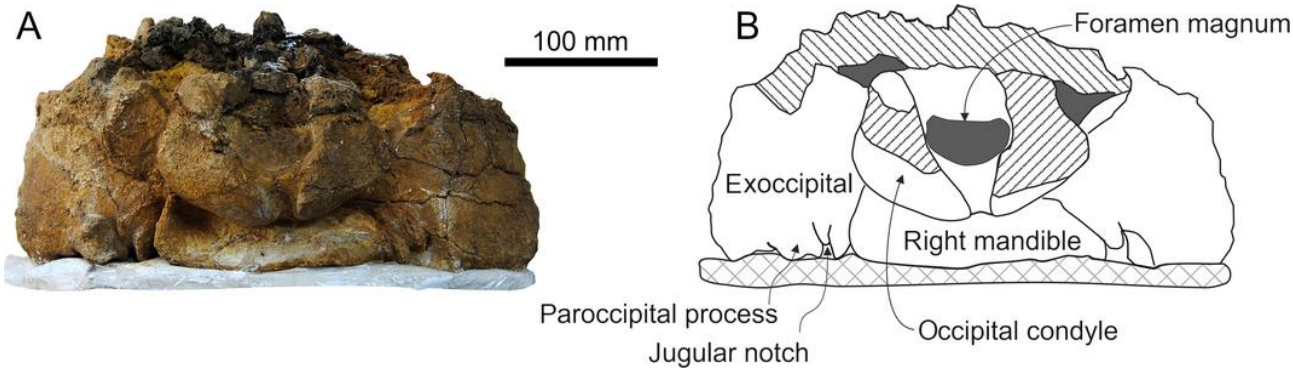

Fig. 27. Skull and right mandible of *Acrophyseter* sp. MUSM 2182, Cerro los Quesos, late Miocene of the Pisco Basin, Peru. A, photograph in posterior view; B, corresponding line drawing. Hatched surfaces for major break surfaces; dark shading for sediment.

Tympanic bulla

The in situ left tympanic (Figs 25, 26; Table 1) displays a sigmoid process that is high on the outer lip and transversely directed. The posterior process forms a massive posterolateroventrally directed rod, with a proximal width of 22 mm. It widens and thickens distally, forming a swollen region between the paroccipital process of the exoccipital and the postglenoid process of the squamosal. The anterior margin of the posterior process follows the postmeatal crest of the squamosal. On the external surface of the skull, the sutures of the process with both the exoccipital and the squamosal are difficult to follow, this region being made of spongy bone marked with grooves and ridges.

Mandibles

Dimensions are provided in Table 2. As in *Acrophyseter deinodon* and *A. robustus* the mandibular symphysis is not ankylosed (Figs 25, 26). The ventral margin of the mandible is regularly convex, with only a slight angle roughly at the level of the symphysis end. The exact lower tooth count is unknown, but considering the upper count similar to *A. deinodon* (12), a similar lower count may be expected (13). As in *A. robustus*, the outline of the moderately elevated coronoid process is regularly curved, differing from the more angular condition in *A. deinodon* (Fig. 28). Located

close to the ventral margin of the bone, the mandibular condyle displays a notched ventral margin.

Fig. 28. Comparison of the shape of the coronoid process in the mandibles of *Acrophyseter deinodon* MNHN SAS 1626 (holotype), *A. robustus* MUSM 1399 (holotype) and *Acrophyseter* sp. MUSM 2182, in left lateral view. All specimens reduced to the same dorsoventral distance between coronoid and condyloid processes. Stippled lines for the outline of the coronoid and condyloid processes in the articulated mandible of *A. robustus* MUSM 1399.

Teeth

As in *Acrophyseter deinodon* and *A. robustus*, teeth are proportionally large with a total length ranging from 76.4 to 110 mm (Table 5). The anteriormost pair of upper teeth is not procumbent, with a roughly vertical longitudinal axis of the crown (Figs 25, 26). Similarly to part of the upper teeth of *A. deinodon*, several detached teeth display a strong curvature, with an angle between the long axis of the crown and the long axis of the proximal part of the root lower than 130° (until 108° in one, presumably lower anterior tooth) (Fig. 29). The short conical crown covered with enamel has a length ranging from 14.5 to 22.2 mm and a diameter at the base ranging from 12 to 16 mm. All the teeth of MUSM 2182 display a distal part of the crown with thinner and smoother enamel than in the proximal part. Indeed, the proximal part of the crown (half or more of its length) bears thicker and more heavily ornamented enamel, with nearly straight longitudinal ridges. The limit between these two parts is clear, marked by a small step. Considering this clear limit, this difference in aspect is difficult to explain with wear only. A similar pattern is described in physeteroid teeth from the Miocene of Europe (Hampe, (2006). The tip of the crown of nearly all the teeth is truncated; the apical surface is plane and smooth. As in the holotype of *A. robustus*, the distal region of the root displays a slight constriction and a smoother surface, probably wear-related. From this area, the root bulges proximally, with a maximum diameter ranging from 25 to 30.5 mm. The proximal end of the root is slender, nearly pointed, sometimes with a short and slender posterior projection. Deep and long occlusal facets similar to those in the holotype of *A. deinodon* are

observed on several detached teeth, from different regions of the jaws. The pulp cavity of each detached tooth is filled and proximally closed.

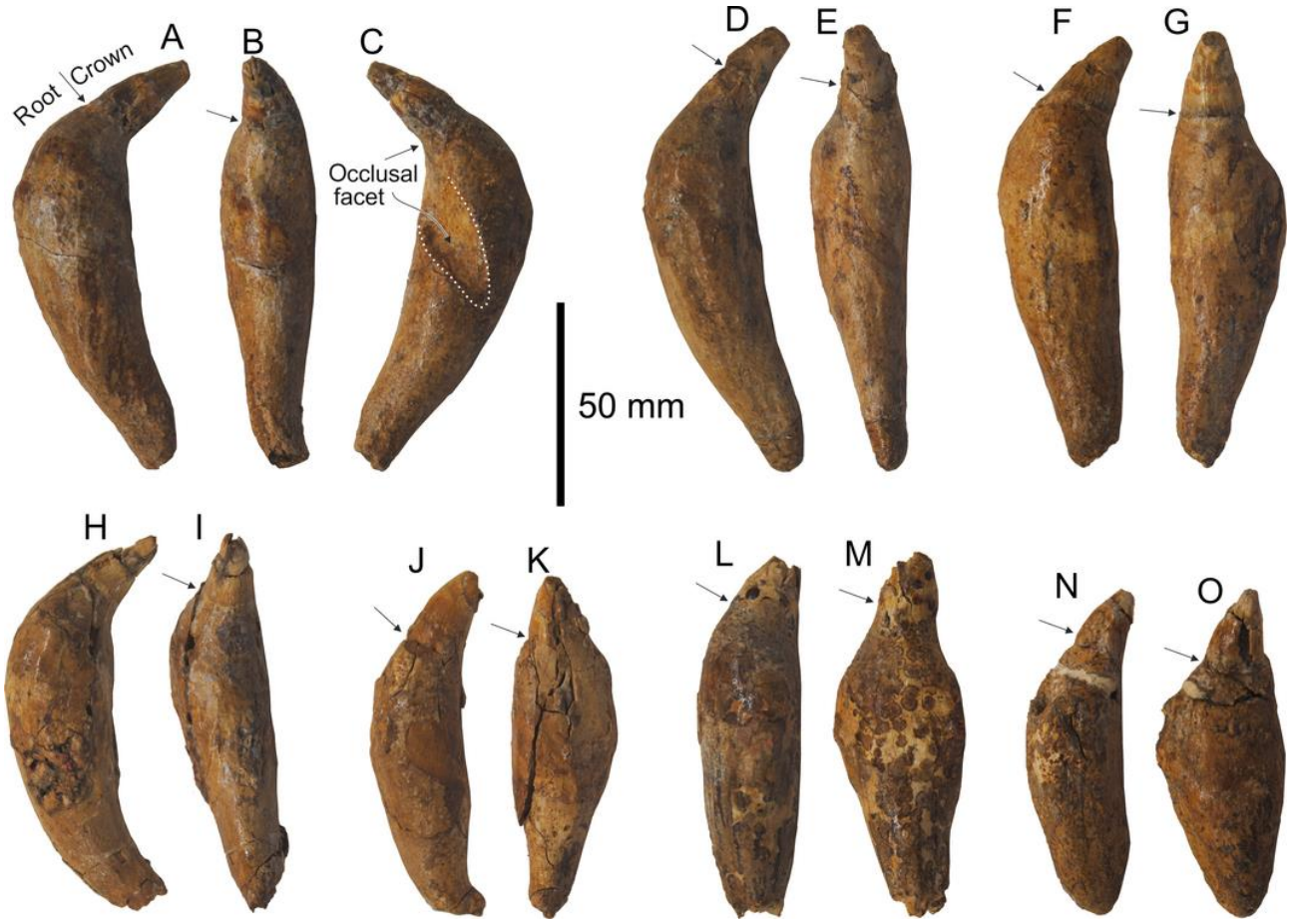

Fig. 29. Detached teeth of *Acrophyseter* sp. MUSM 2182, Cerro los Quesos, late Miocene of the Pisco Basin, Peru. A–C, tooth d (presumably lower anterior left); D–E, tooth a (anterior); F–G, tooth g (medial); H–I, tooth b (anterior); J–K, tooth i (upper posterior); L–M, tooth j (upper posterior); N–O, tooth l (lower posterior). Root–crown boundaries are indicated with arrows; occlusal facet for tooth d is indicated with stippled lines.

Table 5. Measurements (mm) on detached teeth of *Acrophyseter* sp. MUSM 2182

	a	**b**	**c**	**d**	**e**	**f**	**g**	**h**	**i**	**j**	**k**	**l**
Total length	110	+87.6	+108	+95.3	+95.4	+102	99.8	100.6	82.2	+86	+95.2	76.4
Root length	81.5	-	-	82.2	90.3	-	83.0	83.0	70.2	+70.6	+81.5	58.8
Crown length	15.8	18.2	-	22.2	-	-	20.7	19.9	15.5	15.0	e14.5	17.6
Maximum transverse diameter of root	25.0	24.4	20.7	22.4	25.3	26.0	26.4	30.2	25.8	30.5	-	22.4
Maximum mesiodistal diameter of root	25.0	26.1	28.2	25.8	27.6	-	27.2	28.8	21.1	24.0	-	30
Transverse diameter at crown base	-	12.0		13.1	-	-	15.0		15.0	-	-	-
Mesiodistal diameter at crown base	-	13.5	-	12.7	-	-	15.5	16	-	16	-	14.9
Tooth length above gingival collar	40.4	-	-	33.9	-	-	-	-	e37	e35	-	-
Proposed position along tooth rows	ant.	ant.	ant.	ant left low	antmed	antmed	med	postmed up	post up	post up	post up	post low

+, Incomplete; e, estimate; –, no data. Proposed position along the tooth row is provided: ant, anterior; low, lower; med, medial; post, posterior; up, upper. Letters in the first row correspond to letters in caption to Figure 29.

Discussion

The specimen MUSM 2182 shares with *Acrophyseter deinodon* and *A. robustus* the main diagnostic features of the genus *Acrophyseter*: 12 teeth for each upper alveolar groove; deep groove directed anterolaterally along medial wall of tympanosquamosal recess; curved mandible with regularly convex ventral margin in lateral view; and proportionally long and thickened medial lamina of the pterygoid. This specimen shares some diagnostic features of *A. robustus* (and thus differences with *A. deinodon*): rostrum not as pointed in dorsal view and lacking abrupt anterior decrease of height of maxilla in lateral view (a feature corresponding here to a proportionally longer rostrum with more widely spaced alveoli than in *A. deinodon*); absence of a lateral groove on the right side of the rostrum; absence of an additional anterior left premaxillary foramen; and dorsal margin of coronoid process of mandible being smoothly rounded. It further differs from *A. deinodon* in the dorsal closure of the mesorostral groove by the premaxillae in the anterior portion of the rostrum. However, MUSM 2182 differs from *A. robustus* in: lacking a deep sulcus anterior to the main left dorsal infraorbital foramen; presence of a left premaxillary foramen; and possessing several upper teeth more distinctly recurved (angle up to 108°).

Originating from a level distinctly younger in age than the level of A. robustus and probably slightly older (tentative correlation with AGL level) than the level of *A. deinodon* (MTM level), this specimen does not match morphologically either of these two species. Because the facial region is only poorly preserved in MUSM 2182, and because intraspecific variation is currently unknown in the two defined species of *Acrophyseter*, we prefer to keep a generic determination for this specimen, which may prove to belong to a third species of that genus. Furthermore, as noted above, the periotic from the AGL level at Aguada de Lomas referred to *Acrophyseter* aff. *A. deinodon* (MNHN F-PPI 272) has been tentatively regarded as contemporaneous with MUSM 2182. It may thus correspond to the same species as the Cerro los Queso specimen. Finally, because the two specimens are stratigraphically closer to *A. deinodon* than to *A. robustus*, they may actually belong to the former species and the differences noted here may therefore correspond to intraspecific variation.

Livyatan Lambert, Bianucci, Post, Muizon, Salas-Gismondi, Urbina & Reumer, 2010b

Type and only included species

Leviathan melvillei Lambert, Bianucci, Post, Muizon, Salas-Gismondi, Urbina & Reumer, 2010a.

Emended diagnosis

Same as for the only included species.

Livyatan melvillei (Lambert, Bianucci, Post, Muizon, Salas-Gismondi, Urbina & Reumer, 2010a)

Leviathan melvillei Lambert et al., 2010a: fig. 1

Livyatan melvillei Lambert et al., 2010b

Holotype

MUSM 1676, a skull lacking the whole left posterolateral portion, with associated partial mandibles and teeth.

Type locality

Cerro Colorado, Pisco-Ica desert, 35 km SSW of Ica (Fig. 1A). Geographical coordinates 14°20′20.2″S, 75°53′17.4″W, altitude 483 m. The holotype was discovered by Klaas Post on 28 November 2008, during an international expedition in the Pisco Basin. It was collected shortly afterwards by a team directed by Rodolfo Salas-Gismondi.

Type horizon

Lowest beds of the Pisco Formation, approximately 60 m above the unconformity with the late Oligocene to early Miocene Chilcatay Formation, in the lower allomember described in Cerro Colorado (Di Celma et al., 2016; Bianucci et al., 2016; Fig. 30). Radiolarians, diatoms and foraminifers provided a late middle Miocene age (Serravalian, 12–13 Ma) for lowest levels of the Pisco Formation in the northern part of the Pisco Basin (Dunbar, Marty & Baker, 1990). This dating was confirmed with the discovery of the bivalve Anadara sechurana Olsson, 1932 in Cerro Colorado, close to MUSM 1676; this mollusc is indeed found in the lowest levels of the Pisco Formation and the middle Miocene Montera Formation in northern Peru (DeVries, 1998, 2001). Based on this evidence and the associated vertebrate fauna, layers in this locality were previously dated to the late middle Miocene (Serravallian, 12–13 Ma; Bianucci et al., 2010; Lambert et al., 2010a). However, the recent identification in the lower allomember of Lithodesmium reynoldsii (a diatom species ranging from 9.9 to 8.9 Ma; Barron, 2003) indicates a late Miocene (Tortonian) age (Di Celma et al., 2016; Fig. 30). The Tortonian age is confirmed with the 40Ar/39Ar dating of biotite from a local volcanic ash layer (9.0 ± 0.1 Ma; preliminary report in Bosio et al., 2015). This lower allomember yielded numerous marine vertebrate remains, including another undetermined physeteroid, the ziphiid *Messapicetus gregarius*, the pontoporiid *Brachydelphis mazeasi*, another undescribed

pontoporiid, a kentriodontine, at least two cetotheriids and a balaenopteroid, the sea turtle *Pacifichelys urbinai* Parham & Pyenson, 2010, several seabirds and, among others, the sharks *Carcharocles megalodon* and *Cosmopolitodus hastalis* (Bianucci et al., 2010, 2016; Lambert et al., 2010a; Parham & Pyenson, 2010; our pers. observ.).

The specimen was partly covered by a dolomitic concretion, especially along the ventral surface of the rostrum, around and inside dental alveoli (Gariboldi et al., 2015: fig. 2d).

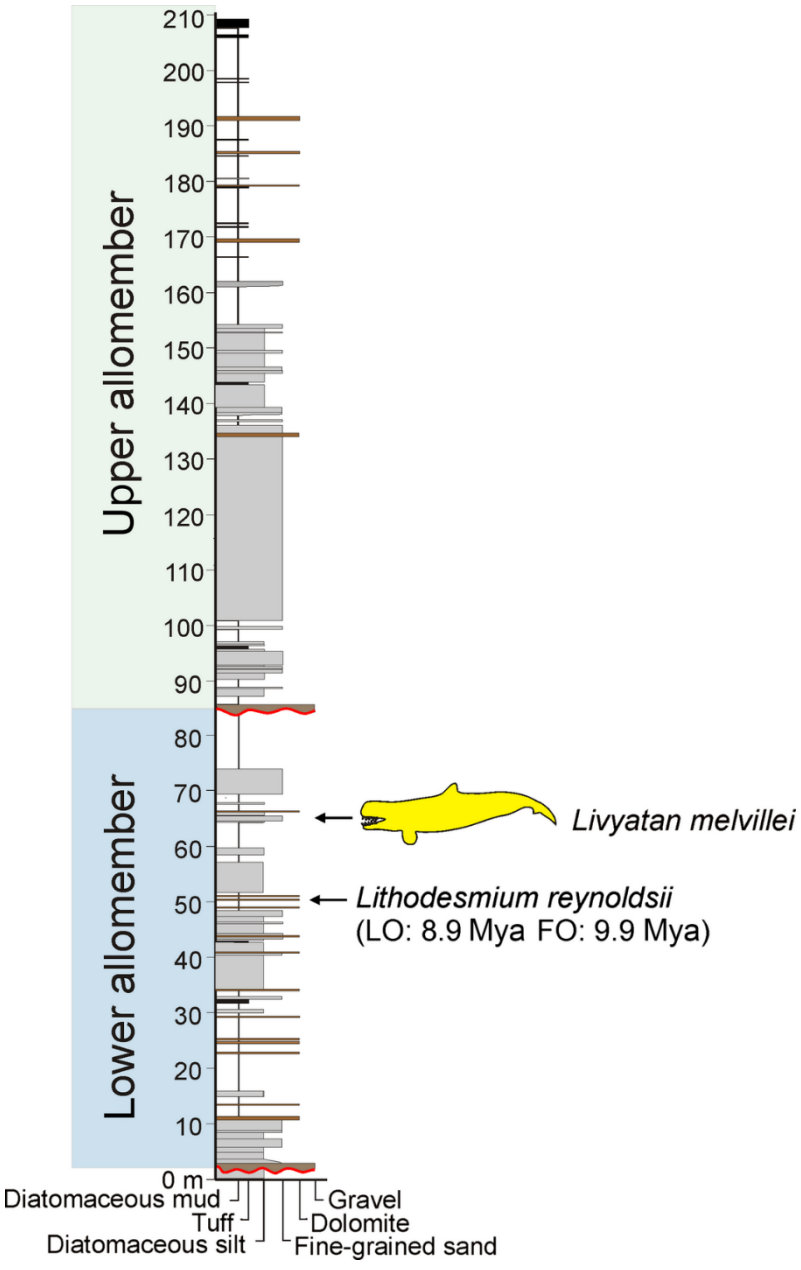

Fig. 30. Stratigraphic column of the late Miocene deposits of the Pisco Formation in the locality of Cerro Colorado, indicating the stratigraphic level of the lower allomember from where the holotype of Livyatan melvillei MUSM 1676 originates. A few metres below the Livyatan level the diatom species Lithodesmium reynoldsii was found, providing a time interval ranging from 9.9 to 8.9 Ma (Barron, 2003). Modified from Bianucci et al. 2016: fig. 4).

Emended diagnosis

Giant physeteroid differing from all other physeteroids in: great anterolateral expansion of the premaxilla on dorsal surface of wide rostrum, reaching lateral margin of latter; absence of premaxillary teeth on the tooth-bearing rostrum; maximum transverse tooth diameter being > 100 mm for most of the upper and lower dentition; and having nine teeth in each upper tooth row. Further differs from all other physeteroids except *Physeter* in having the postorbital width of the skull > 1 m [unknown in *Albicetus oxymycterus* (Kellogg, 1925); Boersma & Pyenson, 2015], from all other physeteroids except *Kogia* in having 11 teeth in each lower tooth row, from all other physeteroids except *Acrophyseter deinodon* and *Kogia* in having the ratio between rostrum length and skull width < 0.95, from all other physeteroids except *Kogia*, *Nanokogia* and *Scaphokogia* in maxilla, premaxilla and vomer all reaching tip of rostrum (unknown in other kogiids), from all other physeteroids except *Aprixokogia*, *Kogia* and *Physeter* in having the supracranial basin extended onto whole dorsal surface of rostrum, and from all other physeteroids except *Kogia*, *Nanokogia*, *Praekogia* and *Scaphokogia* in having a slit-like right antorbital notch. *Livyatan* is further characterized by probable plesiomorphic features, differing from *Kogia*, *Physeter* and several other related taxa in: retention of enamel on teeth; posterior end of upper alveolar groove close to level of antorbital notch; and a high and anteroposteriorly long temporal fossa.

Morphological description of *Livyatan melvillei* and comparison

Skull

Dimensions of the skull are provided in Table 6. Among physeteroids, a skull width similar to *Livyatan melvillei* is only observed in adult males of *Physeter macrocephalus* (e.g. Clarke & Paliza, (1972). The dimensions of the neurocranium are unknown in another large fossil species *Albicetus oxymycterus* (Kellogg, 1925); the estimated condylobasal length of the latter is considerably smaller than in *L. melvillei* (Boersma & Pyenson, 2015), but our own observations suggest a length somewhat greater than the provided estimate. The robust rostrum of L. melvillei is proportionally short, as in *Kogia* and *Acrophyseter deinodon*; rostrum length is about 57% of cbl. The rostrum base is broad and the lateral margins are convex in dorsal view for the anterior half (Figs 31, 32). This anterior region is proportionally transversely wider than in most physeteroids, except *Physeter* and, with an unusual morphology, *Scaphokogia*. The rostrum is dorsoventrally thick, with a dorsal surface transversely concave and, more slightly, longitudinally concave (Figs 31, 33, 34). This concavity testifies to the extension of the supracranial basin until the anterior end of the rostrum, as in *Physeter*. With a more pointed rostrum, *Aprixokogia* and *Kogia* also display a supracranial basin extending anteriorly. On the wide

neurocranium, the supracranial basin deepens and widens posterolaterally, at least on the right side, and is laterally defined by a high wall beyond the level of the antorbital notch. Even if well developed laterally, the supracranial basin does not overhang the right orbit, contrary to *Acrophyseter* and *Zygophyseter*. The temporal fossa is large, with the estimated dorsoventral height roughly equal to the anteroposterior length (Fig. 33). Based on the preserved parts, we estimate that the temporal fossa was not higher than long. The fossa probably occupied most, if not the whole, posterodorsal portion of the neurocranium in lateral view. The temporal fossa is proportionally considerably smaller in *Diaphorocetus, Idiophyseter*, *Kogia*, *Physeter* and probably *Praekogia*, with the roof of the fossa at the vertical level or lower than the dorsal margin of the rostrum in lateral view of all these taxa. The fossa is relatively high, but proportionally anteroposteriorly shorter in *Orycterocetus crocodilinus* and, even more, in *Aulophyseter morricei*. In contrast, the temporal fossa of *Acrophyseter* and *Zygophyseter* is proportionally similar in size to that of *Livyatan.*

Table 6. Measurements (mm) on the skull of *Livyatan melvillei* MUSM 1676 (holotype), modified from Lambert et al. (2010a)

Total length of skull as preserved	270
Condylobasal length	e294
Rostrum length	169
Width of rostrum at mid-length	85
Width of rostrum at base	137
Width of rostrum at antorbital notches	e123
Length of antorbital notch	28
Maximum width of premaxillae on rostrum	69.5
Minimum width of premaxillae on rostrum	e46
Maximum width of mesorostral groove	23
Depth of supracranial basin at mid-length of rostrum	7.5
Length of right upper alveolar row	134
Length of left upper alveolar row	135
Distance between upper right and left first anterior alveoli	17
Distance between upper right and left last posterior alveoli	71
Distance between upper right last posterior alveolus and lateral margin of rostrum	13
Postorbital width of skull	e190
Distance from rostrum tip to left premaxillary foramen	150
Distance from rostrum tip to right bony naris	220.5
Depth of supracranial basin on neurocranium between highest margin of maxilla and lowest part of right premaxilla	56
Distance between anterior margin of preorbital process of maxilla and preserved posterior margin of postorbital process of frontal	50.5
Maximum length of temporal fossa	e66.5
Maximum height of temporal fossa	e64
Bizygomatic width of skull	e197

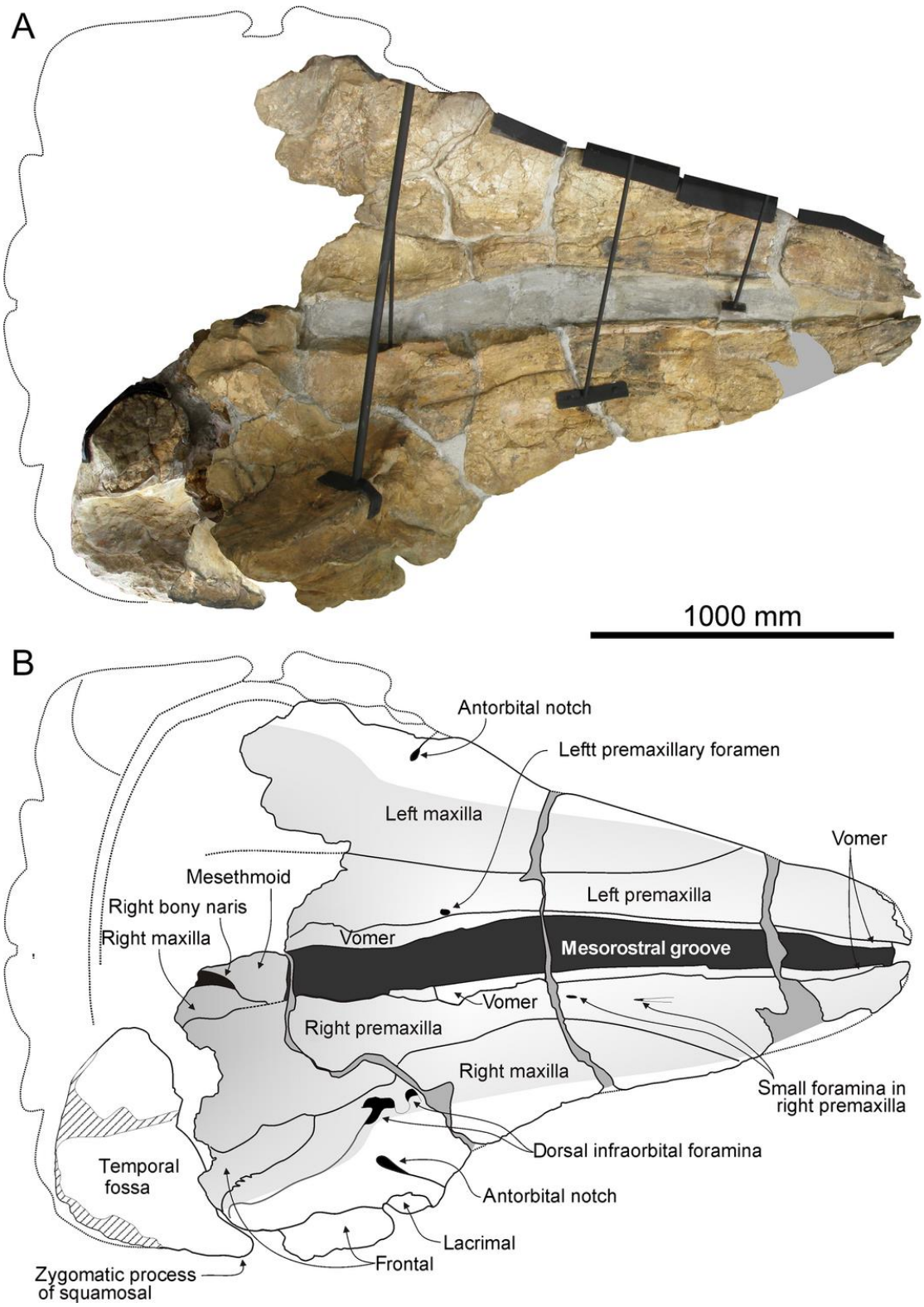

Fig. 31. Skull of *Livyatan melvillei* MUSM 1676 (holotype), Cerro Colorado, early late Miocene of the Pisco Basin, Peru, in dorsal view. A, photograph. B, corresponding line drawing. Light shading for reconstructed parts; hatched surfaces for major break surfaces; dark shading for sediment; stippled lines for incomplete parts. Black metal elements visible on the photo are supporting frames that could not be removed prior to taking the photo.

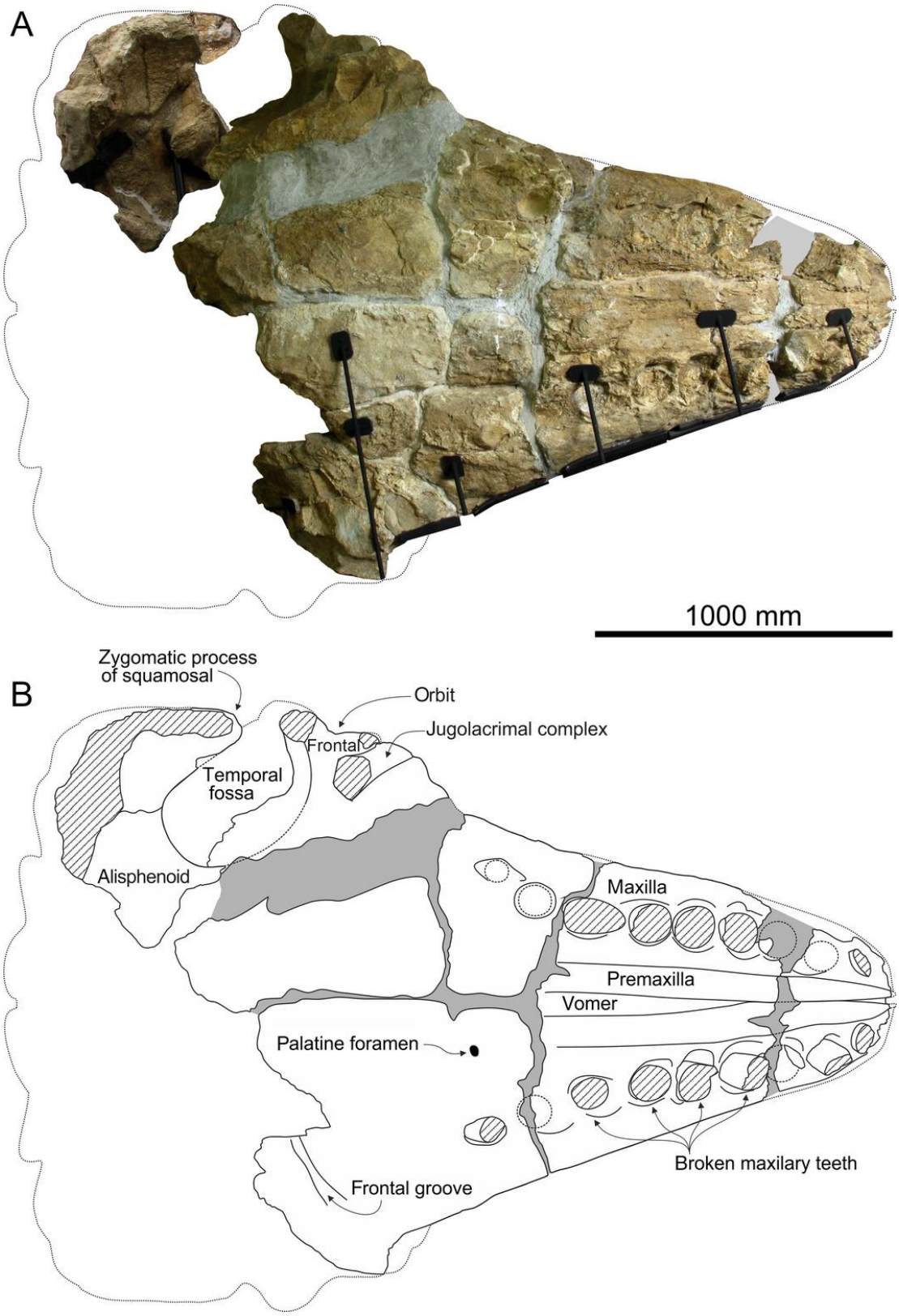

Fig. 32. Skull of *Livyatan melvillei* MUSM 1676 (holotype), Cerro Colorado, early late Miocene of the Pisco Basin, Peru, in ventral view. A, photograph. B, corresponding line drawing. Light shading for reconstructed parts; hatched surfaces for major break surfaces; stippled lines for incomplete parts. Black metal elements visible on the photo are supporting frames that could not be removed prior to taking the photo.

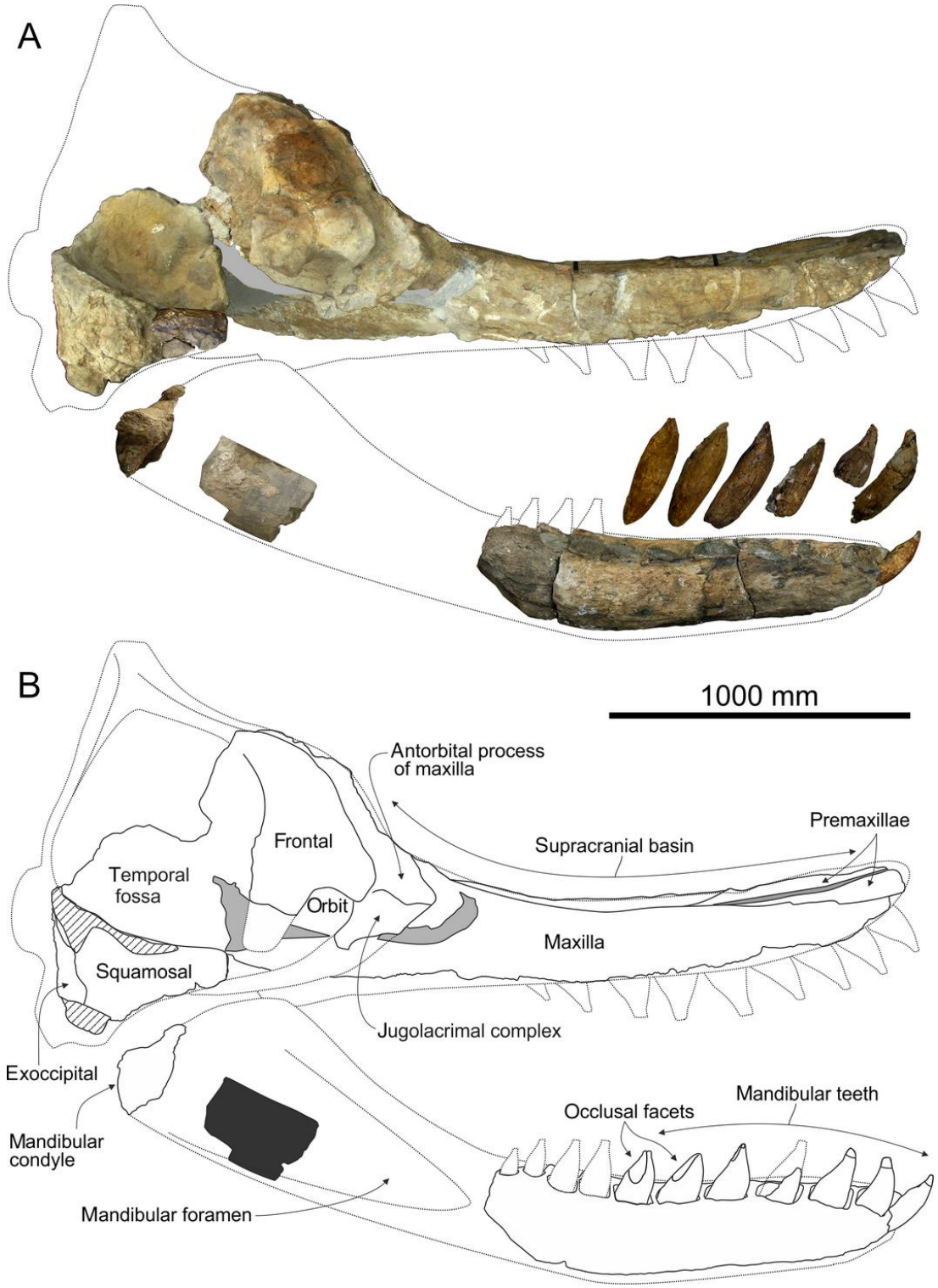

Fig. 33. Skull, mandible and mandibular teeth of Livyatan melvillei MUSM 1676 (holotype), Cerro Colorado, early late Miocene of the Pisco Basin, Peru, in right lateral view. A, photograph. B, corresponding line drawing. Light shading for reconstructed parts; hatched surfaces for major break surfaces; dark shading for sediment; stippled lines for incomplete parts.

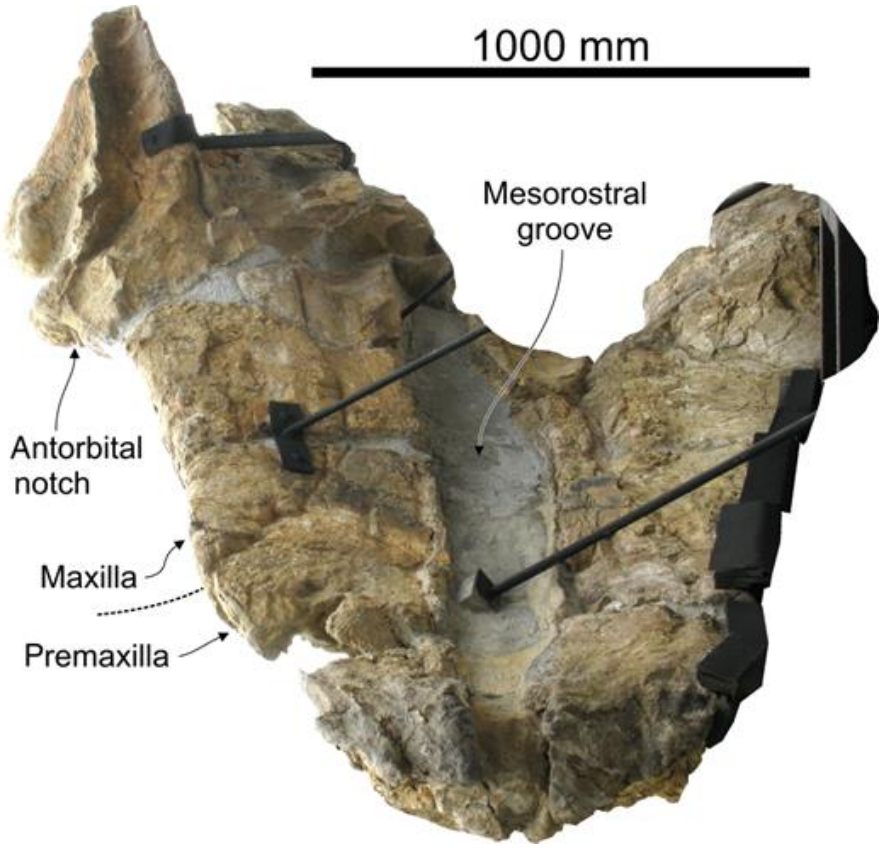

Fig. 34. Skull of *Livyatan melvillei* MUSM 1676 (holotype), Cerro Colorado, early late Miocene of the Pisco Basin, Peru, in anterior to slightly anterodorsal view. Black metal elements are supporting frames that could not be removed prior to taking the photo. Stippled line indicates the level of the premaxilla–maxilla suture.

Premaxilla

In dorsal view, the premaxillae occupy most of the anterior portion of the rostrum (Figs 31, 34). From the apex, each premaxilla reaches the distinctly convex lateral and anterolateral margin of the rostrum for a length of more than 500 mm. In *Physeter*, the premaxillae occupy a much narrower part of the dorsal surface, most of the widening of the rostrum comprising the maxillae. A wide mesorostral groove separates the premaxillae dorsomedially for the whole rostrum length; dorsomedial margins of left and right premaxillae converge anteriorly, but do not contact each other at the rostrum apex. Except for the right premaxilla at the rostrum base, there is no overhanging of the premaxillae on the mesorostral groove. Indeed, each premaxilla is medially defined by the vertical lateral wall of the mesorostral groove, constituted by the vomer. In the anterior part of the rostrum, the dorsal surface of the premaxilla is flat and slightly dorsolaterally sloping; in anterior view, the lateral margin of the premaxilla is distinctly higher than the medial margin, indicating the extension of the supracranial basin until the anterior end of the rostrum. From the

lateral margin of the rostrum, the dorsal premaxilla–maxilla suture turns posteromedially, with the premaxilla progressively narrowing until a minimum width at a level about 500 mm anterior to the antorbital notch. From that level, the premaxilla widens moderately towards the neurocranium. On both sides the premaxilla–maxilla suture is laterally concave for most of its length, except for a slightly convex portion on the right side, anterior to the base of the rostrum.

Small foramina pierce the premaxillae on the rostrum. On the right side, 900 mm from the apex, a 10-mm-wide foramen is followed anteriorly by a narrow sulcus, and 1100 mm from the apex, an 8.5-mm-wide foramen is situated closer to the medial margin of the premaxilla. Due to their anterior position, none of these foramina is interpreted as the right premaxillary foramen. No right premaxillary foramen could be detected, but this might be linked to some damage on the medialmost portion of the premaxilla in the rostrum base area. On the left premaxilla, a foramen 1500 mm from the apex and close to the medial margin of the premaxilla, with transverse and longitudinal diameters of 25 and 29 mm, respectively, is interpreted as the left premaxillary foramen. Additional small foramina might have been originally present more anteriorly, but the superficial layer of the left premaxilla is slightly worn at different levels, a condition that might obscure small morphological features.

A slight depression marks the dorsal surface of the right premaxilla just anterior to the transversely widest level of the rostrum. This concave area, lower than the adjacent maxilla, is separated by a smooth transverse ridge from a much deeper, posteriorly widening depression, considered here as the right premaxillary sac fossa. The transverse ridge is continuous with a crest directed posterolaterally on the right maxilla (margin of supracranial basin, see below). The right premaxilla–maxilla suture is difficult to follow on the neurocranium, due to the poor preservation of this area. We estimate that the suture is directed laterally for a short distance, towards the posterior infraorbital foramen, before taking a more posterior direction. Therefore, the right premaxilla probably does not completely cover the lateral wall of the supracranial basin. On the neurocranium, the floor of the supracranial basin is marked by several breaks, obscuring the interpretation of the various bones involved. Nevertheless, the medial margin of the right premaxilla is higher than the adjoining medial exposure of the right maxilla. If the medial margin of the premaxilla is complete, then the bone does not cross the sagittal plane of the skull at this level. No information is available for the posteriormost portion of the premaxilla. However, the dorsal surface of the bone just lateral to the right bony naris is only moderately sloped, suggesting that the supracranial basin originally extended some distance posterior to this level, before the raised posterior wall.

The dorsal surface of the left premaxilla posterior to the left premaxillary foramen is distinctly lower than the corresponding surface on the right premaxilla, making a

deeper left premaxillary sac fossa. The medial margin of the fossa displays a steep slope along the thick dorsal exposure of the vomer. Based on the preserved parts, no evidence for posterior widening of the left premaxilla exists, contrasting with the condition on the right premaxilla. Therefore, right and left premaxillae are distinctly asymmetrical in the rostrum base and the anterior part of the neurocranium, both for the dorsoventral level of their dorsal surface and for their width.

In ventral view, the premaxillae appear between the maxillae from the apex of the rostrum, contacting each other medially for 685 mm before the ventral exposure of the vomer (Fig. 32). No dental alveoli are entirely located on the premaxilla; only the medial margin of the anteriormost alveoli and possibly their dorsal portion is partly made of the premaxilla. This is a major difference with all other physeteroids bearing functional upper teeth, including *Albicetus oxymycterus*.

Maxilla

The upper surface of the maxilla is flat for the anterior portion of its dorsal exposure, and is slightly upraised laterodorsally. The dorsal surface of the right maxilla becomes more prominent, moderately convex, towards the rostrum base, whereas the surface of the left bone becomes slightly concave. In dorsal view, the lateral margin of the maxilla on the rostrum is regularly concave from the anterior limit of its dorsal exposure to the antorbital notch, diverging markedly at rostrum base. The preserved right antorbital notch is deep (more than 280 mm), opening in an anterolateral direction, and slit-like; its anteromedial and posterolateral walls, respectively made of the lateral margin of the rostrum and the antorbital process of the maxilla, roughly contact each other for most of its extent (Fig. 31). A slit-like antorbital notch is similarly observed in *Acrophyseter robustus* and A. sp. MUSM 2182, *Kogia*, *Nanokogia*, *Praekogia* and *Scaphokogia*. Differing from the condition in Livyatan, the notch is inside the supracranial basin in *Kogia* and *Praekogia*. Only the bottom of the antorbital notch is dorsoventrally open, with a maximum diameter of 25 mm. As mentioned above, an oblique posterolaterally directed crest separates the rostrum base and the antorbital notch from the cranial part of the supracranial basin. The oblique crest, corresponding to the anterolateral wall of the basin, rises abruptly posterodorsally towards the top of the temporal fossa. A deep and wide gutter, originating at the antorbital notch, laterally defines the crest. The lateral limit of the gutter corresponds to a sharp longitudinal crest, leaving from the antorbital process of the maxilla and raising above the supraorbital process of the frontal.

Two dorsal infraorbital foramina are detected medial to the right antorbital notch. One foramen is located on the anterolateral wall of the supracranial basin; this foramen is obliquely elongated, with a maximum length of 122 mm; it probably opened with a posteromedial direction inside the supracranial basin. The second

foramen, just anterior to the first, is smaller with a maximum diameter of 53 mm. In *Physeter*, only one large right dorsal infraorbital foramen (= maxillary incisure) is usually observed along the anterolateral wall of the supracranial basin, whereas several smaller foramina are present inside the basin of *Kogia*.

The right lateral margin of the supracranial basin is roughly at the same transverse level as the lateralmost margin of the rostrum. In the supracranial basin, the right maxilla appears as a narrow strip on the lateral wall of the basin, with a maximum width of 200 mm, 200 mm from its posterodorsolateral preserved end. In this region, the medial maxilla–frontal suture is highly interdigitated, 'ammonite'-like. As in *Physeter*, this suture is far from the sagittal plane of the skull, leaving the right frontal exposed between maxilla and premaxilla on the posterolateral surface of the basin. Medial to the right premaxilla, a narrow strip (a few centimetres) of maxilla occupies the lateral margin of the small right bony naris; the latter is only partly preserved, as a dolomitized inner cast.

In the facial region, most of the left maxilla is lost. Only the antorbital notch is partly preserved.

A deep notch separates the right antorbital process of the maxilla from the corresponding preorbital process of the frontal. The notch is partly filled by a thin bony plate, very probably corresponding to an element of the maxilla, less likely a posteromedial projection of the lacrimal. In lateral view, the anteroposteriorly long antorbital process of the maxilla displays an extended sutural contact with the dorsal surface of the lacrimal/jugal (Fig. 33).

Each maxilla bears nine alveoli (Fig. 32; Table 7). Considering that the premaxilla does not bear alveoli, this tooth count is lower than in any other physeteroid bearing functional upper teeth. The alveolar groove is separated from the lateral margin of the rostrum, particularly in its posterior half. The groove roughly follows the curves of the rostrum, with a convex lateral margin of the groove in the anterior portion, and with alveoli 7–9 directed towards the corresponding antorbital notch. Upper (typically unerupted) teeth in *Physeter* are positioned far medial to the lateral margin of the rostrum, with right and left upper toothrows approaching each other, and aligned with the lower toothrows of the transversely narrow mandibles (see Boschma, 1938: fig. 14). The first anterior right and left alveoli are separated by 170 mm. Alveoli are roughly circular in outline with alveolus 4 as the largest (transverse diameter of 197 mm on the right side, by far the largest diameter for a cetacean maxillary alveolus). The diameter of alveoli decreases progressively anteriorly until alveolus 1 (diameter estimated at 145–150 mm) and posteriorly until alveolus 9 (diameter estimated at 74 mm). Interalveolar septa are ossified and proportionally short, with the distance between successive alveoli not exceeding 49 mm. Lateral to the alveolar groove, the maxilla is dorsoventrally thick, especially at mid-length of

the rostrum (Fig. 33); for example, a thickness of 160 mm is measured between right alveoli 5 and 6.

A major palatine foramen is visible on the left maxilla, 1450 mm from the apex of the rostrum.

Table 7. Transverse diameter (mm) of right/left maxillary alveoli of *Livyatan melvillei* MUSM 1676 (holotype), modified from Lambert et al. (2010a)

Alveolus number	Right	Left
1	e15	e14.5
2	-	-
3	16	-
4	19.7	19.5
5	16.3	18
6	14.9	16
7	-	12
8	10	-
9	e7.4	6.5

e, Estimate; –, no data.

Vomer

Together with the maxillae and premaxillae, the vomer reaches the anterior end of the rostrum (Fig. 31) as in *Kogia*, *Nanokogia* and *Scaphokogia*. The anterior portion of the vomer is slender, forming a thin-walled gutter. The walls abruptly thicken posteriorly; a transverse thickness of 38 mm is measured 230 mm from the apex. From that level, the lateral wall of the vomer narrows and becomes a raised thin sheet along the mesorostral groove (Figs 31, 34). As mentioned above, the vomer is dorsally overhung by the right premaxilla from a level 1180 mm posterior to the apex. As the right premaxilla is incomplete in that region, the overhanging might have originally extended farther anteriorly. Just anterior to the level of the antorbital notch, a thin sheet of vomer may be present medial to the right premaxilla, with a slightly concave dorsal surface. Alternatively, this thin sheet could be made of the premaxilla. On the left side of the mesorostral groove, the vomer is also thickened

from a level some centimetres anterior to the left premaxillary foramen and medial to the left premaxillary sac fossa. This area might correspond to the origin of the nasal plug muscle. The posterior portion of the mesorostral groove is distinctly shifted to the right side.

In ventral view of the rostrum, the vomer is exposed between the premaxillae as a spindle-shaped strip (Fig. 32). The strongly abraded posteriormost portion of the rostrum hides the end of the exposure, as well as most features of the palate.

Frontal

Although partly abraded, the preorbital process of the right frontal is robust and dorsoventrally thick (Fig. 33). Its anterior margin is at the anteroposterior level of the bottom of the antorbital notch. In lateral view, the preorbital process is subcircular and, as mentioned above, separated from the antorbital process of the maxilla by a deep notch. The preorbital process of the frontal is not significantly lower than the lateral margin of the rostrum at its base, differing from *Aprixokogia*, *Aulophyseter morricei*, *Idiophyseter*, *Physeter* and *Scaphokogia*. The orbit is proportionally short (horizontal distance between ventralmost tip of preorbital process and centre of postorbital process 200 mm), with a strongly concave dorsal roof. The postorbital process is only partly preserved, but its robust base is roughly as longitudinally wide as the preorbital process. Based on the subtriangular section on the horizontal break of the postorbital process (anteroposterior length 123 mm; mediolateral length 120 mm), we estimate that the process was originally much longer, probably approaching the apex of the zygomatic process of the squamosal. The posterior surface of the postorbital process, corresponding to the dorsoventrally high anterior wall of the transversely broad and dorsoventrally high temporal fossa, is slightly tilted anterodorsally. The temporal fossa is therefore somewhat anteriorly longer in its dorsal portion than in its ventral portion.

In dorsal view, the right frontal is widely exposed lateral to the maxilla, from the preorbital process to the postorbital process. As mentioned above, in the supracranial basin, the medial portion of the right frontal is exposed between the right maxilla and premaxilla.

In ventral view, the frontal groove is oblique, diverging from the sagittal plane of the skull with an angle of about 60°. No other feature of the orbit region could be detected, due to the poor preservational state of this region.

Lacrimal/jugal

The antorbital portion of the right jugolacrimal complex is partly preserved. It is not possible to distinguish between the two bones. In lateral view, the dorsalmost part of the complex is as long anteroposteriorly as the antorbital process of the maxilla (Fig.

33). The contact with the latter is sinuous and moderately sloping anteroventrally. From this contact, the jugolacrimal complex is directed posteroventrally, forming the robust anterior part of the zygomatic arch. The jugal very probably originally contacted the zygomatic process of the squamosal, ventrally closing the orbit as in most odontocetes (a noticeable exception is the extant *Kogia*).

Squamosal

Only the right squamosal is preserved, and the lateral, dorsal and ventral surfaces of the zygomatic process are damaged (Figs 31–33. The zygomatic process is anteriorly long, with an estimated horizontal length from the anterior tip of the process to the posterior margin of the squamosal of 530 mm. The process is robust; its triangular section at mid-length has a transverse width of more than 175 mm and a vertical height of more than 180 mm. The anterior part of the dorsal margin of the zygomatic process is roughly horizontal; it progressively rises posterodorsally, laterally bordering the posteroventral part of the temporal fossa before joining the temporal crest. The maximum separation between the zygomatic process of the squamosal and the medial surface of the temporal fossa is broad. The preserved squamosal parts of the posterior and posteromedial walls of the temporal fossa are thin, contrasting with the thick anterior and anterodorsal margins made by the frontal. The postglenoid process of the squamosal is lost. However, considering the horizontal section at its base and the slope of the mandibular fossa, this process was probably short. The mandibular fossa is wide and faces anteroventromedially. The tympanosquamosal recess cannot be differentiated from the mandibular fossa. The falciform process is either absent or very reduced. We estimate that the posttympanic process is anteroposteriorly short, as in *Physeter*.

Tympanic bulla

A part of the enlarged posterior process of the tympanic may be preserved posterior to the external auditory meatus. Indeed, the bone in this area is cancellous and this bone is in a position usually occupied by this posterior process in physeteroids (see the condition in *Acrophyseter* above). Even if a suture is detected in section, the outline of this hypothetical large process cannot be inferred. The posterior process is not located within a deep laterally opening notch, unlike *Kogia* and *Praekogia*.

Exoccipital

In posterior view, the right exoccipital has a preserved height of 420 mm. The oblique width between the ventromedial margin and the lateral margin is more than 330 mm. The posterior surface of the exoccipital is slightly concave.

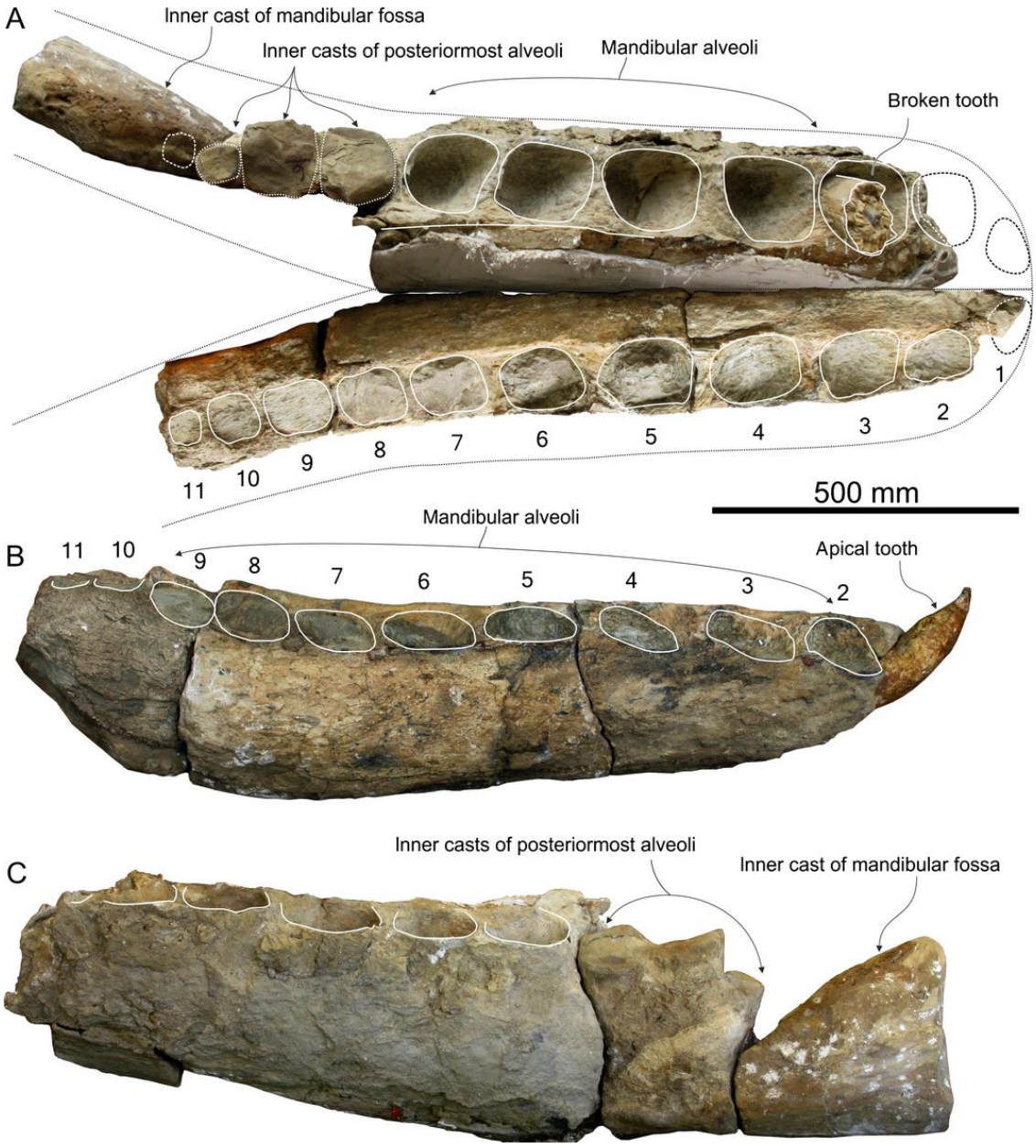

Fig. 35. Mandibles of *Livyatan melvillei* MUSM 1676 (holotype), Cerro Colorado, early late Miocene of the Pisco Basin, Peru. A, dorsal view; B, right lateral view with apical tooth repositioned in the corresponding alveolus; C, left lateral view. Some plaster is retained along the medial wall of the left mandible and alveoli are partly filled with sediment, especially on the right side. Alveoli are delimited by a solid line.

Mandibles

Right and left mandibles are preserved mostly in the symphyseal region (Fig. 35; Table 8). The dolomitized inner cast of the posterior portion of the left mandible provides additional data about the last alveoli and the post-alveolar region. Even if the outer surface of each mandible is abraded, minimum dimensions could be

measured. Each mandible is higher than wide at each level, with a large transverse section, much more robust than in *Physeter* and other large physeteroids, including *Idiorophus*, *Physeterula* and *Zygophyseter*. Based on the better-preserved right side, a count of 11 deep alveoli for each lower jaw is proposed. Here again, this tooth count is lower than in any other physteroid, except for *Kogia* spp. (10–16 in *K. breviceps* and 8–13 in *K. sima*; Caldwell & Caldwell, 1989). The largest alveoli are alveoli 3–6, with transverse diameters ranging from 124 to 134 mm (Table 9). Preserved anterior alveoli are slightly smaller, with a transverse diameter of 122 mm for left alveolus 2. The poorly preserved right alveolus 1 probably corresponds to a detached tooth (see below) with a maximum diameter of the root equal to 81 mm. Therefore, we suggest that a significant decrease of the diameter of the lower alveoli and corresponding teeth only occurs in the first apical position. Posteriorly, the size decrease is more progressive, with transverse diameters of alveoli 8–11 ranging from 115 to 53 mm. The first anterior alveolus is directed anterodorsally, with an angle of about 45° to the horizontal. The anterodorsal slope of more posterior alveoli decreases progressively and more than half the alveoli are roughly dorsally and somewhat laterally directed. Similarly to the upper alveolar grooves, the interalveolar septa are thin. In dorsal view, most of the alveoli, except the posteriormost, are located at a short distance from the lateral margin of the mandible.

Table 8. Measurements (mm) on the mandibles of *Livyatan melvillei* MUSM 1676 (holotype), modified from Lambert et al. (2010a)

Length of lower alveolar groove as preserved: distance between anterior border of right alveolus 2 and posterior border of right alveolus 11	123.0
Maximum height of right mandible (level alveolus 8)	+30.6
Maximum height of left mandible (level alveolus 7)	+36.0
Maximum width of right mandible (level alveolus 5)	+19.3
Maximum width of left mandible (level alveolus 3)	+20.5

+, Incomplete.

Table 9. Transverse diameter (mm) of right/left mandibular alveoli of *Livyatan melvillei* MUSM 1676 (holotype), modified from Lambert et al. (2010a)

Alveolus number	Right	Left
1	-	-
2	12.2	-
3	13.4	12.8
4	13.1	13.1
5	13.4	13.6
6	12.4	13.1
7	12.0	12.1
8	11.5	e12.5
9	11.3	e11.8
10	8.4	+60
11	5.3	-

+, Incomplete; e, estimate; –, no data.

The unfused symphysis extends until the level of the anterior margin of alveolus 8. The medial separation between right and left alveolar grooves progressively increases posteriorly, from the anterior apex to the end of the symphysis, followed by a slightly more abrupt divergence in the postsymphyseal region, related to the divergence of the rami.

In lateral view, the dorsal margin of each mandible remains roughly horizontal for the whole length of the alveolar groove. The ventral margin is slightly convex and rises anterodorsally, with a maximum dorsoventral height of the mandible at the level of alveoli 7–8 (Table 8). Marks on the inner cast of the posterior portion of the left mandible suggest an anteriorly pointed and long mandibular foramen extending nearly until the level of alveolus 11.

A posterior fragment of the right mandible, found attached to the right squamosal, includes a part of the mandibular condyle (Fig. 33). Although the outline of the condyle cannot be assessed, the preserved element suggests that the condyle was close to the ventral margin of the mandible, as in other physeteroids for which the lower jaws are known (see Bianucci & Landini, (2006).

Teeth

As mentioned above, the estimated tooth count for *Livyatan melvillei* is nine teeth for each maxilla and 11 teeth for each mandible. All the teeth preserved are single-rooted, with a roughly cylindrical robust root (Figs 32, 33, 35, 36). Most of the teeth from the upper and lower jaws have a maximum transverse diameter of the root > 100 mm (Tables 10 and 11), differing from all other known physeteroids including *Physeter*, *Albicetus oxymycterus* and the lectotype 45 teeth of *Scaldicetus antwerpiensis* du Bus, 1867. Differing from *Physeter* and kogiids, enamel is observed on the preserved crowns. It should be noted that enamel has been detected on fetal teeth of *Physeter*, being later covered with cementum (Ohsumi, Kasuya & Nishiwaki, 1963).

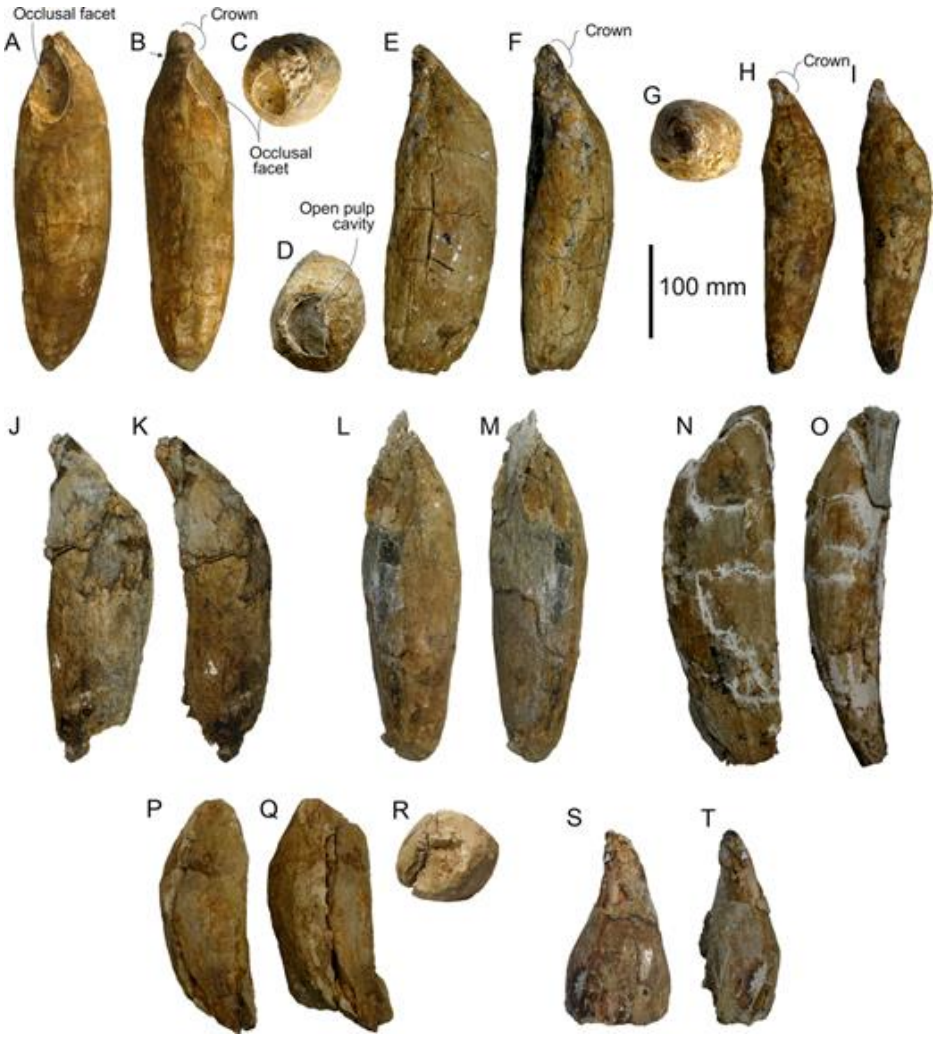

Fig. 36. Detached mandibular teeth of *Livyatan melvillei* MUSM 1676 (holotype), Cerro Colorado, early late Miocene of the Pisco Basin, Peru. A–C, tooth c (presumably right 7); D–F, tooth a (right 5); G–I, tooth e (right 1); J–K, tooth d (right 2); L–M, tooth b (right 6); N–O, tooth h (left 2 or 3); P–R, tooth I (left?); S–T, tooth f (right 3). A, E, H, J, L, N, P, S in labial view; B, F, I, K, M, O, Q, T in distal view; C, G, R in occlusal view; D in ventral view. Occlusal facet and open pulp cavity of tooth c are indicated with white stippled lines.

Table 10. Maximum preserved diameter of right/left maxillary teeth of Livyatan melvillei MUSM 1676 (holotype), modified from Lambert et al. (2010a)

Alveolus number	Right	Left
1	10	9.3
2	-	11.1
3	-	-
4	12.1	11.5
5	11.5	12.2
6	11.5	10.8
7	-	9.6
8	-	-
9	-	-

–, No data.

Table 11. Measurements (mm) on detached mandibular teeth of *Livyatan melvillei* MUSM 1676 (holotype), modified from Lambert et al. (2010a)

Tooth	Proposed position along tooth row	Total length	Crown length	Maximum diameter at crown base	Maximum diameter of root	Diameter of root perp. to maximum diameter	Maximum circumference of root	Height occlusal groove from apex of tooth
e	r1	+31.5	3.1	2.4	8.1	7.1	25	-
d	r2	+32.5	+2.5	2.5	10.7	8.5	31	-
f	r3	-	-	-	11.1	-	-	-
g	r4	-	-	-	+10.4	-	-	-
a	r5	+35.7	-	-	11.1	9.5	33.5	-
b	r6	+36	-	-	11.1	10.0	33.3	+12.5
c	r7	+36.1	-	-	10.2	9.4	31.6	+11.3
h	l2-3	+36.2	-	-	10.6	8.2	31.9	-
i	l?	+32	-	-	+10.2	-	-	+9.6

+, Incomplete; –, no data; ?, exact position unknown. Letters in the first column correspond to letters in caption to Figure 36.

Upper teeth

For the upper dentition, only parts of the roots are preserved in situ: six (1–2; 4–7) could be measured in the left maxilla and five (1; 4–7) in the right maxilla (Table 10). Sections perpendicular to the long axis of the teeth are roughly circular, but because mesial teeth are anteroventrally directed, preserved sections are not perpendicular to the long axis of the tooth, being therefore oval. Transverse diameters of roots at the surface of the alveoli range from 93 to 122 mm, with the most robust teeth at that level being teeth 4–6. These measurements provide only minimum diameters, as the root can be even more robust outside the alveolus, due to the continuous addition of cementum layers on the outer surface of the roots in physeteroids (Hohn, (2002). The dentine–cementum boundary is easily detected based on aspect and colour on the transverse section of the root at the surface of the alveolus; the maximum radial thickness of the cementum ranges from 21 to 28 mm in right maxillary teeth 1 and 4–6.

Lower teeth

For the lower dentition, only the basal part of the root of one left tooth (left tooth 3) is preserved in situ. Nine additional teeth, with varying degrees of preservation, were found detached around the two mandibles (Figs 33, 36; Table 11). Their position in the lower jaws is inferred based on the outline and measurements of the presumed corresponding empty alveoli, as well as the curvature of their root and crown. Mesialmost teeth have a lesser maximum diameter of the root than teeth more intermediate on the tooth row; they are also more distinctly curved, for both the root and the crown. Intermediate teeth are the largest, and their long axis is closer to a straight line. Distalmost teeth also have a smaller root diameter, but they are less curved than mesialmost teeth. Considering the curve of the root and crown, and the position of occlusal facets where present, most of the preserved lower teeth seem to originate from the right mandible. None of the teeth is complete, but some (for example the right teeth 1, 5 and 7) only lack a few fragments at the base of the root or at the apex of the crown. All the well-preserved teeth have a maximum height > 310 mm. The highest measured tooth is left tooth 2–3, with a maximum height of at least 362 mm. The shortest is right tooth 1, at approximately just over 315 mm. However, the height of the distalmost teeth (8–11) is unknown; considering the size of the corresponding alveoli, teeth 10–11 were probably the shortest, as is observed in *Acrophyseter deinodon* above.

Most of the crowns are poorly preserved or completely lacking; this condition is partly based on preservation bias, but also due to wear or breaks during the animal's life. In the best-preserved teeth, crown height is less than one-tenth of tooth height, with a maximum diameter at crown base of 24–25 mm. The crown is covered with

enamel; along break surfaces, a thickness of the enamel layer of about 3 mm could be measured. The enamel surface is nearly smooth, with very subtle longitudinal grooves. However, the preserved surfaces are too small for detecting variation in the degree of surface wear.

The massive roots of the lower teeth have maximum diameters up to 111 mm, which is slightly smaller than the maximum diameter in the largest upper teeth. Transverse sections are oval, obliquely flattened along a mesiolingual to distolabial or mesiolabial to distolingual axis. The flattened sections give a ratio between diameter perpendicular to maximum diameter and maximum diameter of 0.77–0.92. In the mesialmost teeth, the diameter of the root progressively decreases towards the base (e.g. in right tooth 1), whereas in intermediary, less curved teeth, a great diameter is retained for a longer part of the root, with a more abrupt proximal decrease (particularly in right tooth 5). In several teeth, the surface of the root is marked with roughly straight longitudinal grooves.

In several teeth, the apex of the crown is truncated along a subhorizontal plane. At least in two presumably mesial teeth, this truncation probably occurred during the life of the animal, as the surface is smoothly worn. Occlusal attritional wear facets are seen in at least four lower teeth, including right teeth 1 and 6–7 (Fig. 36). The facet runs from the obliquely truncated crown to the distal to distolabial surface of the root, forming in some teeth a deeply excavated fossa. With a height of 96–125 mm, the highest occlusal facets involve 30–35% of the preserved tooth height.

Obviously depending on the basal diameter of the root, the aperture of the pulp cavity is either narrow, as in right tooth 1 with a small basal diameter, or much wider, with a diameter up to 59 mm in right tooth 5. In the extant *Physeter*, the filling of the pulp cavity occurs late in ontogeny; fully adult specimens often display open pulp cavities (e.g. Boschma, 1938).

Phylogeny

Analysis

Starting from the data-matrix of a previous phylogenetic analysis of Physeteroidea (Lambert et al., 2010a), we added 13 characters (see Appendix S1). One character was deleted (projection of longitudinal axis of skull compared to longitudinal axis of body), due to the difficulty to code it unambiguously in many fossil taxa. Several codings were corrected thanks to new observations and/or new interpretations. The final number of characters is 53. We coded seven additional taxa, including the outgroup basilosaurid *Cynthiacetus peruvianus*, *Acrophyseter robustus* sp. nov., *Acrophyseter* sp. MUSM 2182, three Argentinian physeteroids (the early Miocene

Diaphorocetus poucheti and Idiorophus patagonicus, and the late Miocene '*Aulophyseter' rionegrensis*), and the middle to late Miocene Californian species *Idiophyseter merriami* (see Appendices S1 and S2). All the included taxa were directly observed and photographed by at least one of us, except *for Agorophius pygmaeus* Müller, 1849, *Brygmophyseter shigensis*, *I. merriami* and *Idiorophus patagonicus*, for which data were taken directly from the literature (Lydekker, 1893; Kellogg, 1925a; Fordyce, 1981; Hirota & Barnes, 1995; Kimura et al., 2006). For these taxa, a slightly lower number of question marks in the data-matrix would be expected following the direct observation of specimens. All characters were treated as unordered. The analysis was undertaken with the software Paup (version 4b10; Swofford, 2001), using the tree-bisection-reconnection algorithm, for 10 000 replicates and one tree saved per replicate. A preliminary heuristic search, with equal weights for all characters, produced a poorly resolved consensus tree. Therefore, we down-weighted homoplastic characters using the method of Goloboff (1993), with the default value of 3 for the constant k.

Finally, several morphological characters (characters 3, 6, 8, 26, 36, 37 and 44; see Discussion) were optimized using the free software Mesquite (version 3.03; Maddison & Maddison, 2015).

Results

This analysis resulted in three most parsimonious trees with consistency index (CI) 0.60 and retention index (RI) 0.70. The strict consensus of these trees is shown in Figure 37, with bootstrap support values. The only unresolved relationships are found in the genus *Acrophyseter*. Similarly to the result of past analyses (Lambert, 2008; Lambert et al., 2010a; Boersma & Pyenson, 2015; Vélez-Juarbe et al., 2015), Eudelphis is the first stem physeteroid to branch. At the next branching among stem physeteroids, a clade including *Acrophyseter*, *Brygmophyseter* and *Zygophyseter* is recovered, as proposed in three previous analyses (Lambert et al., 2010a; Boersma & Pyenson, 2015; Vélez-Juarbe et al., 2015). This clade is only poorly supported by four characters: widening of the supracranial basin on the right side, overhanging the right orbit (char. 20, state 1; unknown in *Brygmophyseter*); number of mandibular teeth between 12 and 14 (char. 38, state 1); deep and rectilinear narrow groove in ventral surface of squamosal medial to tympanosquamosal recess (char. 47, state 1; only observed in *Acrophyseter*); and lateral margin of atlas convex, with laterally pointed transverse process (char. 52, state 1; unknown in *Brygmophyseter* and many other fossil physeteroids).

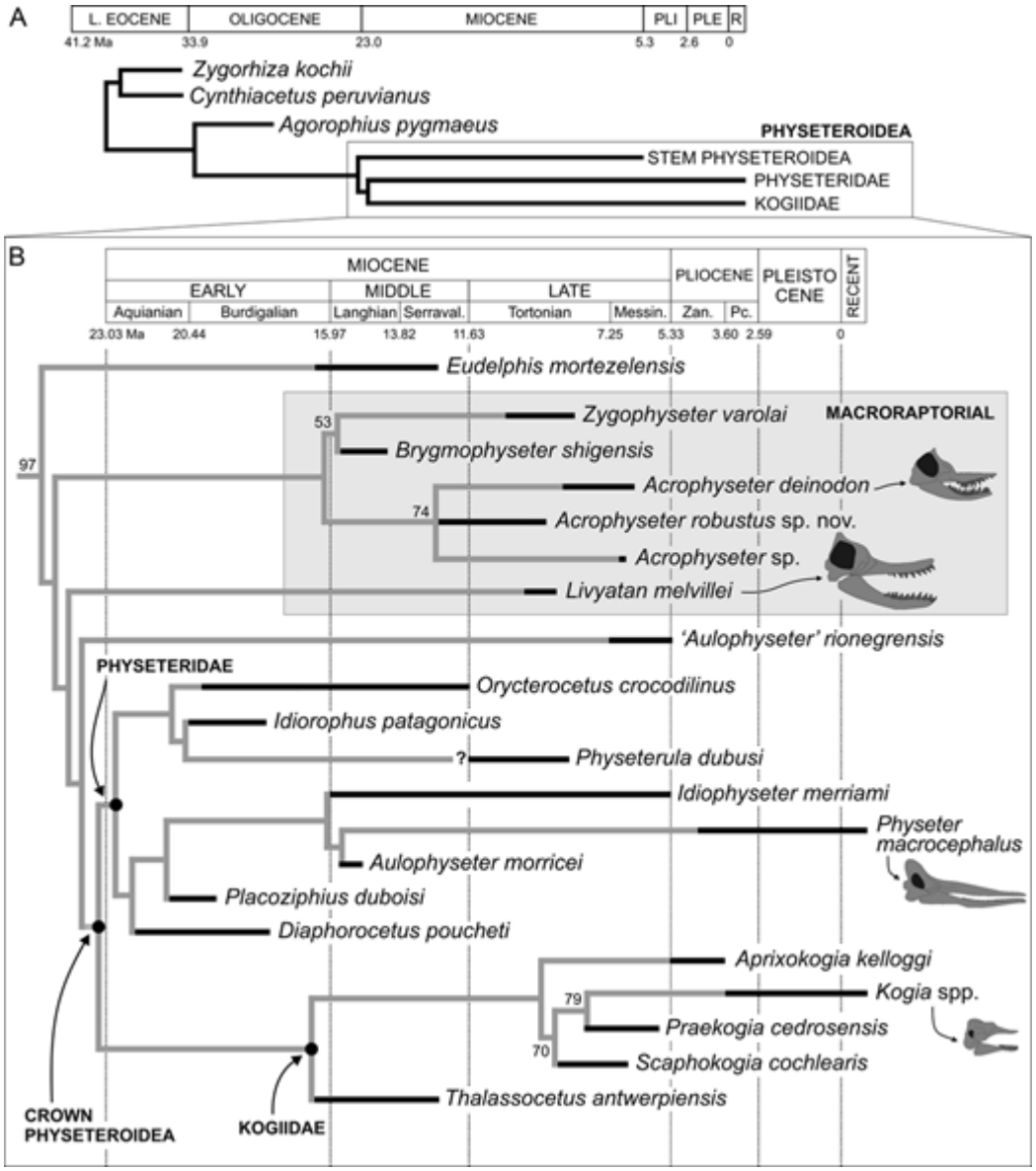

Fig. 37. Consensus of three most parsimonious trees resulting from the cladistic analysis of 53 morphological characters for 21 physeteroids and three outgroups. A, relationships between the paraphyletic stem Physeteroidea, Physeteridae and Kogiidae in a temporal framework; B, detail of the relationships between physeteroids in a temporal framework. Temporal ranges either fill the whole corresponding stage, or, if more precise data are available, start or end before the limits of the corresponding stage. Ranges not discussed in detail in the text are taken from the Paleobiology Database and references therein; Bianucci & Landini, 2006; Uhen, Fordyce & Barnes, 2007; Lambert, 2008; Pyenson et al., 2009; Boessenecker & Churchill, 2015. A paraphyletic group of macroraptorial physeteroid species is inserted in a light grey box. Numbers associated with branches are bootstrap values. Skull outlines for *Acrophyseter deinodon*, *Kogia*, *Livyatan* and *Physeter* are not at the same scale (see Fig. 38 for details).

The genus *Acrophyseter* is defined in this analysis by: antorbital notch transformed into a narrow slit (char. 9, state 2); both nasals present (char. 19, state 0; interpreted as a reversal here; a character often difficult to code in fossil taxa); frontal–maxilla suture making and angle > 35° from the longitudinal axis of the rostrum (char. 25, state 2); and ventral margin of mandible distinctly convex (char. 50, state 1). Confirming the mosaic of similarities and differences observed in MUSM 2182, relationships within Acrophyseter are not resolved: in the three shortest trees, MUSM 2182 is either sister-group to *A. robustus*, or sister-group to *A. deinodon*, or A. deinodon and *A. robustus* are more closely related.

The next, more crownward clade, including *Livyatan*, *'Aulophyseter' rionegrensis*, Kogiidae and Physeteridae, is supported by seven characters: ratio between width of right premaxillary foramen and width of premaxilla at that level ≤ 0.20 (char. 16, state 0; reversal); preorbital process of the frontal at approximately the same level as the lateral margin of rostrum base (char. 24, state 1); falciform process reduced to a simple peg or absent (char. 31, state 2; unknown in Livyatan and 'A.' rionegrensis); transverse compression of posterior lower teeth (char. 39, state 0); no notch in the anterior margin of the basihyal (char. 53, state 2; unknown in *Livyatan* and many other fossil taxa); posteromedial outline of the pars cochlearis flattened (char. 49, state 1; unknown in *Livyatan*); and ratio between length of the zygomatic process and bizygomatic width of skull < 0.35 (char. 46, state 1). The content of this large clade matches a previous analysis (with a lower number of taxa; Lambert et al., 2010a), although the topology somewhat differs. As proposed by Lambert et al. 2010a), *Livyatan* seemingly belongs to a lineage different from the one including the other stem physeteroids with enlarged teeth (*Acrophyseter*, *Brygmophyseter* and *Zygophyseter*). The position of *'A.' rionegrensis* confirms that it is not closely related to *Aulophyseter morricei*, as suggested earlier by several authors (Kazár, 2002; Bianucci & Landini, (2006). The former differs from *A. morricei* in, among others: premaxillae much narrower in dorsal view on the rostrum; a proportionally large left premaxillary foramen; the presence of deep alveoli in the maxilla; the preorbital process being not lower than the dorsolateral margin of the orbit; and the anteroposteriorly much longer temporal fossa, with a correspondingly longer zygomatic process of the squamosal.

Crown Physeteroidea (Kogiidae + Physeteridae) are supported by only two characters: left premaxillary foramen very small or absent (char. 15, state 1) and temporal fossa approximately as long as distance between preorbital process of the maxilla and anterior wall of temporal fossa (char. 26, state 1).

In the analysis, the family Physeteridae includes eight taxa (*Aulophyseter morricei*, *Diaphorocetus*, *Idiophyseter*, *Idiorophus*, *Orycterocetus crocodilinus*, *Physeter*, *Physeterula* and *Placoziphius*), sharing four characters: ratio between rostrum length and skull width ≤ 1.2 (char. 1, state 1; interpreted as a reversal); presence of two large

dorsal infraorbital foramina on the right side (char. 11, state 2); occipital shield flat or concave forming an angle of about 90° with the longitudinal axis of the rostrum (char. 30, state 2); and dorsal process of the periotic anteroposteriorly short but dorsally extended beyond the medial margin of the internal acoustic meatus (char. 48, state 1; interpreted as a reversal). The content of the family differs from several previous analyses (Lambert, 2008; Lambert et al., 2010a; Vélez-Juarbe et al., 2015) in the inclusion of *O. crocodilinus* and *Placoziphius*. These two genera were already proposed as physeterids in two earlier phylogenies (Bianucci & Landini, 2006; Lambert et al., 2008). Among physeterids, the clade including *A. morricei*, *Idiophyseter* and *Physeter* is characterized by: right premaxillary foramen at same level or posterior to antorbital notch (char. 17, state 2); preorbital process of the frontal considerably lower than the lateral margin of rostrum base (char. 24, state 2), and frontal–maxilla suture forming an angle >35° with the longitudinal axis of the rostrum (char. 25, state 2), whereas the more inclusive clade also containing *Placoziphius* is supported by: dorsal exposure of the maxilla on the rostrum wider than the premaxilla all along (char. 4, state 2) and upper alveoli shallow or absent (char. 6, state 1). The Argentinian taxon Idiorophus shares similarities with *Physeterula* and *O. crocodilinus* at the level of the temporal fossa and dimensions, whereas *Diaphorocetus* is seemingly more crownward. However, more complete specimens would most likely further support the phylogenetic affinities of these Patagonian genera. Also, considering the high number of genera within the family, the review of part of the specimens and additional comparisons may result in the placement of several species in the same genus, an investigation beyond the scope of this paper.

The family Kogiidae is the best supported clade among physeteroids, defined based on 14 characters: maxillae, premaxillae and vomer, all reaching the tip of the rostrum (char. 2, state 1; unknown in *Praekogia* and *Thalassocetus antwerpiensis* Abel, 1905); supracranial basin extended onto the whole dorsal surface of the rostrum (char. 3, state 2; unknown in *Praekogia* and *Thalassocetus*); skull width <40 cm (char. 8, state 0); right premaxilla not widened posteriorly (char. 13, state 0; interpreted as a reversal); both nasals absent (char. 19, state 2; unknown in *Aprixokogia*); presence of a sagittal crest (char. 14, state 1); right premaxillary foramen at same level or posterior to antorbital notch (char. 17, state 2); right maxilla reaching the sagittal plane of the skull on the posterior wall of the supracranial basin (char. 21, state 1); long projection of the lacrimal–jugal between frontal and maxilla (char. 23, state 1; unknown in *Thalassocetus*); posterior extension of the posterior process of the periotic parallel to the horizontal plane of the bone (char. 33, state 1; only known in *Kogia* and *Scaphokogia*); no contact between jugal and zygomatic process of squamosal (char. 45, state 2; only known in *Kogia*); postorbital process of the frontal much ventrally extended (char. 43, state 1); symphyseal angle >55° (char.

51, state 2); and ventral margin of mandible concave in lateral view (char. 50, state 2; only known in *Kogia*). The content of the clade is the same as in Lambert et al. 2010a and Vélez-Juarbe et al. (2015), and the only difference (except for the addition of *Nanokogia* and *Kogia* pusilla in the latter) is that *Aprixokogia* is here more crownward than *Thalassocetus*.

Although several taxa were added to the data-matrix compared to previous analyses, the high number of missing data (question marks) due to the fragmentary state and relatively low number of specimens known (and described) for many taxa does not allow well-supported relationships to be recovered for many parts of the tree (as expressed by the generally low bootstrap support values). Indeed, only minor changes in the data-matrix (deletion of characters or taxa) lead to modifications in the content and topology of several clades, especially as regards those taxa included here in the family Physeteridae. We suspect that more complete specimens of *Diaphorocetus*, *Eudelphis*, *Idiophyseter*, *Idiorophus*, *Physeterula*, *Placoziphius* and *Thalassocetus*, as well as an increase in the number of postcranial characters, would modify and hopefully improve physeteroid relationships.

Discussion

Timing of physeteroid radiations

The timing of the origin of each physeteroid clade is discussed in the context of these phylogenetic results (Fig. 37). The oldest described physeteroid is *Ferecetotherium kelloggi*, from the Maikop Group, Chattian (Late Oligocene) of Azerbaidjan (Mchedlidze, 1970). In addition to the low stratigraphic resolution for the type locality, the phylogenetic affinities of the species are difficult to determine due to the fragmentary state of the holotype; indeed, apart from the typically physeteroid-like periotic, figured cranial elements do not display phylogenetically relevant characters. Therefore, this record only indicates an origin of physeteroids before the Oligocene–Miocene boundary. Molecular data provide an estimated divergence time of physeteroids and other extant odontocete lineages during the Early Oligocene (McGowen, Spaulding & Gatesy, 2009; Steeman et al., 2009; Hassanin et al., 2012; see also comments in Vélez-Juarbe et al., 2015). It is thus probable that we still miss the early fossil record of physeteroids and/or that we have not yet succeeded in finding or identifying extinct relatives of the superfamily in Oligocene deposits.

Brygmophyseter is the oldest member of the clade also including *Acrophyseter* and *Zygophyseter*. The type and only known species is *B. shigensis*, from the upper member of the Bessho Formation, Japan, dated to the Langhian (Hirota & Barnes, 1995; Kimura et al., 2006).

Three potential candidates are identified for the oldest physeterid.

Placoziphius duboisi originates from the Edegem Sands Member of the Berchem Formation, Belgium (Van Beneden, 1869; Misonne, 1958; Lambert, 2008). This member is dated based on dinoflagellate cysts from the latest Aquitanian to early Burdigalian (upper part of biozone DN2a and DN2b; Louwye, 2005). The type specimens of *Diaphorocetus poucheti* and *Idiorophus patagonicus* were both found in early Miocene deposits of Argentina (Moreno, 1892; Lydekker, 1893; Cozzuol, 1996; Cione et al., 2011). According to the Paleobiology Database, *D. poucheti* is from the Monte León Formation, the latter having been recently radiometrically dated to the Aquitanian to early Burdigalian (Parras, Dix & Griffin, 2012), whereas *I. patagonicus* is from the partially correlated Gaiman Formation. The vertebrate-bearing levels of this latter unit are tentatively dated to the early Burdigalian, based on radiometric dating of the underlying Sarmiento Formation (Marx & Fordyce, 2015).

The oldest kogiid currently known is probably *Thalassocetus antwerpiensis*, from the Miocene of Belgium. Although stratigraphic information associated with the lectotype is scanty (‘Boldérien d'Anvers’ in Abel, 1905), this information and the external aspect of the bones point to an origin in the Berchem Formation (Misonne, 1958; Lambert, 2008). The vast majority of the cetacean remains found in the Berchem Formation comes from the youngest member, the Antwerpen Sands Member (Misonne, 1958; O. Lambert, pers. observ.). The latter is dated based on dinoflagellate cysts from the latest Burdigalian to Serravallian (biozones DN4–DN7; Louwye, 2005). An upper limit for the age of the lectotype of *T. antwerpiensis* is therefore proposed at the end of the Serravallian.

These lower to middle Miocene earliest physeterid and kogiid records are not too far from the recent molecular estimates for the divergence of the two crown physeteroid families, with a mean age of 24.21 Ma (late Chattian) by McGowen et al. (2009) and an estimate at 21.9 ± 3.6 Ma (late Chattian to early Burdigalian) by Hassanin et al. (2012).

Evolutionary trends

Body size

One of the most striking aspects of the high degree of morphological disparity observed among physeteroids is the diversity of body sizes (Fig. 38). Bizygomatic width of the skull proves to be a relevant proxy for investigating the evolution of body size in a given neocete clade (Lambert et al., 2010a; Pyenson & Sponberg, 2011). When mapping character 8 (bizygomatic or postorbital width, nearly

equivalent in many stem odontocetes) on the consensus tree in Figure 37, different scenarios occur along different lineages (see also Boersma & Pyenson, 2015). In the macroraptorial clade including *Acrophyseter*, *Brygmophyseter* and *Zygophyseter*, a marked increase in size is observed in the subclade of the latter two, with a bizygomatic width higher than 600 mm. Based on skeletal measurements (part of the postcranial skeleton preserved), the body length of *Zygophyseter varolai* was estimated to 6.5–7.0 m (Bianucci & Landini, 2006), whereas an estimate of 4.0–4.3 m is calculated above for *Acrophyseter deinodon*. Even more abrupt, an independent size increase occurs in the lineage of *Livyatan melvillei* (postorbital width of 1900 mm in the latter). Based on a comparison of cranial dimensions with *Physeter* and *Z. varolai*, the body length of L. melvillei was estimated to 13.5 and 16.2–17.5 m respectively, in the range of adult male *Physeter macrocephalus* (Lambert et al., 2010a: Figs 40, 41). Size evolution is more complex within the poorly supported Physeteridae clade, with on the one hand a probable two steps size increase towards *P. macrocephalus* (bizygomatic width up to 2200 mm and body length up to 18.3 m in adult males, but considerably smaller in females; Clarke & Paliza, 1972; Rice, 1989), with *Aulophyseter morricei* as an intermediate stage, and on the other hand a less marked increase towards the seemingly closely related *Idiorophus* and *Physeterula*. Finally, a marked dwarfism unambiguously defines the family Kogiidae, with a bizygomatic width lower than 400 mm in all taxa included in the analysis, as well as in the recently described *Nanokogia* (Vélez-Juarbe et al., 2015).

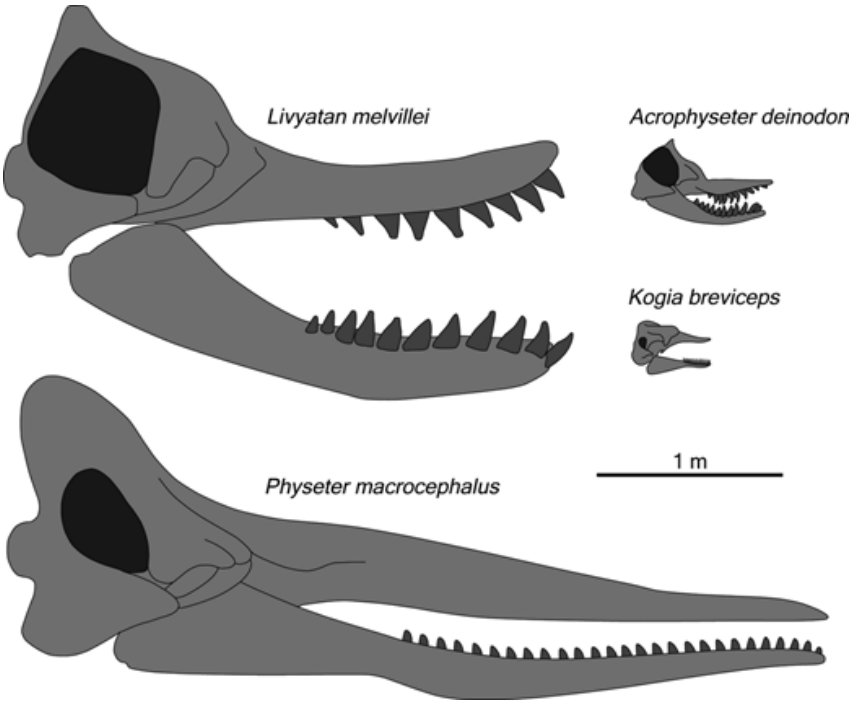

Fig. 38. Comparison of dimensions and shape for the skull, temporal fossa and teeth in the stem physeteroids *Acrophyseter deinodon* and *Livyatan mevillei*, the modern kogiid *Kogia breviceps*, and the modern physeterid *Physeter macrocephalus*. Skulls in right lateral view, all at the same scale. Some parts of the skull are reconstructed in the two fossil species..

Shape and extent of the supracranial basin

This key character of the superfamily is present in all the taxa of the cladistic analysis. However, its extent is limited to the facial area and posteriormost part of the rostrum in many genera. In the latter, the forehead is proposed to have been shorter anterodorsally than in *Physeter* (see for example the reconstruction of *Acrophyseter deinodon* in Fig. 39). Optimized on the consensus tree, the invasion of the rostrum by the supracranial basin (and the related anterodorsal development of the forehead, see Figs 40, 41) is proposed to have occurred independently at least three times among physeteroids: on the branch of Livyatan, on the branch of *Physeter*, and either once among kogiids (reversal in Scaphokogia) or twice (on the branch to *Aprixokogia* and on the branch to *Kogia* + *Praekogia*) (see comments in Vélez-Juarbe et al., 2015; for cranial morphological disparity in kogiids). Parallel evolution for this character is further supported by the markedly different soft tissue organization of the supracranial region in *Kogia* and *Physeter* (Cranford, Amundin & Norris, 1996; Cranford, 1999). In addition, and partly due to the contrast in forehead anatomy, the function(s) of this region most likely differ in these two taxa; although this is subject to debate (Cranford, 1999; Carrier, Deban & Otterstrom, 2002; Huggenberger et al., 2016), Physeter's enormous nose with anteriorly shifted blowhole cannot work acoustically (for echolocation or social acoustic display) and mechanicaly (head-butting hypothesis) in the same way as *Kogia*'s shortened and squarish head. Additionally, the mimicry shown by *Kogia* (with a head that is strikingly shark-like; Caldwell & Caldwell, 1989; Fordyce & Muizon, 2001) could not be applied to Physeter. In this context, it would be premature to propose a function for the enlarged supracranial basin of *Livyatan*, although size and proportions of the skull are somewhat more similar to *Physeter* than to *Kogia*. Nevertheless, considering the highly specialized nasal tracts and surrounding soft structures in the two extant sperm whale genera (Cranford et al., 1996; Cranford, 1999; Huggenberger et al., 2016), production and transmission of sounds probably played a major role in the evolution of the physeteroid supracranial basin.

Fig. 39. Artistic restoration of two individuals of *Acrophyseter deinodon* hunting the contemporaneous seagrass-consuming marine sloth *Thalassocnus natans* in late Miocene waters of the continental shelf off Peru. Art by A. Gennari.

Fig. 40. Artistic restoration of *Livyatan melvillei* preying upon a medium-size (c. 7 m long) cetotheriid baleen whale in early late Miocene waters off Peru. Modified from Lambert et al. 2010a). Art by C. Letenneur.

Fig. 41. Alternative artistic restoration of *Livyatan melvillei* preying upon the stem beaked whale *Messapicetus gregarius* in early late Miocene waters off Peru. Teeth stick out from the gum somewhat more than in Figure 40 and the 'nose' of the whale is more prominent. Art by A. Gennari.

Dental evolution

Proportionally enlarged teeth, as occuring in *Acrophyseter* (Fig. 39), *Brygmophyseter*, *Livyatan* (Figs 40, 41) and *Zygophyseter*, are either interpreted as being inherited from a basilosaurid-like ancestor or did evolve once or twice (in the *Acrophyseter–Brygmophyster–Zygophyseter* clade and in *Livyatan*) in the early evolutionary history of the superfamily.

Reduction of the upper dentition is interpreted here as occuring independently in two physeteroid lineages, among physeterids and among kogiids, leading to the loss of functional upper teeth embedded in alveoli in both *Kogia* and *Physeter* (Fig. 38). By contrast, the loss of dental enamel is proposed here to have occurred once, as the lack (or early covering by cementum) of enamel applies to all crown physeteroids (Kogiidae + Physeteridae) whose dentition is known. Although not occuring fully simultaneously, the loss of the functional upper dention and the loss of enamel may correspond together to a progressive specialization for suction feeding, as demonstrated in *Kogia* and *Physeter* (Werth, 2004, 2006; Bloodworth & Marshall, 2005; Johnston & Berta, (2011). Interestingly, in Physeter the suction process is thought to differ significantly from any other extant odontocete, including *Kogia*; the

exceptionally short and wide tongue of *Physeter*, situated at the very back end of the oral cavity, indicates that suction happens at the level of the oropharyngeal opening (Werth, 2004). This difference suggests that at least an additional step of suction feeding specialization evolved in the lineage of *Physeter*.

Size of temporal fossa

The evolution of the size of the temporal fossa (already partly discussed by Kazár, 2002) is critical for commenting on changes in feeding technique (see above for the interpretation of the jaw muscles masseter, pterygoid and temporalis in *Acrophyseter deinodon*); it is reflected in two characters of the cladistic analysis: (1) length of the temporal fossa compared to the distance between preorbital process of the maxilla and anterior wall of temporal fossa and (2) height of the fossa compared to the total height of the skull. An anteroposteriorly long fossa, as seen in *Acrophyseter*, related genera and *Livyatan*, is interpreted as plesiomorphic. Shortening of the fossa occurs in several steps. The first step (fossa roughly as long as the distance between preorbital process of the maxilla and anterior wall of temporal fossa) occurs at the crown Physeteroidea node (with a reversal in *Aprixokogia*) or independently in physeterids and part of the kogiids (as seen in *Aprixokogia*). The second step (fossa distinctly shorter than the distance between preorbital process of the maxilla and anterior wall of temporal fossa) appears separately in two clades: *Aulophyseter morricei* + *Physeter* and *Kogia* spp. (Fig. 38).

Height of the fossa in *Acrophyseter*, related genera and *Livyatan* is similarly interpreted as plesiomorphic. A drastic reduction of height occurs in the clade including ‘A.’ rionegerensis and crown Physeteroidea, with a reversal, on the one hand, for *Orycterocetus crocodilinus*, *Physeterula* and possibly *Idiorophus*, and, on the other hand, for *Aprixokogia*.

Together, dental reduction (decrease of size and loss of functional upper teeth), enamel loss, and reduction of the length and size of the temporal fossa indicate a progressive reduction in the use of jaws and teeth for raptorial feeding, and further specialization towards suction feeding, as observed in several other odontocete lineages (e.g. several delphinids and crown ziphiids; Werth, 2006; Lambert, Muizon & Bianucci, 2013). Although a general trend can be detected among physeteroids, not all changes occur simultaneously (different combinations of characters are found in different fossil taxa) and some changes occur in parallel in several lineages whereas others seemingly emerge once (eventually followed by reversals). Such a complex process further highlights the great value of fossil species to better characterize the evolutionary history of traits characterizing extant species, especially for clades whose present morphological disparity and ecological diversity proves to be a relict of a formerly much higher degree of disparity and diversity (Vélez-Juarbe et al., 2015).

As for the proposed macrophagy of *Acrophyseter*, *Brygmophyseter*, *Livyatan* and *Zygophyseter*, although some of the morphological features (size of the temporal fossa and teeth, degree of development of the masseter muscle) of these taxa may have been partly inherited from basilosaurid-like ancestors, our interpretation of the jaw muscles of *Acrophyseter* suggests that more developed pterygoid muscles may yet represent a specialization associated with more powerful jaws. Whereas the observation of buccal maxillary exostoses in the holotype of *A. robustus* (Lambert et al., 2014) and of long occlusal facets in teeth of *Acrophyseter*, *Livyatan* and *Zygophyseter* further supports the hypothesis that these stem physeteroids were able to feed via macrophagous biting and tearing, no direct evidence (e.g. bite marks unambiguously attributed to stem physeteroids or stem physeteroid digestive tract contents) is still available. Therefore, proposals for prefered prey types mostly rely upon fossil assemblages and the size ratio between the potential prey and predator (e.g. *Acrophyseter* vs. the aquatic sloth *Thalassocnus* and *Livyatan* vs. a medium-sized cetotheriid or the beaked whale *Messapicetus*; Figs 39–41).

Faunal succession in the Pisco Formation

The Pisco Formation includes a stratigraphical succession of several vertebrate faunal assemblages identified as 'vertebrate levels' by Muizon & DeVries (1985), Muizon (1988) and Lambert & Muizon (2013). Most of these levels have been defined in the southern basin, the Sacaco Basin, and have been given a locality name (Fig. 1B), from the oldest to the youngest: ELJ (El Jahuay), AGL (Aguada de Lomas), MTM (Montemar), SAS (Sud-Sacaco) and SAO (Sacaco). The oldest level outcrops in the northern region of the Pisco Basin, in the Ica area: CLB level (Cerro la Bruja; Fig. 1A). It is noteworthy that some localities include other vertebrate levels than the level bearing their name. For instance, in the locality of Aguada de Lomas, in addition to beds corresponding to the AGL level, beds of the SAS, MTM and ELJ levels are encountered. In the locality of Sud-Sacaco, in addition to beds of the SAS level, beds of the MTM level are also present. Age estimates were provided for these levels by Muizon (1988): CLB, c. 11–13 Ma; ELJ, c. 8–9 Ma; AGL, c. 7.5–7 Ma; MTM, c. 6 Ma; SAS, c. 5 Ma; SAO, c. 4 Ma. Some of these estimates (but not for CLB) were calibrated on the basis of radiometric dates in the Sacaco Basin (Muizon & Bellon, 1980, 1986; see also Lambert & Muizon, 2013). New datings providing slightly to moderately older ages were obtained using zircon U–Pb dating and strontium chemostratigraphic analyses of fossil marine mollusc shells (Ehret et al., 2012), with relatively broad confidence intervals associated with the shell analyses (intervals range from c. 8 to 2 Ma for a late Miocene age). As detailed above, new dates provided by Bianucci et al. (in press) for the Cerro Los Quesos beds (tentatively correlated to the AGL level) are more compatible with the esimates of (Muizon (1988). In spite of these slight age discrepancies, a potentially interesting field of

investigation is the chronological faunal succession following from the relative stratigraphic position of the vertebrate levels in the Pisco Formation. Indeed, several marine mammal genera extend stratigraphically along more than one level. The most spectacular case is that of the marine sloth *Thalassocnus*, which spans c. 4 Myr, from the AGL level to a level younger than the SAO level at Yauca (McDonald & Muizon, 2002; Muizon et al., 2003, 2004; Amson et al., 2014). The five species of *Thalassocnus* currently recognized seem to represent a biostratigraphic, anagenetic lineage (Muizon et al., 2004; Amson et al., 2014; Amson, Muizon & Gaudin, 2016). The monachine phocid *Acrophoca longirostris* was initially described on the basis of specimens from the SAS level, with additional members of the genus in the MTM level at Montemar (*Acrophoca* sp. nov. 1), in the AGL level at Aguada de Lomas (Acrophoca sp. aff. *A. longirostris*), and in the ELJ level at Aguada de Lomas and El Jahuay (Acrophoca sp. nov. 2) (Muizon, 1981; Muizon & DeVries, 1985; our pers. observ.). Another monachine phocid, *Hadrokirus*, is recorded in the SAS level at Sud-Sacaco (*H. martini* Amson & Muizon, 2014) and in beds at Yauca stratigraphically younger than the SAO level (with a specimen much more massive than the holotype of *H. martini*, which could be referred to a different species of Hadrokirus) (Muizon et al., 2004; Amson & Muizon, 2014). The cetotheriid mysticete *Piscobalaena nana* is present in the SAS level at Sud-Sacaco, in the MTM level at Sud-Sacaco and Montemar, and in the AGL level at Aguada de Lomas, whereas *Piscobalaena* sp. nov. is present in the ELJ level at El Jahuay and near Lomas (Bouetel & Muizon, 2006; our pers. observ.). The pontoporiid odontocete *Brachydelphis* is present in the ELJ level at Aguada de Lomas and El Jahuay (B. longirostrisLambert & Muizon, 2013) and in the CLB level at Cerro la Bruja (B. mazeasi) (Muizon, 1988; Lambert & Muizon, 2013). The phocoenid *Piscolithax* occurs in the SAO level at Sacaco and in the SAS level at Sud-Sacaco (*Piscolithax longirostris* Muizon, 1984), and in the MTM and AGL levels at Aguada de Lomas (*Piscolithax* sp.) (Muizon, 1988). The odobenocetopsid odontocete *Odobenocetops* is encountered in the SAS level at Sud-Sacaco (O. peruvianus Muizon, 1993) and in the SAO level at Sacaco (O. leptodon Muizon et al., 1999). Therefore, the stratigraphic extension of the stem physeteroid genus *Acrophyseter* reported here (*A. robustus* in the CLB level, *A. deinodon* in the MTM level and *Acrophyseter* sp. in beds tentatively correlated to the AGL level) is also observed in several other groups of marine mammals. Furthermore, similar observations can be made concerning the penguin genus *Spheniscus* Brisson, 1760, which is present in all the levels of the Pisco Formation and represented by three different species, *Spheniscus urbinai, S. megaramphus* Stucchi et al., 2003 and S. muizoni (Stucchi, 2002; Stucchi et al., 2003; Göhlich, 2007). Biostratigraphical data from the nine genera mentioned above indicate that a succession of several species of the same mammal or bird genus occurs iterativelly in the Pisco Formation. In fact, such faunal extensions appear to be a rule, provided that taxa are well represented in the fossil record; it is likely that a

careful examination of the record for most of the mammal and bird genera of the Pisco Formation (the age of which spans approximately 10 Myr) will reveal a similar succession of closely related species. Whether these successions may represent anagenetic lineages (as already proposed for a fur seal in the Plio-Pleistocene of California; Boessenecker, 2011) remains to be investigated individually for each genus (but see Amson et al., 2016).

Acknowledgements

First of all we would like to thank M. Urbina for finding so many important localities (including Cerro Colorado and Cerro los Quesos) and specimens (including *Acrophyseter* sp. MUSM 2182 and *A. robustus* MUSM 1399) in the Pisco Basin, W. Aguirre, A. Altamirano, E. Díaz, A. Martínez, M. Martínez-Cáceres, R. Salas-Gismondi, J. Tejada, M. Urbina, N. Valencia and R. Varas-Malca for their essential help during fieldwork and visits at the MUSM, W. Aguirre, E. Díaz, the late G. Ramírez and R. Salas-Gismondi for the meticulous preparation of the specimens at the MUSM, and K. Post and J. Reumer for their support with the organization of fieldwork in Peru and their participation in some of the fieldtrips in the Pisco Basin. We also thank R. Vacant and T. Desvignes for the delicate preparation of the specimen MNHN SAS 1626, P. Loubry for the photographs of the latter specimen, and A. Gennari and C. Letenneur for their great artistic reconstructions of *A. deinodon* and *Livyatan melvillei*. We thank the MSNUP for allowing us to re-use the reconstruction of L. melvillei prepared by A. Gennari for a permanent exhibition there. Thanks to D. J. Bohaska, M. Fornasiero, C. Lefèvre, G. Lenglet, J. G. Mead, S. Ploen, L. H. Pomi, C. Potter, N. D. Pyenson, M. A. Reguero, A. Rol, R. Salas-Gismondi, H. van der Es, H. van Grouw, R. van Zelst, R. Varas-Malca and A. Varola for kindly providing access to specimens under their care, to T. DeVries and C. Di Celma for useful discussions about regional geology and stratigraphy, to K. Gariboldi for helpful discussions on diatom biostratigraphy, to J. H. Geisler for the much needed suggestions about cladistic analyses, to M. D. Uhen for his impressive contribution to the marine mammal section of the Paleobiology Database, and to R. W. Boessenecker, J. Corrie and an anonymous reviewer for their detailed reviews and constructive comments for such a long manuscript. The holotype of *A. deinodon* (MNHN SAS 1626) was collected with funds of the Muséum national d'Histoire naturelle (Action Spécifique 1337, 'Paléontologie Andes') and logistical support of the Institut Français d'Études Andines (Lima, Peru). *Acrophyseter* sp. MUSM 2182 was excavated with funds of the 'Action Thématique Muséum' (ATM 'Etat et structure phylogénétique de la biodiversité actuelle et fossile') and of the CNRS (Centre National de la Recherche Scientifique) with logistical support of the Institut

Français d'Études Andines and of the IRD (Institut de Recherche pour le Développement). Discovered by K. Post, the holotype of *L. melvillei* (MUSM 1676) was excavated with funds of the Natuurhistorisch Museum Rotterdam. Part of the fieldwork in Cerro Colorado and Cerro los Quesos was supported by a grant of the Italian Ministero dell'Istruzione dell'Università e della Ricerca (PRIN Project 2012YJSBMK) and by a National Geographic Society Committee for Research Exploration grant (9410-13), both to G. Bianucci.

References

Abel, O. 1905. Les Odontocètes du Boldérien (Miocène supérieur) des environs d'Anvers, *Mémoires du Musée Royal d'Histoire Naturelle de Belgique*, 3 (2), pp. 1-155..

Amson, E., De Muizon, C. 2014. A new durophagous phocid (Mammalia: Carnivora) from the late Neogene of Peru and considerations on monachine seals phylogeny, *Journal of Systematic Palaeontology*, 12 (5), pp. 523-548..

Amson, E., de Muizon, C., Laurin, M., Argot, C., de Buffrénil, V. 2014. Gradual adaptation of bone structure to aquatic lifestyle in extinct sloths from Peru, *Proceedings of the Royal Society B: Biological Sciences*, 281 (1782), art. no. 20140192,

Amson, E., De Muizon, C., Gaudin, T.J. 2017. A reappraisal of the phylogeny of the megatheria (Mammalia: Tardigrada), with an emphasis on the relationships of the Thalassocninae, the marine sloths, *Zoological Journal of the Linnean Society*, 179 (1), pp. 217-236.

Barnes, L.G. 1973. Praekogia cedrosensis, a new genus and species of fossil pygmy sperm whale from Isla Cedros, Baja California, Mexico, *Contrib Sci, Nat Hist Mus Los Angeles County*, 247, pp. 1-20.

Barron, J.A. 2003. Planktonic marine diatom record of the past 18 m.y.: Appearances and extinctions in the pacific and southern oceans, *Diatom Research*, 18 (2), pp. 203-224.

Berzin, A.A. 1972. The Sperm Whale. Israel Program for Scientific Translation (English translation, 1972): Jerusalem.

Bianucci, G., Landini, W. 2006. Killer sperm whale: A new basal physeteroid (Mammalia, Cetacea) from the Late Miocene of Italy, *Zoological Journal of the Linnean Society*, 148 (1), pp. 103-131.

Bianucci, G., Lambert, O., Post, K. 2010. High concentration of long-snouted beaked whales (genus Messapicetus) from the Miocene of Peru, *Palaeontology*, 53 (5), pp. 1077-1098.

Bianucci, G., Di Celma, C., Landini, W., Post, K., Tinelli, C., de Muizon, C., Gariboldi, K., Malinverno, E., Cantalamessa, G., Gioncada, A., Collareta, A., Gismondi, R.-S., Varas-Malca, R., Urbina, M., Lambert, O. 2016. Distribution of fossil marine vertebrates in Cerro Colorado, the type locality of the giant raptorial sperm whale Livyatan melvillei (Miocene, Pisco Formation, Peru), *Journal of Maps*, 12 (3), pp. 543-557.

Bianucci, G., Di Celma, C., Collareta, A., Landini, W., Post, K., Tinelli, C., de Muizon, C., Bosio, G., Gariboldi, K., Gioncada, A., Malinverno, E., Cantalamessa, G., Altamirano-Sierra, A., Salas-Gismondi, R., Urbina, M., Lambert, O. 2016. Fossil marine vertebrates of Cerro Los Quesos: Distribution of cetaceans, seals, crocodiles, seabirds, sharks, and bony fish in a late Miocene locality of the Pisco Basin, Peru, *Journal of Maps*, 12 (5), pp. 1037-1046.

Bloodworth, B., Marshall, C.D. 2005. Feeding kinematics of Kogia and Tursiops (Odontoceti: Cetacea): Characterization of suction and ram feeding, *Journal of Experimental Biology*, 208 (19), pp. 3721-3730.

Boersma, A.T., Pyenson, N.D. 2015. Albicetus oxymycterus, a New Generic Name and Redescription of a Basal Physeteroid (Mammalia, Cetacea) from the Miocene of California, and the Evolution of Body Size in Sperm Whales, *PLoS ONE*, 10 (12), art. no. e0135551

Boessenecker, R.W. 2011. New records of the fur seal Callorhinus (Carnivora: Otariidae) from the Plio-Pleistocene Rio Dell Formation of Northern California and comments on otariid dental evolution, *Journal of Vertebrate Paleontology*, 31 (2), pp. 454-467.

Boessenecker, R.W., Churchill, M. 2015. The oldest known fur seal, *Biology Letters*, 11 (2), art. no. 20140835

Boschma, H. 1938. On the teeth and other particulars of the sperm whale (Physeter macrocephalus L.), *Temminckia*, 3, pp. 151-278.

Bosio, G., Gariboldi, K., Di Celma, C., Gioncada, A., Malinverno, E., Tinelli, C., Villa, I.M., Cantalamessa, G., Collareta, A., Lambert, O., Landini, W., Urbina, M., Bianucci, G. 2015. Tephrochronology and biostratigraphy of two exceptional fossil localities in the Pisco Formation (Peru), *Rendiconti Online Soc. Geol. Ital.*, 35, p. 438.

Bouetel, V., De Muizon, C. 2006. The anatomy and relationships of Piscobalaena nana (Cetacea, Mysticeti), a Cetotheriidae s.s. from the early Pliocene of Peru, *Geodiversitas*, 28 (2), pp. 319-395.

Brand, L., Urbina, M., Chadwick, A., DeVries, T.J., Esperante, R. 2011. A high resolution stratigraphic framework for the remarkable fossil cetacean assemblage of the Miocene/Pliocene Pisco Formation, Peru, *Journal of South American Earth Sciences*, 31 (4), pp. 414-425.

Du Bus, B.A.L. 1867. Sur quelques Mammifères du Crag d'Anvers, *Bulletins de l'Académie Royale des Sciences, des Lettres et des Beaux-Arts de Belgique*, 24 (24), pp. 562-577.

Caldwell, D.K., Caldwell, M.C.1989. Pygmy sperm whale Kogia breviceps (de Blainville, 1838): Dwarf sperm whale Kogia simus Owen, *Handbook of Marine Mammals*, 4, pp. 235-260.

Carrier, D.R., Deban, S.M., Otterstrom, J. 2002. The face that sank the Essex: Potential function of the spermaceti organ in aggression, *Journal of Experimental Biology*, 205 (12), pp. 1755-1763.

Cione, A.L., Cozzuol, M.A., Dozo, M.T., Acosta Hospitaleche, C. 2011. Marine vertebrate assemblages in the southwest Atlantic during the Miocene, *Biological Journal of the Linnean Society*, 103 (2), pp. 423-440.

Clarke, R., Paliza, O. 1972. Sperm whales of the southeast Pacific. Part III. Morphometrics, *Hvalrådets Skrifter*, 53, pp. 1-106.

Cozzuol, M.A. 1996. The record of the aquatic mammals in southern South America, *Munchner Geowissenschaftliche Abhandlungen*, 30 (A), pp. 321-342.

Cranford, T.W. 1999. The sperm whale's nose: Sexual selection on a grand scale*?, Marine Mammal Science*, 15 (4), pp. 1133-1157

Cranford, T.W., Amundin, M., Norris, K.S. 1996. Functional morphology and homology in the odontocete nasal complex: Implications for sound generation, *Journal of Morphology*, 228 (3), pp. 223-285.

Devries, T.J. 1998. Oligocene deposition and Cenozoic sequence boundaries in the Pisco Basin (Peru), *Journal of South American Earth Sciences*, 11 (3), pp. 217-231.

DeVries, T.J. 2001. Molluscan evidence for an Oligocene-Miocene age of 'Paracas' beds in southern Peru, *Boletín de la Sociedad Geológica del Perú*, 92, pp. 57-65.

Di Celma, C., Malinverno, E., Gariboldi, K., Gioncada, A., Rustichelli, A., Pierantoni, P.P., Landini, W., Bosio, G., Tinelli, C., Bianucci, G. 2016. Stratigraphic framework of the late Miocene to Pliocene Pisco Formation at Cerro Colorado (Ica Desert, Peru), *Journal of Maps*, 12 (3), pp. 515-529.

Di Celma, C., Malinverno, E., Cantalamessa, G., Gioncada, A., Bosio, G., Villa, I.M., Gariboldi, K., Rustichelli, A., Pierantoni, P.P., Landini, W., Tinelli, C., Collareta, A., Bianucci, G. 2016. Stratigraphic framework of the late Miocene Pisco Formation at Cerro Los Quesos (Ica Desert, Peru), *Journal of Maps*, 12 (5), pp. 1020-1028.

Dunbar, R.B., Marty, R.C., Baker, P.A. 1990. Cenozoic marine sedimentation in the Sechura and Pisco basins, Peru, *Palaeogeography, Palaeoclimatology, Palaeoecology*, 77 (3-4), pp. 235-261.

Ehret, D.J., Macfadden, B.J., Jones, D.S., Devries, T.J., Foster, D.A., Salas-Gismondi, R. 2012. Origin of the white shark Carcharodon (Lamniformes: Lamnidae) based on recalibration of the Upper Neogene Pisco Formation of Peru, *Palaeontology*, 55 (6), pp. 1139-1153.

Evans, H.E., De Lahunta, A. 2013. Miller´s Anatomy of the Dog, 4th edn. St. Louis: Elsevier Saunders

Fahlke, J.M., Gingerich, P.D., Welsh, R.C., Wood, A.R. 2011. Cranial asymmetry in eocene archaeocete whales and the evolution of directional hearing in water, *Proceedings of the National Academy of Sciences of the United States of America*, 108 (35), pp. 14545-14548.

Fitzgerald, E.M.G. 2011. A fossil sperm whale (Cetacea, Physeteroidea) from the Pleistocene of Nauru, equatorial southwest Pacific, *Journal of Vertebrate Paleontology*, 31 (4), pp. 929-931.

Flower, W.H. 1868. XII. On the Osteology of the Cachalot or Sperm-Whale (Physeter macrocephalus), *The Transactions of the Zoological Society of London*, 6 (6), pp. 309-372.

Fordyce, R.E. 1981. Systematics of the odontocete whale Agorophius pygmaeus and the family Agorophiidae (Mammalia: Cetacea), *Journal of Paleontology*, 55 (5), pp. 1028-1045.

Fordyce, R.E. 1994. Waipatia maerewhenua, new genus and new species (Waipatiidae, new family), an archaic late Oligocene dolphin (Cetacea: Odontoceti: Platanistoidea) from New Zealand, *Proceedings - San Diego Society of Natural History*, 29, pp. 147-176.

Fordyce, R.E. 2002.Simocetus rayi (Odontoceti: Simocetidae) (new species, new genus, new family), a bizarre new archaic Oligocene dolphin from the eastern North Pacific, *Smithsonian Contributions to Paleobiology*, 93, pp. 185-222.

Fordyce, R.E., de Muizon, C. 2001. Evolutionary history of cetaceans: A review, in: Mazin J-M de Buffrénil V (eds), Secondary Adaptation of Tetrapods to Life in Water, München: Verlag Dr. Friedrich Pfeilpp, pp.169-233.

Fraser, F.C., Purves, P.E. 1960. Hearing in cetaceans: Evolution of the accessory air sacs and the structure and function of the outer and middle ear in recent cetaceans, *Bulletin of the British Museum (Natural History), Zoology*, 7 (1), pp. 1-140.

Gariboldi, K., Gioncada, A., Bosio, G., Malinverno, E., Di Celma, C., Tinelli, C., Cantalamessa, G., Landini, W., Urbina, M., Bianucci, G. 2015. The dolomite nodules enclosing fossil marine vertebrates in the East Pisco Basin, Peru: Field and petrographic insights into the Lagerstätte formation, *Palaeogeography, Palaeoclimatology, Palaeoecology*, 438, pp. 81-95.

Göhlich, U.B. 2007. The oldest fossil record of the extant penguin genus Spheniscus - A new species from the Miocene of Peru, *Acta Palaeontologica Polonica*, 52 (2), pp. 285-298.

Goloboff, P.A. 1993. Estimating character weights during tree search, *Cladistics*, 9 (1), pp. 83-91.

Gondar, D. 1975. La presencia de cetaceos (Physeteridae) en el terciario superior (rionegrense) de la prov. de rio negro, *Actas Del Congreso Argentino De Paleontologia Y Bioestratigrafia*, 2, pp. 349-356.

Hampe, O. 2006. Middle/late Miocene hoplocetine sperm whale remains (Odontoceti: Physeteridae) of North Germany with an emended classification of the Hoplocetinae, *Fossil Record*, 9 (1), pp. 61-86.

Hassanin, A., Delsuc, F., Ropiquet, A., Hammer, C., Jansen Van Vuuren, B., Matthee, C., Ruiz-Garcia, M., Catzeflis, F., Areskoug, V., Nguyen, T.T., Couloux, A.2012. Pattern and timing of diversification of Cetartiodactyla (Mammalia, Laurasiatheria), as revealed by a comprehensive analysis of mitochondrial genomes, *Comptes Rendus - Biologies*, 335 (1), pp. 32-50

Heyning, J.E., Mead, J.G. 1996. Suction feeding in beaked whales: Morphological and observational evidence, *Contributions in Science, Natural History Museum of Los Angeles County*, 464, pp. 1-12.

Hirota, K., Barnes, L.G. 1994. A new species of Middle Miocene sperm whale of the genus Scaldicetus (Cetacea; Physeteridae) from Shiga-mura, Japan, *Island Arc*, 3 (4), pp. 453-472.

Hohn, A.A. 2002. Age estimation, in: Perrin WF Würsig B Thewissen JGM (eds), Encyclopedia of Marine Mammals, san Diego: Academic Press, pp. 6-13

Howell, A.B. 1927. Contribution to the anatomy of the Chinese finless porpoise, Neomeris phocaenoides, *Proceedings of the United States National Museum*, 70 (13), pp. 1-43.

Huggenberger, S., André, M., Oelschläger, H.H.A. 2016. The nose of the sperm whale: Overviews of functional design, structural homologies and evolution, *Journal of the Marine Biological Association of the United Kingdom*, 96 (4), pp. 783-806.

Johnston, C., Berta, A. 2011. Comparative anatomy and evolutionary history of suction feeding in cetaceans, *Marine Mammal Science*, 27 (3), pp. 493-513.

Kázar, E. 2002. Revised phylogeny of the Physeteridae (Mammalia: Cetacea) in the light of Placoziphius Van Beneden, 1869 and Aulophyseter Kellogg, 1927, *Bulletin de l'Institut Royal des Sciences Naturelles de Belqique, Sciences de la Terre*, 72, pp. 151-170.

Kellogg, R. 1925. Two fossil physeteroid whales from California, *Carnegie Institution of Washington Publication*, 348, pp. 1-34.

Kellogg, A.R. 1925. A fossil physeteroid cetacean from Santa Barbara County, California, *Proceedings of the United States National Museum*, 66 (27), pp. 1-8.

Kellogg, R. 1927. Study of the skull of a fossil sperm whale from the Temblor Miocene of southern California, *Carnegie Institution of Washington Publication*, 346, pp. 1-23.

Kellogg, R. 1965. Fossil marine mammals from the Miocene Calvert Formation of Maryland and Virginia, *United States National Museum Bulletin*, 247 (2), pp. 1-45.

Kimura, T., Hasegawa, Y., Barnes, L.G. 2006. Fossil sperm whales (Cetacea, Physeteridae) from Gunma and Ibaraki prefectures, Japan; with observations on the Miocene fossil sperm whale Scaldicetus shigenis Hirota and Barnes, 1995, *Bulletin of the Gunma Museum of Natural History*, 10, pp. 1-23.

Kraus, R. 1998. The cranium of Piscogavialis jugaliperforatus n. gen., n. sp. (Gavialidae, Crocodylia) from the Miocene of Peru, *Paläontologische Zeitschrift*, 72 (3-4), pp. 389-406.

Lambert, O. 2005. Phylogenetic affinities of the long-snouted dolphin Eurhinodelphis (Cetacea, Odontoceti) from the Miocene of Antwerp, Belgium, *Palaeontology*, 48 (3), pp. 653-679.

Lambert, O. 2006. First record of a platanistid (Cetacea, Odontoceti) in the North Sea Basin: A review of Cyrtodelphis Abel, 1899 from the Miocene of Belgium, *Oryctos*, 6, pp. 69-79.

Lambert, O. 2008. Sperm whales from the Miocene of the North Sea: A re-appraisal, *Bulletin de l'Institut Royal des Sciences Naturelles de Belqique, Sciences de la Terre*, 78, pp. 277-316.

Lambert, O., De Muizon, C. 2013. A new long-snouted species of the Miocene pontoporiid dolphin Brachydelphis and a review of the Mio-Pliocene marine mammal levels in the Sacaco Basin, Peru, *Journal of Vertebrate Paleontology*, 33 (3), pp. 709-721

Lambert, O., Bianucci, G., de Muizon, C. 2008. A new stem-sperm whale (Cetacea, Odontoceti, Physeteroidea) from the Latest Miocene of Peru, *Comptes Rendus - Palevol*, 7 (6), pp. 361-369.

Lambert, O., Bianucci, G., Post, K. 2009. A new beaked whale (Odontoceti, Ziphiidae) from the middle Miocene of Peru, *Journal of Vertebrate Paleontology*, 29 (3), pp. 910-922

Lambert, O., Bianucci, G., Post, K., De Muizon, C., Salas-Gismondi, R., Urbina, M., Reumer, J. 2010. The giant bite of a new raptorial sperm whale from the Miocene epoch of Peru, *Nature*, 466 (7302), pp. 105-108.

Lambert, O., De Muizon, C., Bianucci, G. 2013. The most basal beaked whale Ninoziphius platyrostrisMuizon, 1983: Clues on the evolutionary history of the family Ziphiidae (Cetacea: Odontoceti), *Zoological Journal of the Linnean Society*, 167 (4), pp. 569-598

Lambert, O., Bianucci, G., Beatty, B.L. 2014. Bony outgrowths on the jaws of an extinct sperm whale support macroraptorial feeding in several stem physeteroids, *Naturwissenschaften*, 101 (6), pp. 517-521.

Lambert, O., Bianucci, G., Urbina, M., Geisler, J.H. 2017. anew inioid (Cetacea, Odontoceti, Delphinida) from the Miocene of Peru and the origin of modern dolphin and porpoise families, *Zoological Journal of the Linnean Society*, 179 (4), pp. 919-946.

Lancaster, W.C. 1990. The middle ear of the archaeoceti, *Journal of Vertebrate Paleontology*, 10 (1), pp. 117-127.

Louwye, S. 2005. The Early and Middle Miocene transgression at the southern border of the North Sea Basin (northern Belgium), *Geological Journal*, 40 (4), pp. 441-456.

Lydekker, R. 1894. Contribution to a knowledge of the fossil vertebrates of Argentina. 2. The extinct Edentates of Argentina, *Anales Del Museo de la Plata*, 3, pp. 1-118.

Maddison, W.P., Maddison, D.R.. 2004. Mesquite: A Modular System for Evolutionary Analysis. Version 3.03. Available at: http://mesquiteproject.org

Martínez-Cáceres, M., de Muizon, C. 2011.A new basilosaurid (Cetacea, Pelagiceti) from the Late Eocene to Early Oligocene Otuma Formation of Peru, *Comptes Rendus - Palevol*, 10 (7), pp. 517-526.

Marx, F.G., Fordyce, R.E. 2015. Baleen boom and bust: A synthesis of mysticete phylogeny, diversity and disparity, *Royal Society Open Science*, 2 (4), art. no. 140434, 14 p.

McDonald, H.G., De Muizon, C. 2002. The cranial anatomy of thalassocnus (xenarthra, mammalia), a derived nothrothere from the neogene of the pisco formation (Peru), *Journal of Vertebrate Paleontology*, 22 (2), pp. 349-365.

McGowen, M.R., Spaulding, M., Gatesy, J. 2009. Divergence date estimation and a comprehensive molecular tree of extant cetaceans, *Molecular Phylogenetics and Evolution*, 53 (3), pp. 891-906.

Mchedlidze, G.A. 1970. Some general characteristics of the evolution of cetaceans, part 1. Tbilisi: Akademia Nauk Gruzinskoi S.S.R., Institut Paleobiologii

Mead, J.G. Fordyce, R.E. 2009. The therian skull: a lexicon with emphasis on the odontocetes, *Smithsonian Contributions to Zoology*, 627, pp. 1-248.

Misonne, X. 1958. Faune du Tertiaire et du Pléistocène inférieur de Belgique (Oiseaux et Mammifères), *Bulletin de l'Institut royal des Sciences naturelles de Belgique*, 34, pp. 1-36

Moreno, F. P. 1892. Noticias sobre algunos cetáceos fósiles y actuales, *Revista del Museo de La Plata*, 3, pp. 383-400.

Murie, D. J. 1873. On the organization of the Caaing whale, Globiocephalus melas, *The Transactions of the Zoological Society of London*, 8 (4), pp. 235-302.

Ohsumi, S., Kasuya, T., Nishiwaki, M. 1963. Accumulation rate of dental growth layers in the maxillary tooth of the sperm whale, *Whales Research Institute, Scientific Reports*, 17, pp. 15-35.

Parham, J. F., Pyenson, N. D. 2010. New sea turtle from the Miocene of Peru and the iterative evolution of feeding ecomorphologies since the cretaceous, *Journal of Paleontology*, 84 (2), pp.231-247.

Parras, A., Dix, G. R., Griffin, M. 2012. Sr-isotope chronostratigraphy of paleogene-neogene marine deposits: Austral basin, southern Patagonia (argentina), *Journal of South American Earth Sciences*, 37, pp. 122-135.

Pyenson, N. D., Irmis, R. B., Lipps, J. H., Barnes, L. G., Mitchell Jr., E. D., McLeod, S. A. 2009. Origin of a widespread marine bonebed deposited during the middle miocene climatic optimum. *Geology*, 37 (6), pp. 519-522.

Pyenson, N. D., Sponberg, S. N. 2011. Reconstructing body size in extinct crown Cetacea (neoceti) using allometry, phylogenetic methods and tests from the fossil record. *Journal of Mammalian Evolution*, 18 (4), pp. 269-288.

Reidenberg, J. S., Laitman, J. T. 1994. Anatomy of the hyoid apparatus in odontoceli (toothed whales): Specializations of their skeleton and musculature compared with those of terrestrial mammals, *The Anatomical Record*, 240 (4), pp. 598-624.

Rice, D. W. 1989. Sperm whale Physeter macrocephalus linnaeus, 1758, in: In: Ridgway, S.H., Harrison, R. (eds.), *Handbook of marine mammals, vol. 4: River dolphins and the larger toothed whales*. London: Academic Press, pp. 177–233

Schulte, H. V. W., Smith, M. D. F. 1918. The external characters, skeletal muscles, and peripheral nerves of Kogia breviceps (blainville), *Bull Am Mus Nat Hist*, 38 (2), pp. 7-72.

Seagars, D. J. 1982. Jaw structure and functional mechanics of six delphinids (Cetacea: Odontoceti). Unpublished Master's thesis, San Diego State University.

Steeman, M. E., Hebsgaard, M. B., Fordyce, R. E., Ho, S. Y. W., Rabosky, D. L., Nielsen, R., . . . Willerslev, E. 2009. Radiation of extant cetaceans driven by restructuring of the oceans, *Systematic Biology*, 58 (6), pp. 573-585.

Stucchi, M. 2002. Una nueva especie de spheniscus (aves: Spheniscidae) de la formación Pisco, Perú, *Boletín de la Sociedad Geológica del Perú*, 94, pp. 17-24.

Stucchi, M., Urbina, M., Giraldo, A. 2003. Una nueva especie de spheniscidae del mioceno tardío de la formación Pisco, Perú, *Bulletin de l'Institut Français d'Études Andines*, 32 (2), pp. 361-375.

Swofford, D. L. 2002. PPAUP: Phylogenetic analysis using parsimony (and other methods). Version 4b10. Sunderland, MA: Sinauer Associates.

Turnbull, W. D. 1970. Mammalian masticatory apparatus, *Fieldiana: Geology*, 18 (2), pp. 149-356.

Uhen, M. D. 2004. Form, function, and anatomy of Dorudon atrox (mammalia, cetacea): An archaeocete from the middle to late Eocene of Egypt. *University of Michigan Papers on Paleontology*, 34, pp. 1-222.

Uhen, M. D., Fordyce, R. E., Barnes, L. G. 2008. Odontoceti, in: Janis, C.M., Gunnel, G.F., Uhen, M.D. (eds), *Evolution of tertiary mammals of North America: Volume 2: Small mammals, xenarthrans, and marine mammals*. Cambridge: Cambridge University Press, pp. 566–606

Van Beneden, P. -. 1869. Sur un nouveau genre de ziphioïde fossile (placoziphius), trouvé à Edeghem, près d'Anvers. *Mém. Acad. R. Sci. Belg.*, 37, pp. 1-12.

Velez-Juarbe, J., Wood, A. R., De Gracia, C., Hendy, A. J. W. 2015. Correction: Evolutionary patterns among living and fossil kogiid sperm whales: Evidence from the Neogene of central America, *PLoS ONE*, 10 (5), article n. e0123909

Vélez-Juarbe, J., Wood, A. R., Pimiento, C. 2016. Pygmy sperm whales (odontoceti, kogiidae) from the Pliocene of Florida and North Carolina, *Journal of Vertebrate Paleontology*, 36 (4), article n. e1135806.

Werth, A. J. 2004. Functional morphology of the sperm whale tongue, with reference to suction feeding, *Aquatic Mammals*, 30, pp. 405-418.

Werth, A. J. 2006. Mandibular and dental variation and the evolution of suction feeding in odontoceti, *Journal of Mammalogy*, 87 (3), pp. 579-588.

Whitmore, F. C., Kaltenbach, J. A. 2008. Neogene Cetacea of the Lee Creek phosphate mine, North Carolina. *Virginia Museum of Natural History Special Publication*, 14, pp. 181-269.

Wible, J. R. 2008. On the cranial osteology of the Hispaniolan solenodon, Solenodon paradoxus Brandt, 1833 (mammalia, lipotyphla, solenodontidae). *Annals of Carnegie Museum*, 77 (3), pp. 321-402.